SISSA **ISAS**

SCUOLA INTERNAZIONALE SUPERIORE DI STUDI AVANZATI
INTERNATIONAL SCHOOL FOR ADVANCED STUDIES

Clustering at high redshift: the sub-millimeter and radio views

Thesis submitted for the degree of
Doctor Philosophiæ

CANDIDATE:
Mattia Negrello

SUPERVISORS:
Prof. Gianfranco De Zotti
Dr. Manuela Magliocchetti

October 2006

Table of Contents

Published Works

Part of the contents of this Thesis has already appeared in the following papers:

- ▷ *Confusion noise at far-infrared to millimetre wavelenghts.*
  Negrello M., Magliocchetti M., Moscardini L., De Zotti G., Granato G. L., Silva L., 2004, MNRAS, **352**, 493-500.
- ▷ *Effect of clustering on extragalactic souce counts with low-resolution instruments.*
  Negrello M., González-Nuevo J., Magliocchetti M., Moscardini L., De Zotti G., Toffolatti L. Danese L., 2005, MNRAS, **358**, 869-874.
- ▷ *Extragalactic source contributions to arcminute-scale Cosmic Microwave Background anisotropies.*
  Toffolatti L., **Negrello M.**, González-Nuevo J., De Zotti G., Silva L., Granato G. L., Argüeso F., 2005, A&A, **438**, 475-480.
- ▷ *The large scale clustering of radio sources.*
  Negrello M., Magliocchetti M., De Zotti G., 2006, MNRAS, **368**, 935-942.

Chapter 1

Introduction

1.1 Overview

Understanding the large scale distribution of galaxies in the Universe is one of primary objectives in modern cosmology. The extensive efforts devoted to this topic are repaid by the wealth of informations that can be extracted from clustering measurements. And indeed, these measurements have been exploited since the 70s' to get insight on the initial conditions of the Big Bang, to constrain the matter content of the Universe and shed light on the physical processes that have operated through the cosmic time.

Although it is now well established that the large scale structure in the distribution of matter arose due to gravitational instability operating from the same primordial perturbations seen as small anisotropies in Cosmic Microwave Background (CMB) radiation, less clear is the way in which luminous galaxies relate to the underlying matter distribution. In fact it has become evident in recent years that this relation is not straightforward and, indeed, galaxies provide us only with a *biased* picture of the distribution of the matter. Moreover the details of the relation between light and matter, encoded in the so called *bias parameter*, depend on many unknowns which range from the intrinsic properties of the sources (mass, luminosity, etc.) to the length-scale sampled and the epoch of observation. Accounting for all these observed dependencies is something theories of galaxy formation are called to do.

The issue of bias has been extensively addressed in the local Universe by taking advantage the new generation of surveys - the 2df Galaxy Redshift Survey (2dfGRS) and the Sloan Digital Sky Survey (SDSS) - which have measured the large scale distribution of low-redshift objects with a level of details and on length scales that were unthinkable just a few years ago. However, in order to have a clear picture of structure formation and evolution, high redshift investigations are needed.

In this thesis I will focus on two classes of high redshift sources: galaxies selected at 850μm and AGN-powered radio sources. The detection of submillimetre radiation from distant galaxies is one of the most recent developments in observational cosmology and has proved to be a challenge for theories of galaxy formation. This is the reason why a major part of the present work will be devoted to this class of sources.
Conversely, the large scale distribution of radio galaxies is a matter of analysis since many decades, but the improvement in clustering estimates achieved by means of the recent large-scale radio surveys can help to better constrain some properties of this class of objects and their cosmic evolution.

1.2 The formation and evolution of large scale structures

In this Section I summarize the main aspects that concur to determine the observed large-scale clustering properties of matter: from the cosmological framework in which perturbations were set and evolved, to the relevant physical processes which affected the spectrum of the primordial fluctuations.

1.2.1 The cosmological framework

The nearly isotropic CMB radiation provides the strongest support to the widely accepted model of a (statistically) homogeneous and isotropic Universe. The geometrical properties of such a Universe are described by the metric of Friedman-Robertson-Walker:

$$ds^2 = -(cdt)^2 + a^2(t)\left[\frac{dx^2}{1-Kx^2} + x^2(d\theta^2 + \sin^2\theta d\phi^2)\right], \qquad (1.1)$$

expressed here in the spherical comoving coordinates x, θ and ϕ. K is the spatial curvature of the Universe, scaled so as to take the values 0 or ± 1; the case $K = 0$ corresponds to a flat cosmic geometry and is the value favored by current CMB measurements. The *scale factor*, $a(t)$, describes the way in which the physical separation between two generic positions in space changes with cosmic time t under the effect of the dynamical evolution of the Universe that is regulated by the Einstein equations:

$$H^2(t) = \frac{8\pi G}{3}\rho - \frac{K}{a^2}c^2, \tag{1.2}$$

$$\frac{\ddot{a}}{a} = -\frac{4\pi G}{3}\left(\rho + 3\frac{p}{c^2}\right), \tag{1.3}$$

where ρc^2 and p are respectively the rest-mass energy density and the pressure of the homogeneous and isotropic fluid that is assumed to fill the Universe. The dots denote the derivative with respect to cosmic time and $H(t) = (\dot{a}/a)$ is the *Hubble parameter*.

Once the equation of state of the fluid is provided, this can be used, together with the above equations, to infer the cosmic evolution of both the functions $a(t)$ and $\rho(t)$. A common assumption is

$$\rho = wpc^2. \tag{1.4}$$

The case $w = 0$ corresponds to a fluid made of collisionless particles, while the case $w = 1/3$ describes a gas of relativistic particles (e.g. photons). By inserting equation (1.4) into equations (1.2)-(1.3) one gets

$$\rho = \rho_0 \left(\frac{a}{a_0}\right)^{-3(1+w)}. \tag{1.5}$$

The time-evolution of the scale factor $a(t)$, and consequently that of $\rho(t)$, depends on the curvature of the Universe: for $K \leq 0$, $a(t)$ is a monotonic increasing function of time (expanding Universe) while for $K > 0$ it first increases up to a maximum value and then decreases to its initial value ("closed" Universe).

According to observations, the main matter components of the Universe are photons, baryons (with their accompanying electrons), a form of non-relativistic (Cold) and non-radiating (Dark) matter (hereafter CDM). In addiction, the Universe is filled by a form

of dark energy characterized by negative pressure: $p = w\rho c^2$ with $w \sim -1$, the case $w = -1$ corresponding to the well known *cosmological constant*. The densities of such components, measured at present epoch and referred to the critical density of the Universe $\rho_{0,\rm cr} = 3/8\pi G(\dot{a}/a)^2$ (the one required for a flat cosmic geometry), are well constrained by combining the results of the 3-years Wilkinson Microwave Anisotropy Probe (Spergel et al. 2006) with other data sets:

$$\Omega_{0,\rm CDM} = \rho_{0,m}/\rho_{0,\rm cr} \sim 0.23 \quad \text{for CDM,} \tag{1.6}$$

$$\Omega_{0,b} = \rho_{0,b}/\rho_{0,\rm cr} \sim 0.045 \quad \text{for baryons,} \tag{1.7}$$

$$\Omega_{0,ph} = \rho_{0,r}/\rho_{0,\rm cr} \sim 10^{-5} \quad \text{for photons,} \tag{1.8}$$

$$\Omega_{0,\Lambda} = \rho_{0,b}/\rho_{0,\rm cr} \sim 0.73 \quad \text{for cosmological constant.} \tag{1.9}$$

The emerging scenario is that of a Universe that is actually dominated by non-relativistic matter, mainly constitute of particles interacting only via gravity. Baryons provide only a marginal contribution to the total matter content of the Universe; this means that the formation of cosmological structure is mainly driven by dark matter, with baryons following within the deep potential wells associated to the collapsing dark matter perturbations.

In this thesis, I will provide results within the cosmological framework set by the above constraints, with $\Omega_{0,m} = \Omega_{\rm CDM} + \Omega_{0,b} = 0.3$ and $\Omega_{0,\Lambda} = 0.7$, if not otherwise stated. I will further adopt $h = 0.7$ for the present-day value of the Hubble parameter, normalized to 100 Km s^{-1} Mpc^{-1}.

1.2.2 Evolution of perturbations

Perturbations in the matter density field ρ are described in terms of the *dimensionless density contrast*

$$\delta(\vec{x}) = \frac{\rho(\vec{x}) - \bar{\rho}}{\bar{\rho}}, \tag{1.10}$$

$\bar{\rho}$ being the mean value of the density in the Universe.
It is often convenient to consider the perturbations as a superposition of plane waves:

$$\delta(\vec{x}) = \frac{1}{(2\pi)^3} \int \delta_{\vec{k}} e^{-i\vec{k}\cdot\vec{x}} d^3k, \tag{1.11}$$

where $\delta_{\vec{k}}$ is the Fourier transform of the density contrast:

$$\delta_{\vec{k}} = \int \delta(\vec{x}) e^{i\vec{k}\cdot\vec{x}} d^3x. \tag{1.12}$$

The advantage of working in Fourier space follows from the fact that, in the linear regime (i.e. $\delta \ll 1$), the equations which describe the evolution of the perturbations are linear in δ and therefore the single modes $\delta_{\vec{k}}$ evolve independently.

Small perturbations in the matter density field are believed to be generated in the early Universe as a consequence of the amplification of quantum fluctuations set during the inflationary era. These fluctuations have subsequently imprinted the CMB radiation which arises from the decoupling of photon from baryonic matter when the Universe was only 400,000 years old. Measurements of the CMB polarization suggest that these seed fluctuations are *adiabatic*, which means that they involve both the matter density and the radiation density in such a way that the total entropy of the system stay constant; as a consequence they induce fluctuations in the spatial curvature by causing variations in the total energy of the system.
CMB data also indicate that the primordial perturbations follow a nearly Gaussian distribution as predicted by standard inflationary models. Deviations from Gaussianity, if present, are expected to be far below the detectability of current CMB experiments. For these reason, the intrinsic temperature fluctuations in the CMB are commonly treated as being Gaussian, and the same assumption is made in most analysis of large-scale structure of the Universe (see e.g. Press & Schechter 1974).

The primordial fluctuations grow under the influence of gravity and, in the early stage of their evolution, are modified by various physical processes once they enter the *cosmological horizon*, $c/H(t)$, the scale over which different parts of a perturbation can be in causal contact with each other at the epoch t. Such physical processes, and therefore the modulation

of the perturbations, depend on the form of matter in the Universe, on its amount and on the amount of radiation.

In the established cosmological paradigm, non relativistic particles (baryons, electrons and CDM) dominate relativistic particles (e.g. photons) in density today. However, at early times, the opposite was true because the density of those two classes of particles scales differently in time: in fact, according to equation (1.5) the densities of matter and radiation increase back in time respectively as a^{-3} and a^{-4}, so that there should be an epoch at which they were equal. The transition from a radiation-dominated Universe to a matter-dominated one occurs roughly at redshift[1] $z_{\rm eq} \sim 2.4 \times 10^4 \Omega_{0,m} h^2$, and that epoch has important consequences for the evolution of perturbations:

- before $z_{\rm eq}$ the dominant energy of radiation drives the Universe to expand so fast that matter has no time to self-gravitate, and any perturbation on scales within the cosmological horizon is frozen at a constant value (Mészáros 1974); on the other hand, perturbations on larger scales, which lie outside the horizon at z_{eq}, are left virtually unscathed by the radiation dominated epoch.

- after $z_{\rm eq}$ perturbations on scales smaller than the horizon can grow again but their amplitude is suppressed with respect to fluctuations on scales above the horizon by an amount corresponding to the lack of growth between horizon entry and matter-radiation equivalence.

Therefore, the horizon scale at matter-radiation equality will be imprinted in the distribution of fluctuations by marking a turn-over in the growth rate of perturbations.

Dark matter particles interact only via gravity so that there is no pressure that could play against the collapse of perturbations. However, the velocity dispersion of the particles can in principle contrast gravity and dissipate the fluctuations, at least on relatively small scales (*free streaming* process). Since this effect is relevant only for relativistic dark matter particles (e.g. "hot" dark matter), in a CDM Universe perturbations can grow on any cosmological scale. This is a peculiar feature of CDM models, in which structure formation

[1] The redshift z is defined as $z = a(t_0)/a(t) - 1$, where t_0 identifies the present epoch.

can proceed in a hierarchical way, from smaller units which then merge to form bigger structures.

For what concerns baryons, the evolution of perturbations in this matter component is affected by the interaction of baryons with photons (via Thomson scattering) in the primordial ionized plasma. When the temperature of the Universe drops to the point (T$\sim$3000 K) where it is thermodynamically favorable for the ionized plasma to form neutral atoms, photons are left free to propagate through the Universe while baryons fall within the deep potential wells associated to the perturbations in the dominant dark matter component. The dark potential wells thus become the sites for the subsequent formation of galaxies. Before the decoupling of photons from baryons, that occurred soon after the matter-radiation equivalence, the pressure of the plasma - mainly supported by radiation - contrasts the collapse of perturbations. The *Jeans scale*, $\lambda_{\rm J} = v_{\rm s}\sqrt{\pi/G\bar{\rho}}$, $v_{\rm s}$ being the sound speed in the photon-baryon gas, marks the transition between the regimes in which gravity dominates over pressure and vice-versa; as a consequence

- perturbations on scales $2\pi/k << \lambda_{\rm J}$ are prevented from growing because of pressure and are converted into acoustic waves,

- perturbations on scales $2\pi/k >> \lambda_{\rm J}$ can grow due gravitational instability

Since the sound speed is very close to the speed of light before decoupling, the Jeans scale is almost equal to the horizon scale and all perturbations below the horizon propagate as acoustic waves. This effect induces smooth oscillations in the distribution of perturbations on scales smaller than the cosmological horizon at the decoupling of baryons from radiation.

The physical processes briefly described above concur to determine the final shape of the distribution of perturbations and hence the clustering properties of matter, which is the issue addressed in the following section.

1.2.3 Clustering of dark matter

The most useful way to describe the clustering properties of a density field δ is by means of the *autocorrelation function* ξ, defined as

$$\xi(\vec{r}) = \langle \delta(\vec{x}+\vec{r})\delta(\vec{x}) \rangle \tag{1.13}$$

where the average $\langle \cdot \rangle$ is made over all the positions $\vec{x}$. From the assumption of statistical homogeneity and isotropy of the Universe, $\xi(\vec{r})$ only depends on the absolute value of the vector $\vec{r}$; therefore we can set $\xi(\vec{r}) \equiv \xi(r)$.
The physical meaning of ξ becomes evident if one considers a discrete distribution of point-sources with average mass m and number density $n(\vec{x}) = \rho(\vec{x})/m$. Each infinitesimal volume of space δV will have a probability

$$\begin{aligned} \delta P(\vec{x}) &= n(\vec{x})\delta V \\ &= \bar{n}[1+\delta(\vec{x})]\delta V \end{aligned} \tag{1.14}$$

of containing a point-source, $\bar{n}$ being the mean number density. Consequently, the joint probability of finding one point-source at $\vec{x}_1$ and another at $\vec{x}_2$ separated by a distance $\vec{r}$ is

$$\begin{aligned} \delta P(\vec{x}_1, \vec{x}_2) &= \delta P(\vec{x}_1)\delta P(\vec{x}_2) \\ &= \bar{n}[1+\delta(\vec{x}_1)]\delta V_1 \bar{n}[1+\delta(\vec{x}_2)]\delta V_2 \ . \end{aligned} \tag{1.15}$$

By taking the average of $\delta P(\vec{x}_1, \vec{x}_2)$ over all the pairs $(\vec{x}_1, \vec{x}_2)$ with a fixed separation r and keeping in mind that - by definition - $\langle \delta \rangle = 0$ we get

$$\begin{aligned} \delta P(\vec{x}_1, \vec{x}_2) &= \bar{n}^2 \delta V_1 \delta V_2 [1 + \langle \delta(\vec{x}_1)\delta(\vec{x}_2) \rangle] \\ &= \bar{n}^2 \delta V_1 \delta V_2 [1 + \xi(r)] \ . \end{aligned} \tag{1.16}$$

The term $\bar{n}^2 \delta V_1 \delta V_2$ is the joint probability for the case of randomly distributed point-sources. Therefore ξ just represents a measure of how the observed distribution of objects deviates from the Poisson case.

The analogous of the correlation function in Fourier space is the *power spectrum*

$$P(\vec{k}) = \frac{1}{(2\pi)^3} \langle \hat{\delta}(\vec{k}' + \vec{k}) \hat{\delta}(\vec{k}') \rangle \ . \tag{1.17}$$

Also in this case, the statistical homogeneity and isotropy of the Universe implies that the power spectrum only depends on the modulus of the vector $\vec{k}$. It can be shown (see e.g. Coles & Lucchin 1995) that $\xi(r)$ and $P(k)$ form a Fourier pair, that is

$$\xi(r) = \frac{1}{(2\pi)^3} \int e^{-i\vec{k}\cdot\vec{r}} P(k) d^3k \tag{1.18}$$

and therefore provide the same amount of information on the clustering properties of the field δ.

The most basic inflationary models predict a scale-invariant spectrum of the fluctuations

$$P(k) \propto k^n \tag{1.19}$$

with a *spectral index* n close to unit as confirmed by the most recent measurements of the CMB spectrum made by the Wilkinson Microwave Anisotropy Probe satellite (WMAP; Spergel et al. 2006). The linearly evolved power spectrum is written in the form

$$P(k,z) = Ak^n T^2(k) D^2(z) \ . \tag{1.20}$$

In this expression the function $D(z)$ is the *linear growth factor* and describes the evolution of a perturbation in the linear regime. A general analytic approximation to $D(z)$ can be found in Carroll et al. (1992). The combined effect of the various processes involved in changing the shape of the original power spectrum is accounted for by the *transfer function* $T(k)$. Semi-analytic approximations for $T(k)$ have been worked out by Bardeen et al. (1986) and Eisenstein & Hu (1998). The normalization of the power spectrum, provided by the parameter A, is usually fixed either by the value of σ_8, that is the local value of the rms of the matter density field δ within a sphere of 8 h^{-1} Mpc comoving-radius, or by the measured amplitude of the CMB fluctuations. Values of σ_8 in the range 0.7-0.9 are supported by a number of data sets on CMB anisotropies, large scale structure, weak lensing and cluster abundances.

In Fig. 1.1 I show the linear power spectrum of cold dark matter as a function of the comoving wave number k (left-hand panel) and the corresponding spatial correlation function, $\xi_{\rm DM}$, as a function of the comoving scale r (right-hand panel), as obtained from

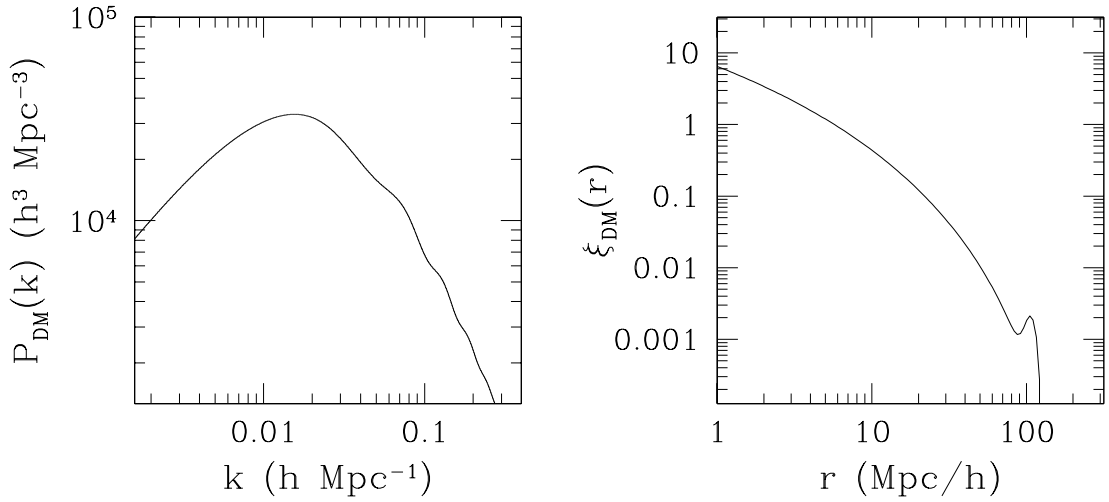

Figure 1.1: *left-hand panel*: the linear power spectrum of dark matter at $z = 0$ as a function of the comoving wave number k, computed from the standard flat Universe with $\Omega_{0,m} = 0.27$, $\Omega_{0,\Lambda} = 0.73$, $\Omega_{0,b} = 0.045$ and $h = 0.72$. Further assumptions are $n = 1$ for the primordial spectral index and $\sigma_8 = 0.9$ for the normalization. *right-hand panel*: the spatial correlation function of dark matter, $\xi_{\rm DM}(r)$, at $z = 0$, as a function of the comoving scale r, computed from the linear power spectrum shown in the left-hand panel by using equation (1.18).

equation (1.18). A primordial spectral index $n = 1$ and a normalization $\sigma_8 = 0.9$ are assumed. Both $P_{\rm DM}$ and $\xi_{\rm DM}$ are calculated at redshift $z = 0$ using the recipe of Eisenstein & Hu (1998) for the transfer function.

The most significant features in the matter correlation function are:

- a sharp cut-off around $r_{\rm cut} \sim 100\ h^{-1}$ Mpc: above such a scale, $\xi_{\rm DM}$ becomes negative and then approaches zero, as follows from the statistical homogeneity and isotropy of the Universe on large scales. The value of $r_{\rm cut}$ depends on that of $\Omega_{0,m}$ since the matter content of the Universe fixes the value of the cosmological horizon at matter-radiation equivalence: by decreasing $\Omega_{0,m}$ the horizon increases its size and much more power is moved to large scales, thus shifting the cut-off scale to higher values;

- a peak just below the cut-off scale: this is due to the baryonic acoustic oscillations imprinted in the power spectrum before the decoupling of photons from matter, and

is sensitive to the value of $\Omega_{0,b}$: the higher the baryon density, the more pronounced the peak is.

It is worth noticing that in the case in which the Universe is filled with a larger amount of baryons, the power spectrum shows significant modulations, reflecting the number of oscillations that were completed before the baryons decoupled from photons and the pressure support dropped. The lack of such large modulations in the real data (see e.g. Spergel et al. 2003, 2006; Cole et al. 2005; Eisenstein et al. 2005) is one of the most solid reasons to believe in collisionless dark matter.
Actually, the CDM paradigm has been tested on a great amount of observations and provides the basic framework to interpret the clustering properties of galaxies.

As a final remark, Fig. 1.1 presents the correlation function of matter evolved in the linear regime. The case in which $\delta \gg 1$ is much more complicated to deal with. In the mildly non-linear regime (i.e. $1 \lesssim \delta \lesssim 10$) some analytic approximations have been developed (Spherical Top-Hat collapse, Zel'dovich Approximation, Adhesion Model; a detailed description of these models can be found in Coles & Lucchin 1995 and Peacock 1999), while in the highly non-linear regime (i.e. $\delta \gtrsim 10$) the only way to follow the evolution of perturbations is by means of N-body simulations (see e.g. Peacock & Dodds 1996; Smith et al. 2003). A detailed analysis of the evolution of structure in this regime is out of the scope of this introduction as throughout this Thesis I will mainly concentrate on the distribution of galaxies on large scales where the linear theory holds.

1.2.4 Clustering of luminous matter

Equation (1.16) is used to define operatively the *spatial two-point correlation function* $\xi_g(r)$ for a given sample of galaxies. In practice, the number of galaxy-pairs is measured as a function of the separation r and then compared, by means of a suitable operator (see e.g. Landy & Szalay, 1993), to that inferred from a distribution of point-sources randomly placed within the same volume of space occupied by galaxies and according to the same selection effects.

The spatial correlation function has long been known to be extremely close to a single power-law (Totsuji & Khara 1969; Peebles 1974):

$$\xi(r) = \left(\frac{r}{r_0}\right)^{-\gamma} \tag{1.21}$$

at least in a limited range of scales, that is $1 \lesssim r \lesssim 10\ h^{-1}$ Mpc for galaxies (Guzzo 2000) and $5 \lesssim r \lesssim 35\ h^{-1}$ Mpc for clusters (Postman 1999), although very recent analyses of the two-point correlation function of galaxies in the local Universe, by taking advantage of larger samples of objects compared to those available up to few years ago, have detected small deviations from the power-law form (Zehavi et al. 2004, 2005; Abazajian et al. 2005; Phleps et al. 2006).

The values of both the slope γ and the *correlation length* r_0 show a dependence on galaxy mass, luminosity, color, morphology, gas content, star-formation activity, and on look-back time. Such dependencies reflect the relations between the formation histories of the extragalactic sources and their large-scale environment. As an example, bright elliptical galaxies selected in the 2dF Galaxy Redshift Survey (Norberg et al. 2002) display higher values of r_0 and of γ when compared to late-type galaxies. This can be naturally explained as a consequence of the well-known density-morphology relation (Dressler 1980): early-type galaxies are far more common than spirals in the central regions of rich clusters, whereas late-type galaxies are commonly found in less dense environments. Also, within the two subsamples of late-type galaxies and ellipticals, the values of the spatial correlation lengths are found to increase with luminosity, more luminous sources being more strongly clustered in space. The dependence of clustering on mass is clear from the comparison of the distribution properties of clusters and galaxies: the former population exhibit values of r_0 exceeding by more than a factor of 2-3 that of local normal galaxies.

The implications of such results are straightforward: luminous matter in general does not trace the distribution of the underlying dark matter otherwise all the cosmic objects should display the same clustering properties. It is thus correct to say that *galaxies are biased tracers of matter*. In order to account for this evidence, the spatial correlation

function of galaxies is commonly assumed to relate to $\xi_{\rm DM}$ via a *linear bias parameter*, b:

$$\xi_{\rm g}(r) = b^2 \xi_{\rm DM}(r). \tag{1.22}$$

Alternatively, a linear relation can be assumed between the density contrast of galaxies and that of dark matter:

$$\delta_{\rm g} = b\delta_{\rm DM}. \tag{1.23}$$

Note that the above definitions are not equivalent since equation (1.22) can be derived from equation (1.23) but the reverse is not true. In this thesis I will always make use of (1.22) in order to define the linear bias parameter. It is worth noticing that b could be also stochastic and non-linear (cf. e.g. Dekel & Lahav 1999; Somerville et al. 2001; Frith, Outram & Shanks 2005, and references therein), but throughout this work I will not consider these possibilities.

How the value of b depends on the intrinsic properties of galaxies and what are the mechanisms responsible for such a dependence are some of the most intriguing questions of modern cosmology.

A first fundamental contribution in this field was provided by Kaiser in 1984. In his work, Kaiser showed that the spatial correlation function of the highest density peaks of a Gaussian random field is much higher than that of the underlying Gaussian field; such a result was used to account for the measured strong clustering of rich Abell clusters. According to the same analysis, the different levels of bias inferred for different populations of sources could be accounted for by assuming that the formation of galaxies takes place in correspondence of matter density peaks whose amplitude varies from one population to another.

A more physically motivated analysis was subsequently proposed by Mo & White (1996) by investigating the density fluctuations of *dark matter halos*, which represent the virialized structures forming from the collapse of dark matter perturbations. It is commonly assumed that the collapse of perturbations occurs at the time in which the density contrast δ reaches a certain threshold δ_c. The latter quantity is estimated from the Top-Hat spherical

model by assuming that the spherical symmetry of the perturbation is preserved during the collapse. An overdense sphere is a very useful nonlinear model, as it behaves in exactly the same way as a closed sub-universe, so that its evolution is regulated by the same set of equations which describe the behavior of the scale factor. For a flat Universe filled only with matter the model gives $\delta_c \sim 1.68$. The spherical top-hat model gives also an estimate of the density inside the halo at the time of virialization which is approximatively $200\bar{\rho}$; such a value is used to define the virial radius that marks the boundary of the halo.

Mo & White have found that the density contrast of hales of mass M, which collapse at redshift z_f and are observed at redshift z (with $z < z_f$), relates to the density contrast of matter, $\delta_{\rm DM}$, in the following way

$$\begin{aligned} \delta_{halos}(M,z) &= b(M,z|z_f)\delta_{\rm DM}(z) \\ &= \left\{1 + \frac{D(z_f)}{\delta_c D(z)}\left[\frac{\delta_c^2}{\sigma^2(M)D^2(z_f)} - 1\right]\right\}\delta_{\rm DM}(z) \end{aligned} \tag{1.24}$$

where $\sigma(M)$ is the variance of the density field, calculated by filtering the field on a scale $R = (3M/4\pi\bar{\rho})^{1/3}$. If we define a characteristic mass, $M_\star$, by imposing $\sigma(M_\star, z_f) = \delta_c$, from equation (1.24) we see that holes of mass $M = M_\star(z_f)$ have $b = 1$ and therefore they trace the distribution of the underlying dark matter at any epoch, while those of mass $M > M_\star(z_f)$ are biased toward higher density regions so that, according to (1.22), they exhibit higher spatial clustering amplitudes when compared to that of the underlying dark matter, in agreement with what predicted by the simple model of Kaiser (1984).

Galaxies are supposed to form at the centers of dark hales due to the cooling and condensation of gas which fragments into stars once it becomes sufficiently dense. If the mass of the halo relates univocally to the observable properties of the galaxies (e.g. luminosity, star-formation activity etc.) than this could easily explain the dependence of clustering on such properties, at least on large scales ($r \gtrsim 1$ Mpc). On smaller scales, clustering is sensitive to the distribution of galaxies within their host hales, which is determined by more complicated physics acting on baryons such as gas-dynamics, radiative cooling and feedbacks (cf. e.g. Benson et al. 2000; Berlind et al. 2003). It can thus be stated that the cosmological model mainly influences the distribution of galaxies on large scales while the

"physics of galaxy formation" determines the clustering of galaxies on small scales.

According to all the above considerations we can state that the analysis of clustering is crucial for the following reasons:

- on *large scales*: it allows to get insights on the cosmic evolution of structures in the Universe by constraining, at each epoch, the typical mass of the halo in which galaxies reside. Moreover it provides independent estimates of the cosmological parameters once the relation between luminous and dark matter, encoded in the bias parameter, is reasonably constrained;
- on *small scales*: it can be used to get insights on the physical processes at work in the formation of galaxies.

In this thesis I will mainly deal with clustering of galaxies on large scales by focusing on high-redshift sources selected at the sub-mm and radio wavebands.

1.3 The submillimetre view of the Universe

A major part of this thesis will be devoted to the class of sources detected, in the last decade, with the Submillimetre Common-User Bolometer Array (SCUBA) camera at the James Clerk Maxwell Telescope (JCMT) (Holland et al. 1999), operating in the atmospheric windows at 450 and 850 μm. The existence of tens of bright sub-mm sources in the sub-degree areas observed with SCUBA have proved to be a challenge for current theories of galaxy formation and have deserved a revision of the processes at work in the baryonic matter component during the formation of structure in the high redshift Universe. In this context, clustering measurements contribute to unveil the real nature of SCUBA-selected galaxies by putting them within a coherent picture for the formation and evolution of galaxies.

About 99 per cent of the energy released by galaxies in the submm and far-IR wavebands is produced by thermal emission from dust grains, the remaining 1 per cent coming from fine-

structure atomic and molecular rotational line emission. The source of energy which powers this emission by heating dust is often unclear, since any intense source of optical/ultraviolet (UV) radiation, such as *young high-mass stars* or *accretion disk surrounding an Active Galactic Nucleus (AGN)*, can produce the desired effect.

The basic parameters necessary to describe emission from dust grains are the temperature T_d and the slope, β, of the emissivity function $\epsilon_\nu \propto \nu^\beta$. The submillimetre emission from distant galaxies is simply modeled as a modified black-body:

$$S_\nu \propto \nu^\beta B(\nu, T_d) = \frac{2h}{c^2} \frac{\nu^{\beta+3}}{e^{h\nu/kT_d} - 1}, \tag{1.25}$$

where $B(\nu, T_d)$ is the Planck function. Values of β in the range 1-2 are usually assumed. Theory predicts $\beta \to 2$ at low frequencies, while the value $\beta \sim 1$ at high frequencies matches the general trend for the interstellar extinction curve that describes the properties of absorption of optical and UV radiation by the Inter Stellar Medium (ISM) (see e.g. Calzetti et al. 2000; Franceschini 2002 for a review).

Note that $S_\nu \propto \nu^{2+\beta}$ in the Rayleigh-Jeans limit (i.e. for $\nu \ll kT_d/h$); this is the key feature that favour the detectability of high-z galaxies at submm-wavelength. In fact, the rapid increase of flux at shorter wavelengths compensate for its decrease due to the effect of distance and the expansion of the Universe. This is clearly illustrated in the right-hand panel of Fig. 1.2 (see also Blain & Longair 1993, their Fig. 2) where I show, as a function of redshift z, and for three wavelengths of observations, 450, 850 and 1100μm, the flux density of a source having a far-infrared SED described by the modified black-body with $T_d = 38$ K, $\beta = 1.5$, and normalized to give a total infrared luminosity[2] $L_{\rm IR} = 5 \times 10^{12}$ L$_\odot$. The values of the parameters adopted here are those typical of Luminous Infrared Galaxies (see next section). For completeness, the SED model, as a function of rest-frame frequency ν, is illustrated in the left-hand panel of the same figure. A standard cosmological model is assumed to convert luminosities into the corresponding flux densities.

[2]By convention, the infrared luminosity corresponds to the energy output in the wavelength interval 8-1000μm.

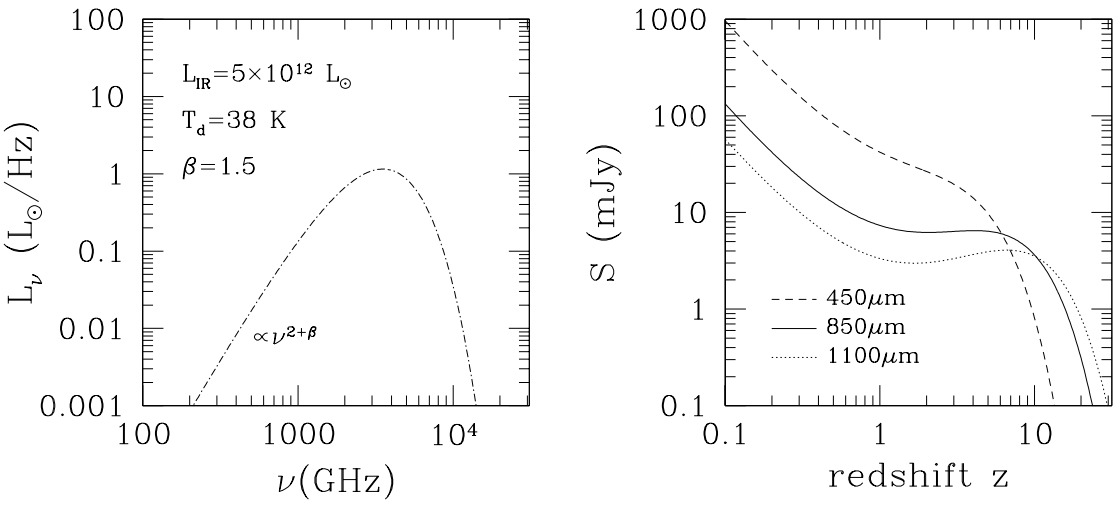

Figure 1.2: *Left-hand panel*: modified black-body spectrum as a function of frequency ν, obtained for a dust temperature $T_d = 38$K, a spectral emissivity $\beta = 1.5$ and a total infrared luminoosity $L_{\rm IR} = 5 \times 10^{12}$ L$_\odot$. *Right-hand panel*: flux density as a function of redshift z, derived from the SED model illustrated in the left-hand panel.

1.3.1 Dust emission in the Universe

The first systematic investigation of dust emission in the Universe was conduced by the InfraRed Astronomical Satellite (IRAS, launched in 1983) which performed the first census of the infrared emission of low redshift ($z \lesssim 0.3$) galaxies in the wavelength range 12-100 μm. Most of the galaxies detected by IRAS are typical spiral galaxies, with relatively low far-IR luminosities (several 10^{10} L$_\odot$); the dust emission in these sources is significantly extended (on the same scale as the 10-kpc stellar disk) and is associated with molecular gas-rich star-forming regions distributed throughout the galaxy (Regan et al. 2001), in which dust is heated by the hot, young OB stars.

IRAS also discovered the high luminosity tail of IR-luminous galaxies (e.g. Sanders & Mirabel 1996). These sources comprise the so-called Luminous Infrared Galaxies (LIRGs) and Ultra Luminous Infrared Galaxies (ULIRGs) which exibit infrared luminosities respectively in the range $10^{11} \lesssim L_{\rm IR} \lesssim 10^{12}$ L$_\odot$ and $L_{\rm IR} \gtrsim 10^{13}$ L$_\odot$. Locally, both LIRGs and ULIRGs are often associated with interacting or merging gas-rich disks, with the fraction

of strongly interacting/merging systems increasing from $\sim$ 10% at $L \sim 10^{10.5-11}$ $L_\odot$ to $\sim$ 100% at $L \gtrsim 10^{12}$ $L_\odot$.

In LIRGs most of the luminosity comes from intense knots of star-formation activity (about 10-100 $M_\odot$ yr^{-1}) which occur in the deeply dust-enshrouded overlapping portion of the interacting galaxies. The ULIRGs phase seems to occur near the end of the merging process when the two disks overlap. However, the nature of the dominant source of emission in such sources, i.e. starburst or dust-enshrouded AGNs, remained unknwon since the advent of Infrared Space Observatory (ISO; Kessler et al. 1996) which performed higher-resolution observations in the mid-IR (2.5-17 μm), where the differences between the SED of starbursts and that of AGN-powered sources are noticeable[3]. ISO has shown that most of the energy from low-redshift ULIRGs is likely generated by star-formation activity rather than AGN accretion. However the fraction of ULIRGs containing AGNs appears to increase at the highest luminosities (Sanders 1999).

The ULIRGs detected by IRAS are generally at low redshift and they do not dominate the local budget of the energy production. As an example, the total infrared luminosity contributed by these galaxies in the IRAS Bright Galaxy Sample (Soifer et al. 1989) accounts for only $\sim$ 6% of the whole infrared emission in the local Universe (Soifer & Neugebauer 1991). Even if interesting objects, these galaxies were believed to be perhaps no more than a local oddity.

It was with the advent of the Cosmic Background Explorere (COBE) satellite that the existence of a significant population of IR-luminous galaxies at high redshift, was thrown to the fore of astronomical debate. In fact, COBE clearly detected the presence of a Far-InfraRed Background (FIRB hereafter) at 140 μm and 240 μm (Puget et al. 1996; Schlegel, Finkbeiner & Davis 1998; Hauser et al. 1998; Fixen et al. 1998). The intensity of the FIRB was surprisingly high, comparable to, or even exceeding, the integrated optical emission from galaxies in the Hubble Deep Field (Hauser et al. 1998). When compared to the cosmic hystory of star-formation derived from optical and UV surveys (Madau et al. 1996)

[3]Starbursts are often characterized by strong, low-excitation, fine-structure lines, prominent Polycyclic Aromatic Hydrocarbon (PAH) features, and a weak $\lambda \geq 10\mu$m continuum, whereas AGNs display a highly excited emission line spectrum with weak or no PAH features, plus a strong mid-IR continuum.

a serious discrepancy become apparent; the CIB detected by COBE required at least a factor two more star-formation than was inferred from in optical and UV surveys, meaning that the integrated star-formation rate at $z \gtrsim 1$ had to be higher than that implied from UV/optical observations by a comparable factor. Furthermore, this star-formation had to be happening in an environment largely surrounded by dust.

The first major step in resolving the CIB came again form the extragalactic surveys carried out by ISO at 7μm and 15μm with ISOCAM, and at 90μm and 170μm with ISOPHOT (see e.g. Genzel & Cesarsky 2000). The picture that emerged from ISO was that very IR-luminous galaxies become substantially more numerous with increasing redshift, making LIRGs and ULIRGs at $z \sim 1$ a cosmologically significant population. While the $0.5 < z < 1.0$ LIRG population seems to be quite similar to LIRGs at lower redshift, ISO also revealed a class of moderate redshift LIRGs with relatively cool dust emission. Furthermore, the high redshift ($z > 0.5 - 1$) ULIRG population is found to exibit a more prevalent level of AGN activity than that found in their local counterparts, although, this result could be either due to luminosity or redshift effects since the most luminous sources are found at higher redshifts.

Though ISO had proved itself remarkably adept at resolving much of the CIB, there remained a significant shortfall between the CIB as measured by COBE and the sources detected by ISO. In fact, the background level at $\lambda > 200\mu$m as determined by FIRAS implied a population of colder sources (i.e. peaking at relatively higher wavelengths), probably $z \gtrsim 1$ systems with IR emission redshifted to longer wavelengths than the objects detected in shallower, $\lambda < 200\mu$m, ISO surveys.

1.3.2 SCUBA-selected galaxies

By operating at substantially longer wavelengths than ISO, namely 850μm and 450μm, SCUBA had the sensitivity to detect these distant cold ULIRGs. SCUBA provided a dramatic leap forward from the pre-existing single-pixel or one-dimensional array instruments. The combination of field of view and sensitivity was sufficient to enable the first

searches for submm-wave emission from previously unknown distant galaxies.

The surveys performed with SCUBA (see next chapter) found a huge population of sub-mm bright (i.e. $S_{850\mu m} \gtrsim 2$ mJy), optically faint sources (Blain et al. 2002, and references therein). Taken together, the sources found in the various sub-mm surveys can explain for around 50% of the CIB detected by FIRAS and, with a resonable extrapolation level, can also account for all of it (Borys et al. 2003). Redshift estimates obtained for a subsample of ~ 70 sub-mm galaxies have shown that they lie at redshifts out to $z = 3.6$, with a median redshift of 2.2 (Chapman et al. 2005). This implies that sub-mm sources are likely to be extremely luminous ULIRGs, with star-formation rates substantially exceeding 1000 $M_\odot$ yr^{-1}. The estimated source counts reveal that the space density of ULIRGs at $z > 1$ was more than 2 orders of magnitude higher than that of their local counterparts confirming that a strong evolution characterizes this population of sources.

One attractive interpretation of the submillimetre galaxy population is that these violent star-forming galaxies represent the progenitors of present-day massive ellipticals (Hughes et al. 1998; Scott et al. 2002) whose properties indicate that the bulk of their star formation activity occurred at high redshift ($z \gtrsim 1$) and in a relatively short time (Thomas, Maraston & Bender 2002; Romano et al. 2002); some pieces of evidence in support of this evolutionary link are sumarized below:

- SCUBA galaxies are located at high redshift (Chapman et al. 2005);
- the star formation rates inferred from the submm flux densities are sufficient to construct the stellar population of even the most massive ellipticals in $\lesssim 1$ Gyr;
- the K-band morphologies of submm-selected galaxies resemble those of radio galaxies, which locally show elliptical morphologies (Lutz et al. 2001);
- the comoving number densities of bright submm sources ($S_{850\mu m} \gtrsim 8$mJy) in the redshift interval $z \sim 2-3$ is comparable to the present-day number density of bright $L \gtrsim 2-3$ $L^\star$ ellipticals (Scott et al. 2002, Borys et al. 2003).

However, while the high star formation rates inferred for submm galaxies is consistent

with the picture of them being protoellipticals, on the other hand they do not provide unambiguous evidence for this conclusion. This is both because the duration of the starburst phase is unknown and because the derived star formation rate is very sensitive to the assumed temperature and Initial Mass Function (IMF) (Larson 1998; Baugh et al. 2005).

Measurements of the clustering properties of bright submm galaxies offer a very powerful tool to unveil the real nature of the submm population and therefore to confirm or reject the evolutionary link between this class of sources and the population of bright ellipticals. In fact, if SCUBA galaxies are protospheroids observed during their major episode of star formation then we expect them to trace the same large scale structure of massive ellipticals which are known to reside in dense environments and to display strong spatial clustering. It follows that submm galaxies should also be associated to the highest density peaks in the matter distribution and their positions in sky should be strongly correlated. Such an hypothesis seems to be supported by the first tentative measurements of the spatial correlation function of bright submm galaxies (Blain et al. 2004, and references therein) (see also next chapter) and by the detection of SCUBA galaxies in overdense regions set at high redshift around bright radio galaxies and QSO; sites which probably identify distant proto-clusters (Chapman et al. 2001; De Breuck et al. 2004; Stevens et al. 2004).

1.3.3 Hints on clustering from the unresolved background

The available samples of SCUBA-selected galaxies comprise only few tens of sources distributed over sparse sub-degree areas of the sky (see next chapter). It is thus clear that a definitive result on the clustering of submm galaxies awaits a much larger sample of objects. However, a powerful complement to direct identifications of the individual sources (by means of high resolution observations) is that of studing the statistical properties of the FIRB light contributed by *unresolved* extragalactic sources. The large scale structure of galaxies can produce correlated anisotropies in the FIRB and indeed, indications of correlated brightness fluctuations on the angular scales expected from faint unresolved dusty galaxies have been claimed in the 850-μm SCUBA image of the *Hubble Deep Field* North (Peacock et al. 2000) in deep 175-μm ISO images (Lagache & Puget, 2000; Kiss et al. 2001)

and, more recently, on 160-μm Spitzer map (Grossan & Smoot 2006).

Scott & White (1999) worked out preliminary estimates of the angular correlation function of the FIRB at 850 μm by assuming that the infrared sources have clustering properties like that of $z \sim 3$ Lyman-Break galaxies (LBGs; Giavalisco et al. 1998). Althought they viewed the FIRB as a contaminant of the CMB data (and were therefore interested in a rough estimate of what these correlations might possibly be) their results enphasized that the intensity fluctuations owing to clustering could be larger than the primary anisotropy signal on scales smaller than about 10 arcmin and will be detectable with the High Frequency Instrument (HFI) of the upcoming ESA/Planck satellite (Lamarre et al. 2003).

Haiman & Knox (2000) and Knox et al. (2001) have subsequently improved the work of Scott & White by discussing in more detail the measurements of the correlation of unresolved submm galaxies on arcminute angular scales in the context of CMB experiments. They concluded that the correlated signal can carry important information about the nature and evolution of the submm galaxy population. Subsequent works by Magliocchetti et al. (2001) and Perrotta et al. (2003) have reached similar conclusions by using a more physically grounded model for SCUBA-like galaxies (Granato et al. 2001) and performing accurate predictions for Planck/HFI. They found that the signal due to clustering of unresolved SCUBA-like galaxies will be detectable in the shorter-wavelength channels of HFI if the analysis is restricted to low-dust regions (e.g. to high enough Galactic latitude regions). This means that crucial information on the clustering properties of faint sub-mm/far-infrared galaxies (and hence on physical properties such as their mass and/or the amount of baryons involved in the star-formation process) will reside in the Planck maps, at least at frequencies greater than 353 GHz.

On the line traced by the cited works, in this thesis I will address the issue of the large scale clustering of SCUBA-like galaxies by taking into exam a number of effects arising from the correlation of the *background* source population. Submm galaxies will be treated within the recently proposed model of Granato et al. (2004) which succesfully reproduces the observed counts and redshift distribution of SCUBA sources.

The first step I will take is that of exploiting the result by Peacock et al. (2000) concerning the angular clustering of the unresolved sources at 850μm, to derive constraints on the correlation length of SCUBA galaxies and on the typical mass of the halo in which these sources reside. Armed with these constraints I will address the effect of clustering in increasing the source confusion for sub-mm/far-IR observations. Source confusion set a potential limitation to any astronomical observation (see e.g. Scheuer 1957, 1974; Condon 1974): for any finite-resolution observations, sources sufficiently close to one another on the sky will seem to overlap, or "confuse" one another, and such a confusion limits the accuracy to which the flux and position of individual sources can be measured, hence being a source of noise for the observation. This limitation is particularly acute in the sub-mm/far-IR wavebands, since the longer wavelengths (relative to optical), combined with the necessity for space-based instrumentation (with the implied smaller telescope aperture) tend to lead to relatively poor resolution, relative to that of ground-based optical observations. By improving the probability of having close pairs of sources falling within the telescope-beam, clustering contributes to enhance the effect of confusion. Therefore it is crucial to account also for the contribution of clustering when dealing with confusion in current and next generation of far-infrared surveys which aim at resolving the FIRB.

I will then focus on the effect that the clustering of unresolved sources have on the estimates of the extragalactic source counts when the latter are collected by means of low-resolution instruments. In fact, in low-resolution surveys, what is measured is the summed contribution of clustered sources falling within the resolution element of the telescope. The counts of bright intensity peaks are therefore shifted to higher flux levels compared with the counts of individual sources detected with high-resolution instruments. The effect is particularly relevant for sources which strongly cluster in space as it is expected for SCUBA-selected galaxies. I will address this issue by providing an accurate formalism to deal with it and will show how such effect, instead of being seen exclusively as a problem, can be exploited in the sub-mm waveband to detect high redshift proto-clusters, whose statistical properties are very useful to test theories of structure formation.

Finally, it is interesting to note that different experiments, performed in the last year with the Berkeley-Illinois-Maryland Association Array (BIMA: Dawson et al. 2002),

the Cosmic Background Imager (CBI: Mason et al. 2003; Readhead et al. 2004) and the Arcminute Cosmology Bolometer Array Receiver (ACBAR: Kuo et al. 2004), and aimed at measuring the anisotropies of the CMB, have detected, on angular scales below few arcminutes, a signal in excess of the expected primordial CMB anisotropies. The origin of this signal will be addressed in this work by taking into account the contribution from both faint radio sources and submm galaxies and by including the clustering contribution from the latter population.

1.4 The radio view of the Universe

The other population on which this thesis focuses is that of extragalactic radio sources. Although representing only a small fraction of all galaxies, radio sources provide a significant sample for clustering studies. In fact, since radio emission is unaffected by dust extinction and the sources detected in this waveband lie at relatively high redshift ($\langle z \rangle \sim 1$), radio surveys can cover very large areas of the sky and sample very large volumes thus probing the structure of the Universe up to several hundreds of Mpc.

1.4.1 Radio emission from extragalactic sources

The primary emission mechanism in virtually all radio sources is *synchrotron emission* from relativistic electrons spiralling around the magnetic fields within the host galaxy. In most of radio sources, the spectrum of the synchrotron emission is well approximated by a power-law, $S_\nu \propto \nu^\alpha$. For many, but not all, radio sources, $-1.0 \lesssim \alpha \lesssim -0.5$ and they are said to have a *steep spectrum*; sources with $\alpha > -0.5$ are referred to as *flat spectrum* sources, and those rare sources with $\alpha > 0$ are referred to as *inverted spectrum* sources.

However, departures from simple power laws with fixed α are frequently observed. This can be determined on one hand by *electron aging*: the higher the energy of an electron, the shorter it takes to radiate a given fraction of that energy. Since high frequency synchrotron emission is dominated by high energy electrons, the effect of aging is to steepen the radio spectrum at high frequencies. Another cause of curvature in the SED of radio sources is *opacity*: as the optical depth rises, the source spectra invert, with $2 \lesssim \alpha \lesssim 2.5$

for fully opaque sources. The result is a peak in the SED at a frequency that is higher for increasing values of both the optical depth and the magnetic field.

The radio emission can be related either to ongoing star forming processes or to the accretion activity onto supermassive black hole within the galaxy.

In "normal" star-forming galaxies (i.e. those with no evident energetic contribution from a central supermassive black hole) the remnants of Type II and Type Ib supernovae, originating from stars more massive than ~ 8 $M_{\odot}$, are thought to accelerate most of the relativistic electrons. Furthermore, massive stars ionize the HII regions and free-free emissions from such regions is also observed in the radio spectra of star-forming galaxies. In these sources the free-free spectrum is in general flat ($\alpha \sim -0.1$) while the synchrotron spectrum is steep ($\alpha \sim -0.8$) and dominates the radio output below 30 GHz. The radio continuum from a typical starburst galaxy accounts for only a tiny fraction of its bolometric luminosity; therefore, in large-scale radio surveys like the NVSS and the Faint Images Radio Sky Survey at Twenty centimeters (FIRST; Becker, White & Helfand 1995), which reach fluxes of few mJy (at 1.4 GHz), the bulk of the radio population is provided essentially by radio-loud galaxies hosting an AGN.

1.4.2 Radio-loud AGNs

AGNs are believed to be powered by gravitational energy coming from a massive black hole sitting in the center of the galaxy.

Expecially at low frequencies (i.e. a few hundred MHz) the radio emission comes from pairs of extremely large lobes set on opposite sides of the host galaxy. These lobes are often several hundred kiloparsec in length and can be separated from the galaxy by a similar distance. Elongated structures, colled *jets*, are also present, connecting the central galaxy to the side lobes. Fanaroff & Riley (1974) have organized these extended radio galaxies into two main classes according to the their radio morphology:

- *Fanaroff-Riley type-I (FRI)*: the lobes are brightnest near the galaxy and grow dimmer as one looks farther away; the jet can be seen on both sides of the central galaxy and

exibits often a turbulent structure;

- *Fanaroff-Riley type-II (FRII)*: the lobes are edge-brightened and have very bright, very small hot spots near the outer surface of the lobes. The jet is usually very narrow and well aligned with the outer structure but its emission is relatively weak compared to the lobes and is virtually only on one side.

It is plausible that the different shape observed for jets and lobes in FRI and FRII galaxies is due to the way in which the jet penetrates the intergalactic medium (IGM): in FRI, jets dissipate their kinetic energy by entering the IGM whereas in FRII they mantein their integrity until they impact on the IGM in a shock.

Interestingly, the morphological differences between FRI and FRII also seem to mirror their radio power properties: at low luminosities, $P_{178MHz} \lesssim 10^{24}\ h^{-2}$ W Hz^{-1} sr^{-1}, the vast majority of radio sources have an FRI radio structure, while at higher luminosities, $P_{178MHz} \gtrsim 10^{24}\ h^{-2}$ W Hz^{-1} sr^{-1}, the majority of radio galaxies have FRII radio structure.

There are other classes of radio-loud objects in which, especially at higher frequencies (i.e. several GHz), the region responsible for the bulk of the radio emission is unresolved even on arcsecond angular scales and the radio emission is essentially core-dominated. The populations of *radio-loud quasars* and of *BL Lac objects* belong to this class of compact objects.

The division between lobe- and core-dominated radio galaxies correlates with the spectrum. When the flux is dominated by extended lobes, the spectrum is usually fairly well described by a power-law with spectral index $-1 \lesssim \alpha \lesssim -0.5$. On the other hand, most core-dominated sources have spectra that are more nearly flat ($S_\nu \sim constant$). This is interpreted as due to the presence of separate optically thick regions within the emitting source: those of progressively greater optical depth and magnetic field are responsable for the production of the higher frequency portions of the spectrum and their combination results in a spectrum that is approximately flat.

1.4.3 The environment dependence of radio activity

The mechanism of ignition of radio activity in AGNs is still almost unknown. Recent studies of the environment dependence of the AGN fraction (Best 2004 and references therein), have suggested that the radio-emission in AGN-powered galaxies is connected to the large scale environment (group, cluster, etc.) of the radio source, with much less dependence on its local environment (i.e. the local galaxy surface density). Interestingly radio-loud AGNs are often found to be hosted by large ellipticals which are are known to inhabit density-enhanced regions (Prestage & Peacock 1989; Hill & Lilly 1991; Zirbel 1996a, 1996b, 1997). However, radio-loud AGNs do not simply trace the distribution of elliptical galaxies which, indeed, seem to be sampled by optically bright AGNs (i.e. quasars; see Magliocchetti 2006 and refernces therein). In fact, AGNs which show enhanced radio emission are found to be associated - at least in the local Universe - with structures which are about an order of magnitude more massive than those that host radio-quiet AGNs and quasars (Peacock & Nicholson 1991; Magliocchetti et al. 2004). This evidence points to the conclusion that the presence of a supermassive black hole and the availability of cold gas that fuels the black hole, although essential, are not sufficient conditions for the ignition of AGN radio-activity.

The observed enviroment dependence of radio-loud AGNs fraction strongly supports the argument that galaxy interactions or mergers may provide the mechanism for the ignition of the radio activity. However it is worth noticing that this hint comes from analysis performed at low redshift (i.e. $z \lesssim 0.3$) by combining the local 2dF Galaxy Redshift Survey with large radio surveys, although the bulk of the population of radio-loud AGNs lies at $z \sim 1$ (see e.g. Dunlop & Peacock 1990).

In order to investigate the typical environment and/or halo mass of radio-loud AGNs at high redshift, a powerful tool is offered by the analysis of the angular clustering of radio sources in the available 2D large-scale surveys. Therefore, in chapter 6 I will exploit the clustering estimates obtained form the NRAO VLA Sky Survey (NVSS; Condon et al. 1998) - the largest existing radio survey - with the aim of constraining the typical mass of the

halo in which AGN-powered radio galaxies reside, and its cosmic evolution.

1.5 Plan of the Thesis

The work is organized as follows:

- In chapter 2 I briefly discuss the tentative measurements of clustering of SCUBA galaxies (and of powerful infrared sources in general). I then introduce the physical model of Granato et al. (2004) adopted here to deal with SCUBA-like sources and propose two simple models for their spatial clustering. By normalizing these models to reproduce the 850μm background source fluctuations I will derive information about the typical mass of the halo in which SCUBA galaxies reside.

- Chapter 3 presents detailed predictions for the confusion noise due to extragalactic sources in the far-IR/(sub)-millimeter channels of ESA/ISO, NASA/Spitzer, ESA/Herschel and ESA/Planck satellites. Such predictions also include the contribution from clustering of unresolved SCUBA sources.

- In chapter 4 I investigate the effect of clustering on source count estimates obtained with low resolution instruments. A suitable model to deal with such an effect is proposed. I also present some applications to the 850μm-channel of Planck/HFI and compare predictions with the output of numerical simulations.

- Chapter 5 quantifies the extragalactic source contribution to arcminute-scale CMB fluctuations as measured by CBI, BIMA, and ACBAR experiments, including the effect from clustering of SCUBA-like galaxies.

- In chapter 6 I analyse the angular clustering of radio sources with $S_{1.4\mathrm{GHz}} > 10$ mJy on large angular scales (up to 10°), a regime that has not been extensively investigated up to now. I derive information on the cosmic evolution of radio AGNs and the typical mass of the dark matter haloes in which they reside. The dependence of theoretical predictions on the adopted cosmological framework is also taken into account.

- Finally, chapter 7 summarizes the results obtained in this work.

Chapter 2

Clustering of SCUBA galaxies

2.1 Introduction

Both theoretical arguments and observational hints support the idea that SCUBA-selected galaxies strongly correlate in space, although an unambiguous detection of the clustering signal associated to this class of objects has not been obtained yet. This is mainly due to the small number statistic provided by the existing sub-degree samples which contain only few tens of sources. Moreover, it is worth noticing that SCUBA-selected galaxies are typically very faint in the optical waveband so that obtaining an estimate of redshift (and therefore of distance) for these objects is not an easy task. When information on redshift is not accessible, the clustering analysis is inevitably restricted to the 2-D distribution of the sources onto the sky. However, SCUBA galaxies are spread over a wide redshift range (because of the strong negative K-correction, as discussed in the previous chapter) so that their spatial clustering signal is strongly diluted when projected onto the sky.

Since SCUBA surveys have resolved only a fraction of the 850μm background, important complementary information is provided by the analysis of the background intensity fluctuations. Such analysis is important also with reference to the studies of anisotropies of the Cosmic Microwave Background since the expected high spatial clustering of SCUBA-like galaxies should significantly contribute to background fluctuations on arcminute scales, as

pointed out by some theoretical works (see Scott & White 1999, Magliocchetti et al. 2001, Perrotta et al. 2003).

Peacock et al. (2000) have analyzed the contribution of clustering of unresolved ($S < 2$ mJy) SCUBA sources to the 850μm background fluctuations detected in the *Hubble Deep Field* North and have found some hints of a positive clustering of the background source populations. In this chapter I will exploit the result of Peacock et al. to derive constraints on the spatial correlation length of SCUBA galaxies and on the typical mass of the dark matter halo in which they reside. Sub-millimeter galaxies will be treated within the physically grounded model of Granato et al. (2004) which accounts for the observed counts and redshift distribution of the sources.

Section 2.2 provides the basic formalism needed to relate the clustering properties of extra-galactic sources in 2-D and 3-D spaces; in the same Section I further discuss the tentative measurements of the clustering of SCUBA-selected galaxies in the existing sub-degree samples. Section 2.3 presents the evolutionary model proposed by Granato et al. (2004). In Section 2.4 I perform a theoretical analysis of the result by Peacock et al. (2000). Conclusions are summarized in Section 2.5.

2.2 Clustering of submillimeter-selected galaxies

2.2.1 Two-point angular correlation function: formalism

The clustering properties of a 2-D distribution of sources can be quantified by means of the two-point *angular* correlation function, $w(\theta)$.

In analogy to the spatial two-point correlation function, ξ, the angular one measures the excess probability of finding pairs of objects at angular separation θ with respect to a random distribution of objects:

$$\delta P_{12}(\theta) = n_{\Omega}^2[1 + w(\theta)]\delta\Omega_1\delta\Omega_2 \tag{2.1}$$

where n_{Ω} is the mean surface density of the sources while $d\Omega_1$ and $d\Omega_2$ are the solid angle elements containing the objects.

The functions, $\xi(r)$ and $w(\theta)$ are not independent. In fact the latter can be obtained by projecting the former along the line of sight of the observer, and weighting the contribution from the redshift z by the corresponding number density of the sources, $\mathcal{N}(z)$, at that redshift:

$$w(\theta) = \int_{z_{\min}}^{z_{\max}} dz_1 \mathcal{N}(z_1) \int_{z_{\min}}^{z_{\max}} dz_2 \mathcal{N}(z_2) \xi[r(z_1, z_2, \theta)] \times \left[\int_{z_{\min}}^{z_{\max}} dz \mathcal{N}(z) \right]^{-2} . \quad (2.2)$$

Note that this expression implicitly assumes that the intrinsic luminosity of a galaxy is statistically independent of its position relative to other galaxies (*Limber hypothesis*; Limber 1953) so that ξ is just a function of the separation r between the sources and not of their luminosities.

In equation (2.2) r represents the comoving spatial distance between two sources located at redshifts z_1 and z_2 and separated by an angle θ on the sky. For $r \ll r_H(z)$, $r_H(z)$ being the Hubble scale at the relevant redshift (see chapter 1), and for the case of a flat Universe, r can be approximated by

$$r^2 = r_c^2(z_1) + r_c^2(z_2) - 2 r_c(z_1) r_c(z_2) \cos\theta, \quad (2.3)$$

where $r_c(z)$ is the *line-of-sight comoving distance* of a source located at redshift z. Again, for a flat cosmic geometry, one has

$$r_c(z) = \int_0^z \frac{c}{H_0 E(z')} dz'; \quad (2.4)$$

with

$$E(z) = \sqrt{\Omega_{0,m}(1+z)^3 + \Omega_{0,\Lambda}} . \quad (2.5)$$

The function $E(z)$ just describes the time evolution of the Hubble parameter, $H(z) = H_0 E(z)$.

A simplified version of equation (2.2) can be derived in the small angle approximation ($\theta \ll 1$ rad) by setting $\delta z = z_2 - z_1$ and assuming that clustering is appreciable only among sources characterized by a redshift separation $\delta z \ll 1$, which is equivalent to postulate that the scale of appreciable clustering is much smaller than the Hubble scale $r_H(z)$:

$$w(\theta) = \int_{z_{\min}}^{z_{\max}} dz \mathcal{N}^2(z) \int_{z_{\min}-z}^{z_{\max}-z} d(\delta z) \xi[r(\delta z, \theta), z] \times \left[\int_{z_{\min}}^{z_{\max}} dz \mathcal{N}(z) \right]^{-2} \quad (2.6)$$

with

$$r^2 = \left[\frac{c}{H(z)}\right]^2 \delta z^2 + [r_c(z)\theta]^2. \tag{2.7}$$

Equation (2.6) - commonly known as Limber (1953) equation - is used to derive constraints on the spatial clustering of the sources under exam once their angular correlation function is measured and a suitable model for their redshift distribution is available.

When dealing with an unresolved background of extragalactic sources with flux below the detection limit S_d, it is possible to define an autocorrelation function, $C(\theta_\star, S_d)$, of the flux fluctuations, δS, due to the unresolved source population, as a function of the angular separation $\theta_\star$ between two directions of observations defined by the vectors $\mathbf{r_1}$ and $\mathbf{r_2}$ (see De Zotti et al. 1996):

$$\begin{aligned} C(\theta_\star, S_d) &= \langle \delta S(\mathbf{r_1}, S_d) \delta S(\mathbf{r_2}, S_d) \rangle \\ &= \int\int_{\mathcal{Z}} dz_1 dz_2 \int\int_{\mathcal{L}} dL_1 dL_2 \frac{L_1 K(z_1)}{4\pi d_L^2(z_1)} \frac{L_2 K(z_2)}{4\pi d_L^2(z_2)} \\ &\quad \times \int\int_{\rm beam} d\Omega_1 d\Omega_2 \langle \delta\mathcal{N}(L_1, \mathbf{r_1}) \delta\mathcal{N}(L_2, \mathbf{r_2}) \rangle f(\theta_1, \phi_1) f(\theta_2, \phi_2) \ . \end{aligned} \tag{2.8}$$

In this expression, $\delta\mathcal{N}(L, \mathbf{r})$ represents the fluctuation around the mean number $\mathcal{N}(L, z)$ of sources with luminosity L and redshift z and writes:

$$\mathcal{N}(L, z) \equiv \frac{dV}{dz d\Omega}(z) \Phi(L, z) \ . \tag{2.9}$$

where Φ is the luminosity function of the objects and $dV/dzd\Omega$ is the comoving volume element, defined as

$$\frac{dV}{dz d\Omega} = \frac{c}{H_0} \frac{d_L^2(z)}{E(z)(1+z)^2} \ , \tag{2.10}$$

$d_L(z)$ being the luminosity distance at redshift z.

In equation (2.8), integration in the angular variables is made within the dimension of the telescope beam; $f(\theta, \phi)$ is the response function of the detector and the angles (θ_1, ϕ_1) and (θ_2, ϕ_2) are meant to be measured from the axes $\mathbf{r_1}$ and $\mathbf{r_2}$, respectively. In the same equation, $K(z) = (1+z)L[\nu(1+z)]/L[\nu]$ is the $k-$correction for monochromatic observations at frequency ν; integration in redshift is performed within the interval $\mathcal{Z} = [z_{\rm min}, z_{\rm max}]$, where

the sources are expected to exist, while the integration in luminosity runs over the interval $\mathcal{L} = [L_{\rm min}, \min[L_{\rm max}, L(S_d, z)]]$, where $L_{\rm max}$ and $L_{\rm min}$ are the maximum and minimum intrinsic luminosities of the sources, and $L(S_d, z)$ is the luminosity corresponding to the flux density S_d at the redshift z, i.e. $L(S_d, z) = S_d 4\pi d_L^2(z)/K(z)$.

If the luminosities of the sources are statistically independent of their positions, one gets:

$$\begin{aligned}\langle \delta\mathcal{N}(L_1, \mathbf{r_1}) \delta\mathcal{N}(L_2, \mathbf{r_2}) \rangle &= \mathcal{N}(L_1, z_1) \delta^D(\mathbf{r_2} - \mathbf{r_1}) \delta^D(L_2 - L_1) \\ &\quad + \mathcal{N}(L_1, z_1) \mathcal{N}(L_2, z_2) \xi(|\mathbf{r_2} - \mathbf{r_1}|, z) \ , \end{aligned} \tag{2.11}$$

δ^D being the Dirac function. The first term on the right-hand side corresponds to a Poisson distribution of point sources, while the second one is due to clustering with a two-point spatial correlation function ξ.

For values of $\theta_\star$ much greater than the dimension of the telescope beam [which implies $\theta_\star \gg \theta_1, \theta_2$ in equation (2.8)] the autocorrelation function of background fluctuations can be written as follows:

$$C(\theta_\star, S_d) = \int_{\mathcal{Z}} dz_1 I(z_1, S_d) \int_{\mathcal{Z}} dz_2 I(z_2, S_d) \xi(z_1, z_2, \theta_\star) \times \left[\int_{\rm beam} d\Omega f(\theta, \phi) \right]^2 \tag{2.12}$$

where $I(z, S_d)$ is the intensity of the radiation emitted, per unit interval in redshift, by sources below the flux threshold S_d:

$$I(z, S_d) = \frac{1}{4\pi} \frac{c}{H(z)} \frac{j_{\rm eff}(z, S_d)}{(1+z)^2}, \tag{2.13}$$

and $j_{\rm eff}$ is the effective comoving volume emissivity at redshift z contributed by same objects:

$$j_{\rm eff}(z, S) = \int_{\mathcal{L}} dL K(z) L \Phi(L, z). \tag{2.14}$$

Starting from equation (2.12), it is possible to define the angular two-point correlation function of the background source population in analogy to what done for resolved sources [see equations (2.2)-(2.6)]. This is obtained by dividing $C(\theta_\star, S_d)$ for the square of the background radiation intensity contributed by the objects with flux lower than S_d which fall within the telescope beam. As a result one gets the following expression, under the same simplifying assumptions made to derive equation (2.6) from equation (2.2):

$$w(\theta_\star, S_d) = \int_{z_{\rm min}}^{z_{\rm max}} dz I^2(z, S_d) \int_{z_{\rm min}-z}^{z_{\rm max}-z} d(\delta z) \xi[r(\delta z, \theta_\star), z] \times \left[\int_{\mathcal{Z}} dz I(z, S_d) \right]^{-2}. \tag{2.15}$$

This expression will be exploited in section 2.4 to derive constraints on the spatial two-point correlation function of SCUBA-like galaxies.

2.2.2 Angular clustering of SCUBA galaxies

Blank-sky surveys carried out with SCUBA have identified a total of ~ 100 sources in disparate areas of the sky. These survey fields include:

- the Hubble Deep Field North (Hughes et al. 1998; Borys et al. 2003; Serjeant et al. 2003; Wang et al. 2004);
- the Hawaii deep-field regions (Barger et al. 1998, 1999)
- the Lockman Hole East and the ELAIS N2 region in the 8-mJy survey (Fox et al. 2002; Scott et al. 2002);
- the Canada-France Redshift Survey (CFRS) fields by the Canada-United Kingdom Deep Submillimeter Survey (CUDSS) (Eales et al. 1999).
- the *Spitzer* northern continuous viewing zone (Sawicki & Webb 2005);
- the area covered by the SCUBA Half-Degree Extragalactic Survey (SHADES; Mortier et al. 2005) which comprises the Lockman Hole East and the Subaru/*XMM-Newton* Deep Field (SXDF). However, data sets from this survey have not been provided yet.

The first attempt to measure the angular clustering of SCUBA galaxies was made by Scott et al. (2002) in the 8-mJy survey covering the 260 arcmin^2 of the combined Lockman Hole East and the ELAIS N2 regions but it proved inconclusive because of the small-number statistics (the sample consists of only few tens of sources). Even the subsequent analysis performed by Borys et al. (2003) in a 165 arcmin^2 region surrounding the Hubble Deep Field North provided no clear evidence of clustering. On the other hand, Webb et al. (2003) have found $\omega(\theta) = (4.4 \pm 2.9)\theta^{-0.8}$ (θ in arcsec) for sources with $S_{850\mu m} > 3$ mJy in the two main CUDSS fields which cover a total area of 110 arcmin^2. The result is consistent with an angular clustering at least as strong as that seen for Lyman Break Galaxies (Giavalisco & Dickinson 2001) and Extremely Red Objects (EROs; Daddi et al. 2000)

but the relatively large error on this estimate makes the measured signal still compatible with zero.

As already mentioned, the angular clustering signal is strongly diluted by the broad redshift distribution of the sources. Thus redshift measurements would be crucially important. They are however difficult not only because SCUBA-selected galaxies are faint in the optical, but also because the broad ($\sim$15 arcsec) beam of SCUBA represents a further difficulty for unambiguous optical identifications. A way to ease this problem is offered by radio observations which can take advantage of a better angular resolution than that achievable in the sub-mm waveband. This method exploits the tight far-infrared-radio correlation observed for star-forming galaxies. Extensive efforts (e.g. Ivison et al. 2002, 2005; Chapman et al. 2003a, 2003b, 2005; Wang et al. 2004) have produced radio identifications for $\sim$50-70 per cent of the brighter submm sources. These radio detections have been successfully exploited to derive accurate (i.e. sub-arcsec) positions for submm galaxies, thus facilitating further spectroscopic studies. As a result, the redshift distribution of 73 bright ($\bar{\mathrm{S}}_{850\mu\mathrm{m}}$ $\sim$6 mJy) galaxies in seven independent fields have been obtained by Chapman et al. (2005). The mean redshift of the sources is $z \sim 2.2$. The sample contains a surprisingly large number of "associations", i.e systems of submillimeter galaxies with Mpc-scale separations and redshifts within 1200 km s^{-1}, thus providing tentative evidence of strong clustering of such sources at $z \simeq 2-3$. By using a simple pair-counting approach, appropriate for this small, sparse submillimeter galaxy sample, Blain et al. (2004) have found a comoving correlation length of $\sim 6.9 \pm 2.1\ h^{-1}$ Mpc. This can be considered, so far, the most reliable estimate of the spatial clustering of SCUBA galaxies.

Very recently, detections of large samples of high-z star-forming galaxies have been made with the Spitzer Space Telescope (formerly SIRTF, the Space Infrared Telescope Facility; Werner et al. 2004) thanks to its ability to map large areas of the sky in the infrared (from 3.6μm up to 160μm) to greater depths than any previous observatory.

Farrah et al. (2006) have used the Spitzer data to measure the spatial clustering of ultraluminous infrared galaxies with $S_{24\mu\mathrm{m}} > 0.4$ mJy, over the redshift range $1.5 \lesssim z \lesssim$

3. In order to select high redshift, IR-luminous star-forming galaxies, these authors have considered the 1.6μm emission feature, which arises due to the photospheric emission from evolved stars. When this feature is redshifted into one of the four channels of the Infrared Array Camera (IRAC) of Spitzer (3.6, 4.5, 5.8, and 8 μm) than that channel exhibits a peak, or "bump", compared to the other three channels (Simpson & Eisenhardt 1999; Sawicki 2002). The presence of a detectable 1.6μm feature demands a minimum mass of evolved stars of $\sim 10^{11}$ $M_\odot$. The further requirement that the sources have $S_{24\mu m} > 0.4$ mJy demands an IR luminosity of $\gtrsim 10^{12}$ $L_\odot$ which implies star formation rates of $\gtrsim 200$ $M_\odot$ yr^{-1}. Farrah et al found that the objects in their sample cluster very strongly with a clustering amplitude that is consistent with populations residing in dark matter halos with masses of $\gtrsim 10^{13}$ $M_\odot$.

2.3 An evolutionary model for submm galaxies

The 850μm counts have represented a challenge for models of galaxy formation. In fact, predictions of semianalytic models (Devriendt & Guiderdoni 2000; Cole et al. 2000; Sommerville, Primack & Faber 2001; Menci et al. 2002) are persistently unable to account for the surface density of massive galaxies at substantial redshifts detected by (sub-)millimeter surveys with SCUBA (Blain et al. 2002; Scott et al. 2002) and the Max Planck Millimeter Bolometer array (MAMBO; Bertoldi et al. 2002), unless ad hoc adjustments are introduced. The difficulty follows from the fact that the standard cold dark matter scenario tends to imply that most of the star formation occurs in relatively small galaxies that later merge to form bigger and bigger objects. On the contrary, the data indicate that galaxies detected by (sub-)millimeter surveys are mostly very massive, with very high star formation rates, at $z > 2$. Therefore all these data are more consistent with the traditional 'monolithic' scenario, according to which elliptical galaxies formed most of their stars in a single burst, at relatively high redshifts, and underwent essentially passive evolution thereafter. But how to reconcile the 'monolithic' scenario with the standard scenario of structure formation from primordial density perturbations?

Since what we observe is luminous matter, a way to overcome this difficulty may be

provided by processes acting on baryons during the formation of galaxies, in particular the *feedbacks*, first of all from supernovae explosions, which release large amounts of mechanical energy, capable of unbinding the gas in weekly bound, low mass systems, but also from the active nuclei which were found to be ubiquitous in the centers of spheroidal galaxies (Kormendy & Richstone 1995; Magorrian et al. 1998). These feedbacks can actually reverse the order of formation of visible galaxies compared to that of dark halos: large galaxies form their stars first, while the star formation is delayed in smaller halos. At the same time, processes associated to the star formation activity have a profound effect on the evolutionary history of nuclear activity.

All these issues have been addressed and put in a coherent scenario of structure formation, for the first time, by Granato et al. (2001; 2004; GDS04 hereafter). Their model accounts for the observed properties of SCUBA-selected galaxies and for many other observables (see Cirasuolo et al. 2005; Shankar et al. 2006; Lapi et al. 2006; De Zotti et al. 2006).

In the GDS04 model, submillimetre-selected sources are interpreted as spheroids observed during their major episode of star-formation, whose evolution and duration, shorter for more massive objects, is substantially affected not only by supernova feedback, but also by the growth of a central super-massive black hole (SMBH), and by the ensuing QSO activity. The relative importance of the QSO feedback, compared to supernovae, increases with the galaxy mass. This scenario, first explored in a phenomenological way by Granato et al. (2001), has been substantiated by GDS04 in a model which follows, using simple semi-analytic prescriptions, the evolution of baryons within dark matter halos with total mass $M_{\rm vir}\gtrsim 2.5\times 10^{11}M_{\odot}$, forming at $z\gtrsim 1.5$ at the rate predicted by the canonical hierarchical clustering scenario. The mass and redshift cuts are meant to crudely filter out the halos associated with disk and irregular galaxies, whose formation is not quantitatively addressed by GDS04. However, disk and irregular galaxies are envisaged as associated to halos virializing at lower redshifts, eventually incorporating most of the less massive haloes which virialized at earlier times and may become galactic bulges.

The GDS04 model predicts that in the less massive halos (characterized by a

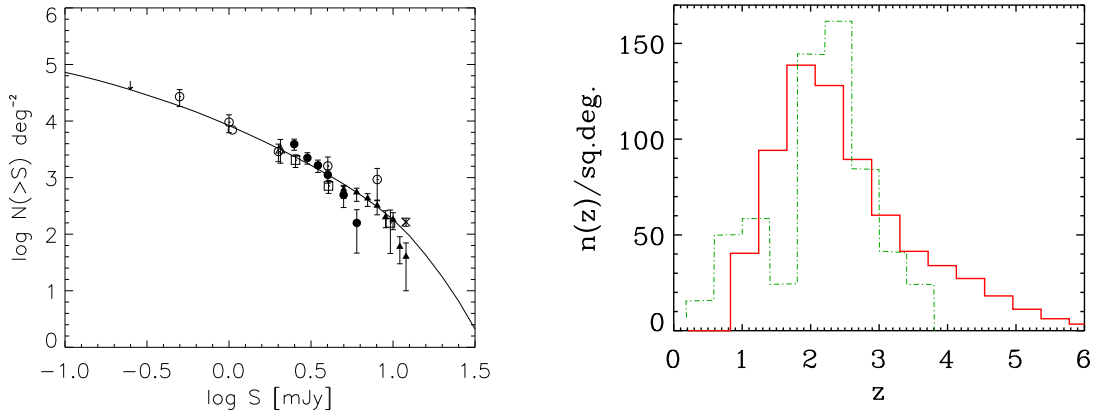

Figure 2.1: *Left-hand panel*: 850μm extragalactic source counts as predicted by the model of Granato et al. (2004; *solid line*) compared with SCUBA counts by Blain et al. (1999; *open circles*), Hughes et al. (1998; *asterisk and open triangles*), Barger, Cowie & Sanders (1999; *open squares*), Eales et al. (2000; *filled circles*), Chapman et al. (2002; *filled triangles*), Borys et al. (2002; *filled squares*). *Right-hand panel*: 850μm redshift distribution of SCUBA galaxies with $S_{850\mu\mathrm{m}} \geq 5$ mJy. The solid line shows the prediction based on the model of Granato et al. (2004) while the dotted-dashed line is the redshift distribution derived from the sample of Chapman et al. (2005).

shallower potential well) the supernova heating is increasingly effective in slowing down the star formation and driving gas outflows, resulting in an increase of the star/DM ratio with increasing halo mass. As a consequence, the star formation is higher within the most massive halos and even higher if they virialize at substantial redshifts. In this way, physical processes acting on baryons effectively reverse the order of formation of galaxies compared to that of DM halos (antihierarchical baryon collapse scenario).

In the more massive halos, the higher star formation rate (compared to that of less massive halos), implies a faster inflow toward the central black hole since the higher radiation drag induce a faster loss of angular momentum of the gas (Umemura 2001; Kawakatu & Umemura 2002; Kawakatu et al. 2003). The model assumes that the kinetic energy carried by outflows driven by active nuclei is proportional to $M_{\mathrm{BH}}^{3/2}$, so that this mechanism can inject in the inter stellar medium (ISM) of massive galaxies a sufficient amount of energy to unbind it. As a result the time required to sweep out the ISM, thus halting both the star formation and the BH growth, is again shorter for larger halos. For the most massive galaxies

($M_{\rm vir} \gtrsim 10^{12}$ M$_\odot$) virializing at $3 \lesssim z_{\rm vir} \lesssim 6$, this time is less than 1 Gyr, so that the bulk of the star formation may be completed before type Ia supernovae can significantly increase the Fe abundance of the ISM. This process can then account for the excess $\alpha-$element/Fe ratio, compared to solar ($\alpha-$enhancement; Trager et al. 2000a, 2000b; Thomas et al. 2002), seen in the largest E/S0 local galaxies which is in fact suggestive of very intense but short star formation activity. Moreover, the interplay between star formation and nuclear activity determines the relationship between BH masses and the mass, or velocity dispersion, of the host galaxy, observed in local galaxies (Ferrarese & Merrit 2000; Gebhardt et al. 2000; Tremaine et al. 2002). The model predictions are in excellent agreement with the observational data (Granato et al. 2004 but see also Cirasuolo et al. 2005; Shankar et al. 2006; De Zotti et al. 2006).

In order to get predictions for the submillimetre counts and the corresponding redshift distribution, the model has been coupled with GRASIL (Silva et al. 1998, see http://web.pd.astro.it/granato), a code computing in a self-consistent way the chemical and spectrophotometric evolution of galaxies over a wide wavelength interval, from far-ultraviolet to radio. The code translates the SFR and the mass in stars, as derived from the GDS04 model, into more directly observable quantities such as broad-band luminosities, including dust extinction. The predicted 850μm source counts and the corresponding redshift distribution are found to be in very good agreement with the data, as shown in Fig. 2.1.

Note that, according to GDS04 (but see also Granato et al. 2001), the high-redshift QSO activity marks and concurs to the end of the major episode of star formation in spheroids. Thus, a clear evolutionary link between SCUBA sources and high-redshift QSOs is implicit in the model. GDS04 also establish a close link between the submillimetre population and Lyman-Break Galaxies and Extremely Red Objects. The former are interpreted as the optical counterpart of low to intermediate mass primeval spheroidal galaxies, with a duration of the star-formation burst $T_B \sim 1-2$ Gyr and a star-formation rate ranging from a few to a hundred M$_\odot$ yr^{-1}. EROs are instead seen as either dust-obscured or passively evolving massive galaxies in which the ISM has been swept out and the combination of

redshift and aging have made them extremely red. The GDS04 model can thus be tested against measurements of LBGs and EROs clustering (see e.g. Magliocchetti et al. 2001).

In this thesis, the GDS04 model will be assumed as the basic tool to deal with submillimetre galaxies.

2.4 Clustering contribution to the background fluctuations at 850μm

Peacock et al. (2000, hereafter P00) carried out a power-spectrum analysis of the 850μm map of the northern *Hubble Deep Field* by Hughes et al. (1998), after subtracting sources brighter than $S_d = 2\,\mathrm{mJy}$. They found, for multipole numbers ℓ in the range $10^4 \lesssim \ell \lesssim 5 \times 10^4$, some evidence of power in excess of the sum of instrumental noise and of estimated Poisson fluctuations due to unresolved sources. Such excess power can be accounted for by source clustering described by an angular correlation function of the form:

$$w(\theta) = (\theta/\theta_0)^{-0.8} \ ; \tag{2.16}$$

with θ_0 in the range 1–2 arcsec. As made clear by P00, however, the estimated amplitude of Poisson fluctuations is rather uncertain due to our poor knowledge of the 850μm counts below 2 mJy, and the possibility that they account entirely for the detected confusion noise cannot be ruled out. The more recent data on the faint 850 μm counts (Chapman et al. 2002; Smail et al. 2002; Knudsen & van der Werf 2003) are in good agreement with the analysis by P00 and lend support to their estimate of the angular correlation function.

Here I will derive information on the clustering properties of SCUBA-like galaxies by trying to reproduce the data of P00. As I will show below, an angular correlation function with the amplitude suggested by P00 is consistent with a number of other data on clustering of SCUBA galaxies themselves (although, again, the significance of the clustering detection is not very high) and of other populations which are closely linked to these galaxies, such as EROs.

To compare with the results by P00 I assume $S_d = 2\,\mathrm{mJy}$ (for which the model of GDS04 yields a background intensity $I_{850\mu\mathrm{m}}(S_d) = 6.6 \times 10^{-19}$ erg/s/cm^2/Hz/sr) and then

estimate the angular correlation function of the background source population by means of equation (2.15).

For what concern the two-point spatial correlation function of proto-spheroids, $\xi_{\rm sph}$, I will consider both a phenomenological, power-law model (Model 1) and a physically motivated model (Model 2). Both models are normalized to equation (2.16) with $\theta_0 = 1$"–2" in the range of scales probed by P00 (see Fig. 2.2).

2.4.1 Model 1

The first model assumes the usual power-law shape:

$$\xi_{\rm sph}(r,z) = \left[\frac{r}{r_0(z)}\right]^{-1.8} \quad . \tag{2.17}$$

In view of the tight connection between spheroidal galaxies and active nuclei at their centers, entailed by the GDS04 model, I further assume that the correlation length, r_0, is constant *in comoving coordinates*, as suggested by quasar data (Croom et al. 2001; Outram et al. 2003) at least in the redshift interval $0.5 \leq z \leq 2.5$–3.

From equation (2.6), I find that the range of values of r_0 corresponding to $\theta_0 = 1''$–$2''$ is:

$$r_0 = 8.3 \pm 1.3 \text{ Mpc/h} \ , \tag{2.18}$$

very close to the range of values found for bright 2QZ quasars ($r_0 = 8.37 \pm 1.17\,$Mpc/h; Croom et al. 2002), and fully consistent with the tentative estimate of the correlation length of SCUBA galaxies obtained by Blain et al. (2004): $r_0 = 6.9 \pm 2.1 \ h^{-1}$ Mpc. The above value of the comoving correlation length is also compatible with the ones measured for bright local elliptical galaxies (Loveday et al. 1995; Guzzo et al. 1997; Norberg et al. 2002; Madgwick et al. 2003), supporting the link between these objects and the population of SCUBA sources.

2.4.2 Model 2

In this second model I assume the standard theoretical recipe for clustering evolution in a ΛCDM universe, with a redshift dependent bias factor. Under the assumption

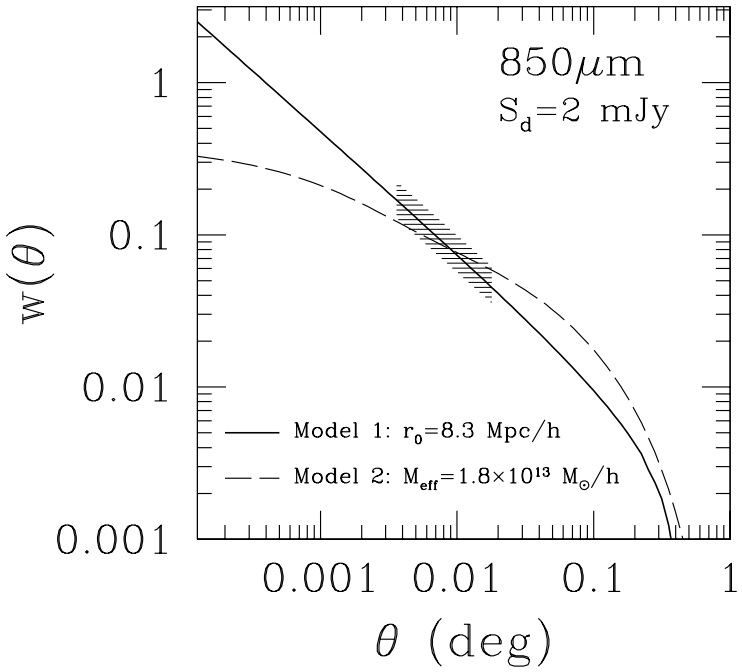

Figure 2.2: Comparison of the adopted models for the angular correlation function with equation (2.16) with $\theta_0 = 1$"–2", in the interval of angular scales probed by P00. The long-dashed curve has been obtained using the prescriptions by Peacock & Dodds (1996) for generating the dark matter power spectrum.

of a single object per halo, which is expected to hold for massive objects at high redshift ($z \gtrsim 1$) and is implicit in the GDS04 model, the bias parameter, b, can be written as a function of an effective dark-matter halo mass, $M_{\rm eff}$ (which is close to the minimum halo mass, cf. Moscardini et al. 1998), and of redshift (see, e.g., Mo & White 1996; Sheth & Tormen 1999). I can then write the spatial correlation function of star-forming spheroids as

$$\xi_{\rm sph}(r,z) = b^2(M_{\rm eff},z)\xi_{\rm DM}(r,z)\ . \tag{2.19}$$

I adopt a CDM spectrum for density fluctuation with the spectral index $n = 1$ and the transfer function of Bardeen et al. (1986):

$$T(k) = \frac{\ln(1+2.34q)}{2.34q} \times \left[1+3.89q+(16.1q)^2+(5.46q)^3+(6.71q)^4\right]^{-1/4}. \tag{2.20}$$

where $q = k/\Gamma$, with k in h Mpc^{-1}, and Γ is the power spectrum *shape parameter* (Sugiyama 1995)

$$\Gamma = \Omega_{0,m} h \exp\left[-\Omega_{0,b}(1 + \sqrt{2h}/\Omega_{0,m})\right]. \tag{2.21}$$

A normalization $\sigma_8 = 0.8$ is assumed (see e.g. Lahav et al. 2002, Spergel et al. 2006). I will use the practical fitting formula by Peacock & Dodds (1996) to evolve the dark matter power spectrum into the non-linear regime.

The effective mass $M_{\rm eff}$ is determined by the condition that, in the range of angular scales probed by P00, the model correlation function matches the measured one. Using the analytic formulae by Sheth & Tormen (1999) for the bias factor, I find:

$$M_{\rm eff} = 1.8 \times 10^{13} M_{\odot}/{\rm h} \ , \tag{2.22}$$

consistent with the estimates by Moustakas & Somerville (2002) for ERO halo masses (the minimum mass of ERO dark matter haloes is estimated to be $\sim 10^{13} M_{\odot}/{\rm h}$, while the galaxy number-weighted average halo mass is $\simeq 5 \times 10^{13} M_{\odot}/{\rm h}$). Note that EROs are either massive dusty galaxies like SCUBA galaxies, or evolved giant ellipticals, a later evolutionary phase of SCUBA galaxies, in the scenario discussed by GDS04.

For a virialization redshift $z_{\rm vir} \lesssim 4$, GDS04 predict a ratio $M_{\rm eff}/M_{\rm sph} \sim 40$, where $M_{\rm sph}$ is the present-day mass in stars of spheroids (see Figure 5 of their paper). Thus $M_{\rm eff}$ corresponds to a mass in stars of $\simeq 6 \times 10^{11}$ M$_{\odot}$, compatible with values for the stellar masses inferred for SCUBA galaxies (Smail et al. 2003) and for high-z galaxies with very red near-IR colors (Saracco et al. 2004).

As a last remark, it is worth noticing that (as also illustrated by Fig. 2.2) Models 1 and 2 widely differ on small angular scales. The small scale flattening of $w(\theta)$ implied by Model 2 is due to the fact that at high redshifts ($z \gtrsim 2$) density perturbations are close to the linear regime, even on very small scales.

2.5 Conclusions

In this chapter, I have described the existing tentative measurement of the clustering properties of SCUBA-like galaxies. They seem to indicate that such sources are strongly clustered in space. I have provided I further support to this expectation by reproducing the clustering contribution of submillimetre galaxies to the background fluctuations at 850μm as measured by Peacock et al. (2000). In doing this, I have treated SCUBA galaxies according to the physical model of Granato et al. (2004) which succesfully reproduces both the counts and the redshift distribution of 850μm sources.

By assuming that the spatial correlation function of SCUBA galaxies has a power-law form with slope $\gamma = 1.8$ and a redshift-independent spatial correlation length, I infer $r_0 \sim 8\ h^{-1}$ Mpc (comoving). On the other hand, a more physical model, that accounts for the evolution of the dark matter correlation function and of the bias parameter, provides a typical mass of the halo hosting SCUBA galaxies of the order of $10^{13}\ h^{-1}\ \mathrm{M}_{\odot}$.

These results support the existence of an evolutionary link between high-z submillimetre galaxies and local massive ellipticals, the former objects being proto-spheroids observed during their major episode of star-formation.

Chapter 3

Source confusion at far-infrared to millimeter wavelengths

3.1 Introduction

In this chapter I address the issue of the effect of clustering in increasing the confusion noise, and therefore the flux limit for source detection, for far-IR/sub-millimeter surveys. As already pointed out in chapter 1, the effect is particularly relevant for confusion limited surveys with poor spatial resolution since, for small enough angular scales, the ratio of Poisson-to-clustering fluctuations decreases with increasing angular scale (De Zotti et al. 1996). I will mainly concentrate on surveys in the ISOPHOT 175 μm channel, in the Spitzer (formerly SIRTF) MIPS 160 μm channel, and on those performed with Herschel/SPIRE and with Planck/HFI instruments.

All current estimates of the confusion noise for the above instruments (Blain et al. 1998; Dole et al. 2001; Xu et al. 2001; Franceschini et al. 2001; Rowan-Robinson 2001; Lonsdale et al. 2003; Lagache et al. 2003; Rodighiero et al. 2003; Dole et al. 2003, 2004; Jeong et al. 2006) do in fact only take into account the Poisson contribution. An attempt to allow also for the effect of clustering in the Planck mission was worked out by Toffolatti et al. (1998) although their treatment of infrared galaxies (and of their clustering properties) suffered

from the lack of tight observational constraints at sub-mm wavelengths.

The model of Granato et al. (2004), adopted here, provides a step forward with respect to the Toffolatti's approach since it fixes the volume emissivity of sub-mm sources as a function of cosmic time, that is one of the key ingredients to derive the amplitude of the fluctuations. The other key ingredient, namely the correlation function, will be treated by means of the two models described in the previous chapter.

The layout of this chapter is as follows. In Section 3.2 I describe the formalism needed to deal with source confusion noise. Section 3.3 summarizes the main aspects of the models adopted for the sources of interest here. In Section 3.4 I present some applications and discuss the main results. Conclusions are summarized in Section 3.5.

3.2 Confusion noise due to clustered sources: the formalism

The variance, σ_N^2, of intensity fluctuations due to sources with flux below the detection limit S_d, within the same telescope beam, is obtained by setting $\theta_\star = 0$ in the expression for the autocorrelation function $C(\theta_\star, S_d)$ of flux fluctuations introduced in the previous chapter [equation (2.8)]. By assuming again that the luminosities of the sources are statistically independent of their positions (see chapter 2, equation (2.11)] one gets

$$\sigma_N^2(S_d) = \lim_{\theta_\star \to 0} C(\theta_\star, S) = \sigma_P^2(S_d) + \sigma_C^2(S_d) \ , \tag{3.1}$$

where σ_P^2 is the Poisson contribution to the variance:

$$\sigma_P^2(S_d) = \int_{beam} d\Omega f^2(\theta,\phi) \times \int_{\mathcal{Z}} dz \frac{dV}{dz d\Omega}(z) \int_{\mathcal{L}} dL \left(\frac{LK(z)}{4\pi d_L^2(z)} \right)^2 \Phi(L,z) \ , \tag{3.2}$$

while σ_C^2 is the contribution owing to the the clustering of the background source population which, in the small angle approximation ($\theta_1, \theta_2 << 1$ rad) and assuming that the maximum scale of appreciable clustering is much smaller than the Hubble radius, $c/H(z)$, can be written as:

$$\begin{aligned} \sigma_C^2(S_d) &= \left(\frac{1}{4\pi} \frac{c}{H_0} \right)^2 \int_{\rm beam} d\Omega_1 d\Omega_2 f(\theta_1,\phi_1) f(\theta_2,\phi_2) \\ &\times \int_{\mathcal{Z}} dz \frac{j_{\rm eff}^2(z,S_d)}{(1+z)^4 E^2(z)} \int_{z_{\rm min}-z}^{z_{\rm max}-z} d(\delta z) \xi[r(\delta z,\vartheta),z] \ , \end{aligned} \tag{3.3}$$

where ϑ is the angular separation[1] in the sky of the points having spherical coordinates (θ_1,ϕ_1) and (θ_2,ϕ_2).

In the following analysis, the spatial response function of the detector, $f(\theta, \phi)$, will be assumed to be axially symmetric and Gaussian:

$$f(\theta, \phi) = e^{-(\theta/\Theta)^2/2} \ , \tag{3.4}$$

where Θ relates to the beam Full Width at Half Maximum (FWHM) of the instrument through

$$\Theta = \frac{\mathrm{FWHM}}{2\sqrt{2\ln 2}} \ . \tag{3.5}$$

The quantity σ_N will be referred to as *confusion noise*. The detection limit, S_d, for a confusion limited survey, is defined by:

$$S_d = q \times \sigma_N(S_d) \ , \tag{3.6}$$

where the parameter q is usually chosen in the range [3,5]. Hereafter I will adopt $q = 5$.

3.3 Extragalactic sources in the far-infrared and sub-millimeter wavebands: evolutionary models

The extragalactic source counts in the far-IR/sub-mm wavebands are contributed by various classes of sources which comprise

- high-z protosheroidal galaxies, detected by SCUBA at 850 μm;
- late type "normal" galaxies which show moderate star formation activity;
- starburst galaxies, which are characterized by a burst of intense star formation, although the rate at which stars are formed and the related infrared luminosity are much lower than those associated to bright SCUBA-selected sources;

[1] In the small angle approximation: $\vartheta^2 = \theta_1^2 + \theta_2^2 - 2\theta_1\theta_2\cos(\phi_1 - \phi_2)$

- canonical radio sources, whose emission in the far-IR/sub-mm waveband is due to synchrotron radiation rather than dust-reprocessed light, as it is the case for the classes of objects cited above.

The relative importance of these populations of sources, as predicted by the models adopted here and illustrated below, is shown in Fig. 3.1, for observations performed at wavelengths ranging from 175 μm up to 3000 μm.

According to the model of Granato et al. (2004), SCUBA-like galaxies are important in the flux ranges $\sim$1-100 mJy at far-IR wavelengths and $\sim$1-10 mJy in the sub-mm waveband. At higher fluxes, the counts exibit a very steep decline as a result of the combined effect of the strongly negative k-correction - due to the steep increase with frequency of dust emission - and of cosmological evolution.
In order to account for the contribution of clustering of SCUBA-like galaxies to source confusion noise in far-IR/sub-mm surveys, I will adopt, in the following analysis, the spatial two-point correlation function provided by the two models illustrated in the previous chapter.

Late-type, normal galaxies and starburst galaxies dominate the bright tail of the counts at far-infrared wavelengths. To deal with these sources I adopt a phenomenological approach (e.g. Franceschini et al. 2001; Takeuchi et al. 2001; Rowan-Robinson 2001; Gruppioni et al. 2002; Lagache et al. 2003), which consists in simple analytic recipes to evolve their 60μm local luminosity functions (Saunders et al. 1990) and appropriate templates for the spectral energy distributions (SED) in order to extrapolate the predictions to different wavelengths. The prescriptions adopted here are those defined by Silva et al. (2005), which provide reasonable fits to the results of IRAS and ISO surveys. Briefly, normal late-type galaxies are assumed to undergo a pure luminosity evolution, with their luminosity function, $\Phi_{\rm LT}$, described by

$$\Phi_{\rm LT}[L(z), z] = \Phi_{\rm LT}[L(z)/(1+z)^{1.5}, z = 0], \tag{3.7}$$

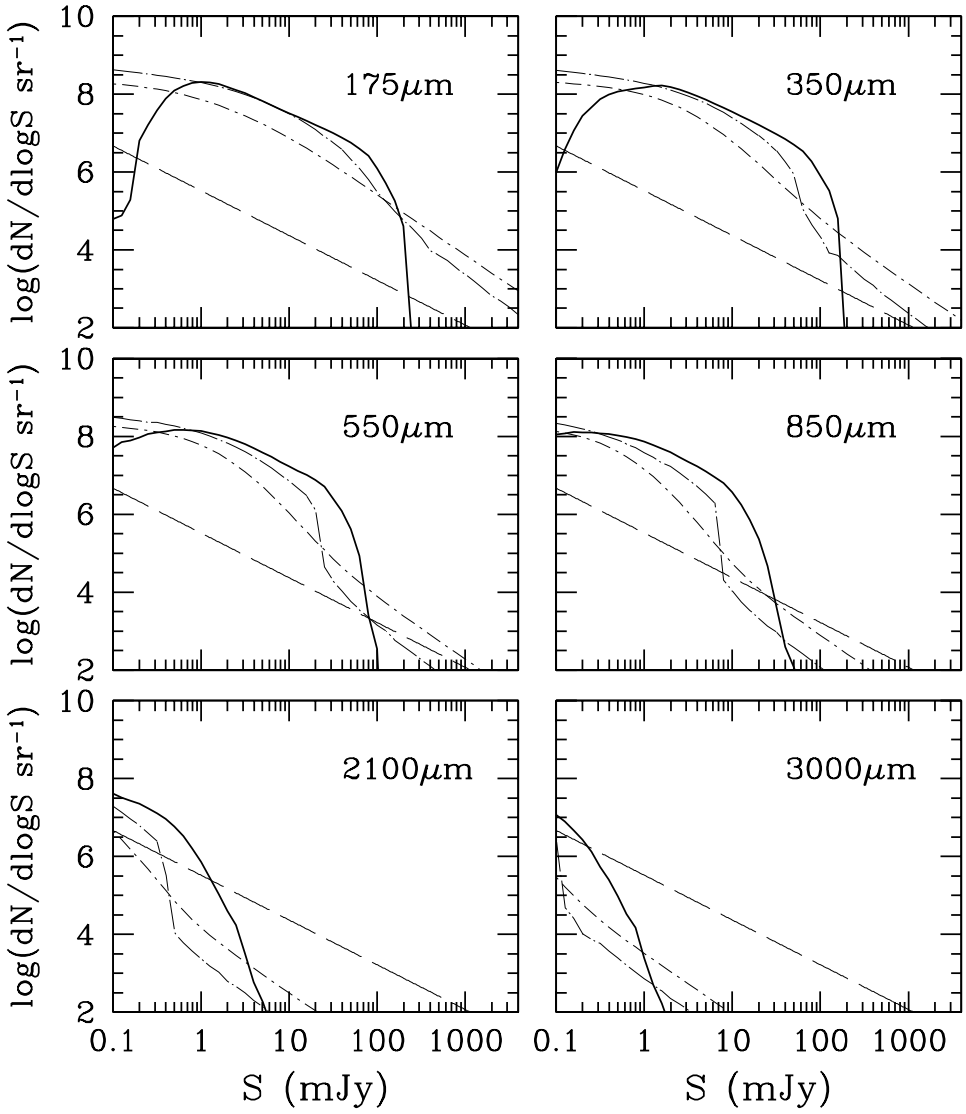

Figure 3.1: Differential extragalactic source counts at various wavelengths ranging from 175μm up to 3000μm. The solid curve shows the contribution from proto spheroids as predicted by the model of Granato et al. (2004) while the other curves describe the contributions from spiral galaxies (dotted/short-dashed line), starburst galaxies (dotted/long-dashed line) and extragalactic radio sources (long-dashed line). See text for details about the way in which the counts of the the various classes of sources have been computed.

and to have the SED of the Sc galaxy NGC 6946. The SED of the galaxy NGC 6090 is adopted for starburst galaxies and the luminosity function of these objects, $\Phi_{\rm SB}$, is assumed to evolve both in luminosity and in density, according to the following prescription

$$\Phi_{\rm SB}[L(z),z] = \Phi_{\rm SB}[L(z)/(1+z)^{2.5}, z=0](1+z)^{3.5}. \tag{3.8}$$

The evolutionary laws for both populations were assumed to apply up to $z = 1$; then the luminosity functions were kept constant up to $z_{\rm cutoff} = 1.5$.

Spiral and starburst galaxies are relatively weakly clustered (Fisher et al. 1994; Loveday et al. 1995; Guzzo et al. 1997; Madgwick et al. 2003), so that their contributions to the confusion noise turn out to be dominated by Poisson fluctuations. In the following I will therefore neglect their contribution to σ_C.

At millimeter wavelengths the composition of the bright counts drastically changes since flat spectrum radio sources take over. Their counts have been estimated in a very simple manner, by extrapolating the 15 GHz differential counts, $n(S_{\rm Jy}) = 51 S_{\rm Jy}^{-2.15}\,{\rm Jy}^{-1}{\rm sr}^{-1}$ (Waldram et al. 2003), with a spectral index equal to zero (i.e. assuming a flux density constant with frequency, that is $S \propto \nu^{-\alpha}$ with $\alpha = 0$), consistent with the WMAP results (Bennett et al. 2003). This choice for the spectral index is likely to increasingly overestimate the counts with increasing frequency as the radio-source spectra steepen both because emitting regions become optically thin and because of electron aging effects. However, this has little impact on our results since at sub-millimeter wavelengths radio sources are anyway a minor component.

Although radio sources are rather strongly clustered (Magliocchetti et al. 1998; Blake & Wall 2002a,b; Overzier et al. 2003, Magliocchetti et al. 2004), their clustering signal is highly diluted due to the broadness of their luminosity function (e.g. Dunlop & Peacock 1990) so that their σ_C is small when compared to σ_P and can therefore be neglected (Toffolatti et al. 1998; Argüeso et al. 2003).

Table 3.1: Estimated confusion noise and detection limits, S_d (neglecting instrumental noise as well as emissions within our Galaxy and fluctuations of the cosmic microwave background) for several far-IR/(sub)-millimeter instruments: the 175μm channel of ISOPHOT, the 160μm channel of Spitzer and the three channels of Herschel/SPIRE. Shown are the Poisson contributions (σ_P) due to spiral galaxies (sp), star-forming galaxies (sb), radio-galaxies (rg) and star-forming spheroids (sph). For the latter, I also give the clustering fluctuations ($\sigma_{C,sph}$). At each wavelength, three cases are shown: Poisson contributions only (first line), Poisson plus clustering contribution from star-forming spheroids with a correlation function of the form $\xi_{\rm sph}(r,z) = (r/r_0)^{-1.8}$ with $r_0 = 8.3\,{\rm Mpc/h}$ (*model 1*, second line), Poisson plus clustering contribution from star-forming spheroids with a correlation function of the form $\xi_{\rm sph}(r,z) = b^2(M_{\rm eff},z)\xi_{\rm DM}$ with $M_{\rm eff} = 1.8\times10^{13}\ M_\odot/{\rm h}$ (*model 2*, third line). I have assumed $q = 5$, so that $S_d = 5\times(\sigma^2_{P,sp}+\sigma^2_{P,sb}+\sigma^2_{P,rg}+\sigma^2_{P,sph}+\sigma^2_{C,sph})^{1/2}$.

λ (μm)	ν (GHz)	FWHM (arcsec)	$\sigma_{P,sp}$ (mJy)	$\sigma_{P,sb}$ (mJy)	$\sigma_{P,rg}$ (mJy)	$\sigma_{P,sph}$ (mJy)	$\sigma_{C,sph}$ (mJy)	S_d (mJy)
ISOPHOT								
			20	29	2	40	-	264
175	1714	94.0	21	29	2	40	45	350
			21	29	2	40	38	327
Spitzer/MIPS								
			5.0	9.1	0.4	11.2	-	76.4
160	1875	35.2	5.3	9.3	0.4	11.5	8.2	88.3
			5.1	9.3	0.4	11.4	6.0	83.2
Herschel/SPIRE								
			2.0	3.9	0.1	4.6	-	31.7
250	1200	17.4	2.1	4.1	0.1	4.8	2.6	35.7
			2.1	4.0	0.1	4.7	1.8	33.7
			2.5	5.0	0.2	6.9	-	44.2
350	857	24.4	2.6	5.1	0.2	7.3	4.1	50.6
			2.5	5.0	0.2	7.1	3.1	47.9
			1.7	3.3	0.2	5.8	-	34.6
500	600	34.6	1.7	3.3	0.3	6.0	3.8	40.1
			1.7	3.3	0.3	6.0	3.2	38.6

Table 3.2: Same as in Table 3.1 but for the case of Planck/HFI.

λ (μm)	ν (GHz)	FWHM (arcsec)	$\sigma_{P,sp}$ (mJy)	$\sigma_{P,sb}$ (mJy)	$\sigma_{P,rg}$ (mJy)	$\sigma_{P,sph}$ (mJy)	$\sigma_{C,sph}$ (mJy)	S_d (mJy)
Planck/HFI								
			45	65	7	116	-	705
350	857	300	50	66	10	116	250	1439
			51	66	10	116	266	1510
			18	29	5	55	-	323
550	545	300	19	29	7	55	117	671
			19	29	8	55	137	757
			5	9	3	20	-	115
850	353	300	6	9	5	20	42	241
			6	9	5	20	53	288
			1.2	2.2	1.9	4.9	-	29.2
1380	217	300	1.3	2.2	2.5	4.9	10.1	59.0
			1.3	2.2	2.8	4.9	13.3	73.2
			0.5	0.7	2.0	1.8	-	13.9
2100	143	426	0.5	0.7	2.6	1.8	4.2	26.5
			0.5	0.7	2.8	1.8	5.7	33.5
			0.2	0.3	2.5	0.7	-	12.9
3000	100	552	0.3	0.3	2.8	0.7	1.8	17.1
			0.3	0.3	3.0	0.7	2.6	20.0

3.4 Applications and discussion

Tables 3.1-3.2 give the estimated contributions to the confusion noise and the corresponding detection limits S_d for all the populations previously described. These are obtained by adopting $q = 5$ in equation (3.6) in the case of:

i) the 175 μm channel of the Imaging Photo-Polarimeter of the ESA's ISO satellite (ISOPHOT);

ii) the longest wavelength channel (160 μm) of the Multiband Imaging Photometer (MIPS)

of NASA's Spitzer (formerly SIRTF) satellite;

iii) all channels (250, 350 and 500 μm) of the Spectral and Photometric Imaging REceiver (SPIRE) of the ESA's Herschel satellite scheduled for launch in 2007;

iv) all channels (350, 550, 850, 1380, 2100, and 3000 μm) of the High Frequency Instrument (HFI) of the ESA's Planck satellite, to be launched jointly with Herschel.

The values for the angular resolutions (FWHM) have been taken from Dole et al. (2001; ISOPHOT), Lonsdale et al. (2003; MIPS/Spitzer), Griffin et al. (2000; SPIRE/Herschel), and Lamarre et al. (2003; HFI/Planck).

As discussed above, forming spheroidal galaxies are the only population, among those considered here, whose fluctuations can be significantly affected clustering. I have therefore only presented in Tables 3.1-3.2 results for the instruments and the wavelengths where this population gives an important contribution to the confusion noise. For each channel, the first line corresponds to pure Poisson fluctuations while the second and the third lines include the contributions of clustering based on *model 1* and *model 2*, respectively. The increment of Poisson fluctuations when I allow for the effect of clustering is obviously due to the increment of S_d.

The relative importance of the contributions from each class of objects as a function of the flux limit is illustrated in Fig. 3.2 and in Fig. 3.3 respectively for the case of Herschel/SPIRE and Planck/HFI. The flattening of the function $\sigma_{C,sph}(S_d)$ at bright flux densities follows from the fact that the main contribution to this term does not come from sources just below the detection limit, as is frequently the case for Poisson fluctuations, but from sources at redshifts where the effective volume emissivity, $j_{\rm eff}$ [see equation (3.3)], is maximum.

For power-law differential counts, $n(S) \propto S^{-\beta}$, $\sigma_P \propto S_d^{(3-\beta)/2}$ if $\beta < 3$. This power-law behaviour, obeyed by $\sigma_{P,rg}$ because of our adoption of the power-law representation of the counts by Waldram et al. (2003), must break down at faint flux densities, where the counts must converge, and must flatten at bright flux densities ($S \gtrsim 1$ Jy), where the slope of the

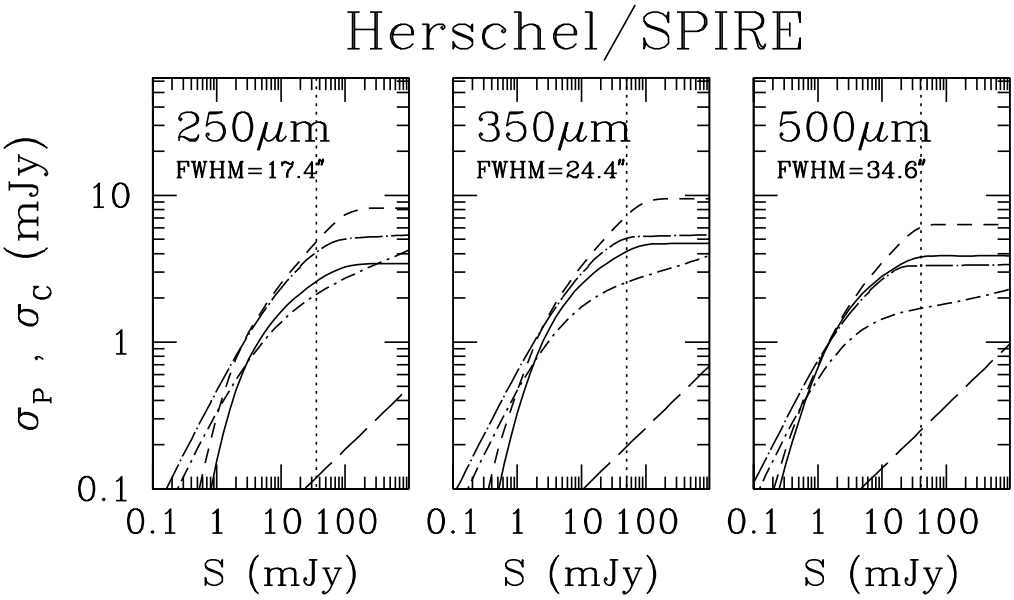

Figure 3.2: Poisson confusion noise σ_P as a function of the flux density S for spiral galaxies (dotted–short-dashed line), starburst galaxies (dotted–long-dashed line), radio-sources (long-dashed line) and star-forming spheroids (short-dashed line) for the channels of Herschel/SPIRE. The confusion noise due to clustered star-forming spheroids, $\sigma_C(S)$, (*model 1* with $r_0 = 8.3$ Mpc/h) is shown by the solid line. The vertical dotted lines correspond to the detection limit S_d obtained by taking into account both Poisson and clustering fluctuations.

counts approaches the Euclidean value (Bennett et al. 2003). Since the survey by Waldram et al. (2003) covers the flux density range 10–1000 mJy, in the hypothesis that the counts start converging not far below 10 mJy, I may have somewhat overestimated fluctuations due to radio sources.

The slope of the bright counts of normal late-type galaxies is close to the Euclidean value ($\beta \simeq 2.5$), while that of starburst galaxies is somewhat steeper due to their relatively strong evolution (see Fig. 3.1). Correspondingly, for both the above populations σ_P is a flatter function of S than what results for radio galaxies, and is flatter for starbursts than for normal galaxies.

On the other hand, the bright tail of the counts of forming spheroidal galaxies is extremely steep ($\beta > 3$), as a consequence of the combined effect of strong evolution and negative K-correction. Thus, the main contribution to $\sigma_{P,sph}(S_d)$ comes from relatively

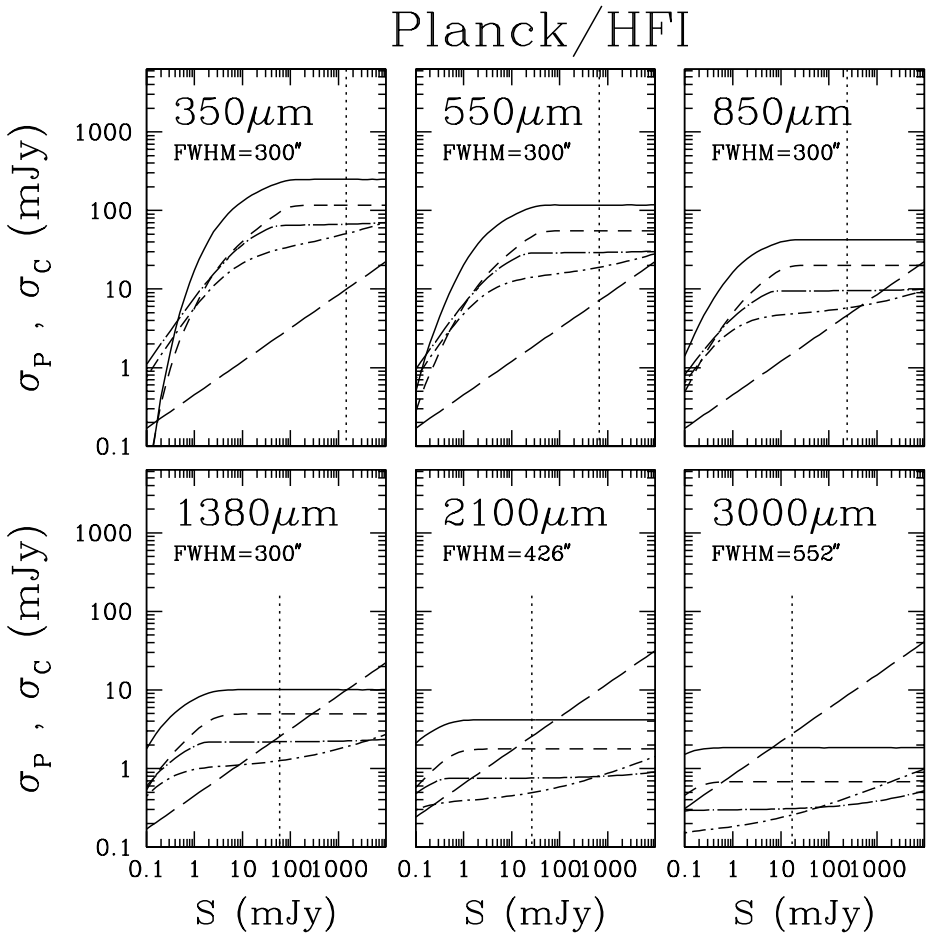

Figure 3.3: Same as in Fig. 3.2 but for the case of Planck/HFI

faint sources and this quantity is essentially constant for large enough values of S_d.

Clustering accounts for 10–20% of the total confusion noise, depending on the assumed model for $\xi_{\rm sph}$, for the 160 μm MIPS channel and the SPIRE channels, but its contribution increases up to 35–40% of the total confusion noise for the 175 μm ISOPHOT channel, and dominates the fluctuations due to extragalactic sources in the case of Planck/HFI, except in the longest wavelength channel where Poisson fluctuations due to radio sources take over. However, higher resolution surveys can be used to subtract such sources down to flux

densities well below the estimated S_d, thus decreasing their contribution to fluctuations. It is worth noticing that a similar task is much more difficult in the case of forming spheroidal galaxies since the main contribution to their clustering fluctuations comes from very faint flux densities.

As noted above, the ratio of clustering-to-Poisson fluctuations increases with decreasing angular resolution. In fact [see equation (3.2)], $\sigma_P \propto \Theta$ while, if $\xi(r) = (r/r_0)^{-\gamma}$ with $\gamma = 1.8$, $\sigma_C \propto \Theta^{1.6}$ (De Zotti et al. 1996). It may also be noted that, as a consequence of the different dependence of $w(\theta)$ on angular scale (see chapter 2, Fig. 1), the values of σ_C implied by *model 1* exceed those given by *model 2* for higher resolution surveys, while the opposite happens for lower resolution surveys, such as those of Planck/HFI.

Our estimates – obtained with the inclusion of the clustering contribution – of the confusion noise for the 175 μm ISOPHOT channel are in good agreement with the observational determination by Dole et al. (2001) in the FIRBACK survey fields, once I allow for the different flux limit. These authors find a confusion noise of 45 mJy when adopting a $3\sigma_N$ detection limit of 135 mJy, while I adopt a $5\sigma_N$ limit of 327–350 mJy (see Table 3.1, bearing in mind that σ increases with S_d). The possibility of a significant contribution from clustering in the 175 μm FIRBACK survey was discussed by Perrotta et al. (2003) and Dole et al. (2003).

In spite of the different models used and of the different criteria adopted to define the limiting flux densities, our estimates of Poisson fluctuations are in reasonable agreement with those by Rowan-Robinson (2001), Dole et al. (2003) and Xu et al. (2003) for MIPS/Spitzer and by Lagache et al. (2003) for SPIRE/Herschel and HFI/Planck. At the wavelengths (160 and 850 μm) where the models are tightly constrained by the data, differences are generally within 20–30 per cent, our predictions being on the high side. At other wavelengths, our estimates tend to be higher than those of other authors by up to 50 per cent.

As briefly discussed in the introduction of this chapter, a preliminary attempt to allow for the effect of clustering of evolving dusty galaxies was carried out by Toffolatti et al. (1998), who assumed $\xi(r) = [r/r_0(z)]^{-1.8}$ and constant clustering in physical coordinates (stable

clustering model: $r_0(z) = r_0(z=0)(1+z)^{1-(3+\epsilon)/1.8}$ with $\epsilon = 0$, in comoving coordinates). They further adopted an Einstein-de Sitter universe (i.e. a flat Universe filled only with matter) and set $r_0(z=0) = 10$ Mpc/h. Their model yielded a comoving correlation scale length at $z = 3$, $r_0(z=3) \simeq 4$ Mpc/h, i.e. about a factor of 2 smaller than what indicated by current data (see Blain et al. 2004). Correspondingly, they have probably substantially underestimated the clustering fluctuations.

Recently, Takeuchi & Ishii (2004) have estimated the effect of clustering with reference to the Japanese AKARI (formerly known as ASTRO-F; Murakami 1998) satellite that will perform an all sky survey in 4 far-IR bands, in the wavelength range 2-180 μm. They find that, between 60 and 170 μm, clustering increases by ~ 10 per cent the detection limit derived considering only Poisson fluctuations. Their result is thus compatible with our estimate for the MIPS/Spitzer 160μm channel.

It must be stressed that only fluctuations due to extragalactic point sources have been considered here. Additional contributions of varying importance (depending on the wavelength and on the position in the sky of the surveyed area) come from Galactic (synchrotron, free-free, interstellar dust) and zodiacal emissions. At millimeter wavelengths the graininess of the sky is actually dominated by fluctuations of the cosmic microwave background. Further fluctuations may be produced by Sunyaev-Zel'dovich effects in groups and clusters of galaxies. Last, but not least, in order to provide a complete determination of the sensitivity of a survey one also has to allow for instrumental noise. Therefore, the values of S_d quoted in Tables 3.1-3.2 must only be regarded as lower limits.

3.5 Conclusions

In this chapter I have presented detailed predictions for the confusion noise due to extragalactic sources in the far-IR/(sub)-millimeter channels of ESA/ISO, NASA/Spitzer, ESA/Herschel and ESA/Planck satellites, including the contribution from clustering of unresolved SCUBA-like galaxies. Clustering is found to increase the confusion noise, compared to the case of purely Poisson fluctuations, by 10–15% for the lowest frequency (and lowest

angular resolution) Spitzer and Herschel channels, by 25–35% for the 175 μm ISOPHOT channel, and to dominate in the case of Planck/HFI channels for $\nu \geq 143$ GHz.

It is worth noting that, although the calculations performed here make use of a specific evolutionary model for SCUBA-like galaxies (Granato et al. 2004), the results are strongly constrained by the observed counts and by data on the redshift distribution of SCUBA sources, and therefore are not expected to be heavily model dependent. The main uncertainty arises from the poor observational definition of the source clustering properties, for which I have assumed the two models described in the previous chapter.

Chapter 4

Effect of clustering on extragalactic source counts with low-resolution instruments

4.1 Introduction

It has long been known (Eddington 1913) that the counts (or flux estimates) of low signal-to-noise sources are biased high because there are more faint sources on top of positive noise fluctuations than bright sources on top of negative ones. Contributions to the noise arise both from the instrument and from source confusion. The latter, which may dominate already at relatively bright fluxes in the case of low-resolution surveys, comprises the effect of Poisson fluctuations and of source clustering. For angular scales where the correlation of source positions is significant, the ratio of clustering to Poisson fluctuations increases with angular scale (De Zotti et al. 1996), so that the confusion limit can be set by the effect of clustering. This is the case for some far-IR and for sub-mm surveys from space, due to the relatively small primary apertures and to the presence of strongly clustered populations (i.e. SCUBA-like galaxies).

While the effect of Poisson confusion on source counts has been investigated both analyti-

cally (Scheuer 1957; Murdoch et al. 1973; Condon 1974; Hogg & Turner 1998) and through numerical simulations (Eales et al. 2000; Hogg 2001; Blain 2001), the effect of clustering received far less attention. The numerical simulations by Hughes & Gaztañaga (2000) focused on the sampling variance due to clustering. More recently, algorithms successfully simulating the 2D distribution of clustered sources over sky patches as well as over the full sky have been presented by Argüeso et al. (2003) and González-Nuevo et al. (2005), who also discussed several applications. Some efforts have been made to quantify theoretically the effect of clustering on the confusion noise (see also the detailed analysis performed in chapter 2) but not on the source counts.

In this chapter, I will use the counts of neighbors formalism (Peebles 1980, hereafter P80) and numerical simulations to address this problem. The formalism is described in Section 4.2; Section 4.3 describes the simulations and presents applications to the 850 μm survey with Planck/HFI and to the 500 μm Herschel/SPIRE surveys. In Section 4.4 I briefly discuss the possibility of studying proto-clusters at high-z by combining Planck and Herschel observations. Section 4.5 summarizes the main conclusions.

4.2 Formalism

While in the case of a Poisson distribution a source is observed on top of a background of unresolved sources that may be either above or below the all-sky average, in the case of clustering sources are preferentially located in over-dense environments and one therefore measures the sum of all physically related sources in the resolution element of the survey (on top of Poisson fluctuations due to unrelated sources seen in projection).

If the beam-width corresponds to a substantial fraction of the clustering size, the observed flux is, generally, well above that of any individual source. Thus, to estimate the counts one cannot refer to the source luminosity function, but must define the distribution of luminosities, $L_{cl}(z)$, of source "clumps", as a function of redshift z. It has long been known (Kofman et al. 1994; Taylor & Watts 2000; Kayo et al. 2001) that a log-normal function is remarkably successful in reproducing the statistics of the matter-density distribution

found in a number of N-body simulations performed within the CDM framework, not only in weakly non-linear regimes, but also in more strongly non-linear regimes, up to density contrasts $\delta \approx 100$. Furthermore, it displays the correct asymptotic behavior at very early times, when the density field evolves linearly and its distribution is still very close to the initial Gaussian one (Coles & Jones 1991).

If light is a (biased) tracer of mass, fluctuations in the luminosity density should obey the same statistics of the matter-density field. I therefore adopt a log-normal shape for the distribution of L_{cl}. Such a function is completely specified by its first (mean) and second (variance) moments, that can be evaluated by using the counts of neighbors formalism.

The mean number of objects inside a volume V centered on a given source, $\langle N \rangle_p$, is [see equation (36.23) of P80]:

$$\langle N \rangle_p = n \int_V [1 + \xi(r)] dV \ , \tag{4.1}$$

where n is the mean volume density of the sources and ξ is their two-point spatial correlation function. The excess of objects (with respect to a random distribution) around the central one is then given by the second term on the right-hand side of this equation. The variance around the mean value $\langle N \rangle_p$ can instead be written as [equation (36.26) of P80]:

$$\langle (N - \langle N \rangle_p)^2 \rangle_p = \langle N \rangle_p + n^2 \int_V \int_V [\zeta(r_1, r_2) + \xi(r_{12}) - \xi(r_1)\xi(r_2)] dV_1 dV_2 \ . \tag{4.2}$$

If the first term on the right-hand side dominates, the variance is approximately equal to the mean, as in the case of a Poisson distribution.

The second term on the right-hand side of equation (4.2) is related to the skewness of the source distribution and exhibits a dependence on the reduced part of the three-point angular correlation function, ζ, for which I adopt the standard hierarchical formula:

$$\zeta(r_1, r_2) = Q[\xi(r_1)\xi(r_2) + \xi(r_1)\xi(r_{12}) + \xi(r_{12})\xi(r_2)]. \tag{4.3}$$

In the local Universe, observational estimates of the amplitude Q indicate nearly constant values, in the range $Q \simeq 0.6$–1.3, on scales smaller than ~ 10 Mpc/h (Peebles & Groth 1975; Fry & Seldner 1982; Jing & Boerner 1998, 2004). On larger scales, i.e. in the weakly non-linear regime where $\xi \lesssim 1$, the non-linear perturbation theory - corroborated by N-body

simulations - instead predicts Q to show a dependence on the scale (Fry 1984; Fry et al. 1993; Jing & Boerner 1997; Gaztañaga & Bernardeau 1998; Scoccimarro et al. 1998).

From equations (4.1) and (4.2) I can derive, at a given redshift z, the mean luminosity of the clump, $\overline{L}_{cl}$, and its variance, $\sigma^2_{L_{cl}}$:

$$\overline{L}_{cl}(z) = \overline{L}(z) + \int_{\mathcal{L}} dL' L' \Phi(L', z) \cdot \int_V [1 + \xi(r, z)] f(\theta) dV \tag{4.4}$$

and

$$\begin{aligned} \sigma^2_{L_{cl}}(z) &= \sigma^2_L + \int_{\mathcal{L}} dL' L'^2 \Phi(L', z) \int_V [1 + \xi(r, z)] dV \\ &+ \left[\int_{\mathcal{L}} dL' L' \Phi(L', z)\right]^2 \cdot \int \int_V [\zeta(r_1, r_2, z) + \xi(r_{12}, z) - \xi(r_1, z)\xi(r_2, z)] f(\theta_1) f(\theta_2) dV_1 dV_2 . \end{aligned} \tag{4.5}$$

In both the above equations, luminosities are given for unit frequency interval and are computed at the wavelength $\lambda_e = \lambda_o/(1+z)$, where λ_o is the wavelength of observation. The range of integration in luminosity is $\mathcal{L} = [L_{\min}, L_{\max}]$, where $L_{\min}$ and $L_{\max}$ are, respectively, the minimum and the maximum intrinsic luminosity of the sources. Φ is the luminosity function (LF) of the sources, while $f(\theta)$ is the response function of the instrument supposed to carry out the observations. I will assume $f(\theta)$ to be axially symmetric and Gaussian:

$$f(\theta) = e^{-(\theta/\Theta)^2/2}, \tag{4.6}$$

with

$$\Theta = \frac{\mathrm{FWHM}}{2\sqrt{2 \ln 2}} , \tag{4.7}$$

FWHM being the Full Width at Half Maximum of the instrument.

In equation (4.4) $\overline{L}(z)$ represents the mean luminosity of the sources located at redshift z

$$\overline{L}(z) = \frac{\int_{\mathcal{L}} dL' L' \Phi(L', z)}{\int_{\mathcal{L}} dL' \Phi(L', z)} \tag{4.8}$$

and accounts for the fact that the resolution element of the telescope is assumed to contain at least one source. The second term on the right-hand side of equation (4.4) adds the mean contribution of the neighbors.

The first term on the right-hand side of equation (4.5) accounts for fluctuations around $\bar{L}(z)$, that is

$$\sigma_L^2(z) = \frac{\int_{\mathcal{L}} dL'[L' - \bar{L}(z)]^2 \Phi(L', z)}{\int_{\mathcal{L}} dL' \Phi(L', z)}, \tag{4.9}$$

while the other two terms arise from the fluctuations of neighbor luminosities (second term) and of neighbor numbers (third term).

From the assumed log-normal shape of the distribution of L_{cl}, the probability that the sum of luminosities of sources in a clump at redshift z amounts to L_{cl} is then given by:

$$p(L_{cl}, z) = \frac{\exp\left[-\frac{1}{2}[\ln(L_{cl}) - \mu_g(z)]^2/\sigma_g^2(z)\right]}{\sqrt{2\pi\sigma_g^2(z)}L_{cl}}\ , \tag{4.10}$$

where

$$\mu_g(z) = \ln\left[\frac{\overline{L}_{cl}^2(z)}{\sqrt{\sigma_{L_{cl}}^2(z) + \overline{L}_{cl}^2(z)}}\right], \tag{4.11}$$

$$\sigma_g^2(z) = \ln\left[\frac{\sigma_{L_{cl}}^2(z)}{\overline{L}_{cl}^2(z)} + 1\right]. \tag{4.12}$$

An estimate of the "clump" luminosity function, $\Psi_{\rm clump}(L_{cl}, z)$, is then provided by equation (4.10) apart from the normalization factor that can be obtained by imposing conservation of the luminosity density:

$$\int_{\mathcal{L}_{cl}} \Psi_{\rm clump}(L_{cl}, z) L_{cl} dL_{cl} = \int_{\mathcal{L}} \Phi(L, z) L dL\ , \tag{4.13}$$

The integration in L_{cl} is performed in the range $\mathcal{L}_{cl} = [L_{cl,\rm min}, L_{cl,\rm max}]$ where $L_{cl,\rm min}$ and $L_{cl,\rm max}$ are respectively the minimum and the maximum luminosity of the clumps.
Note that, according to equation (4.13) the shift to higher luminosities of $\Psi_{\rm clump}$ compared to Φ is compensated by a decrease of the former function compared to the latter at low luminosities, as low luminosity sources merge to produce a higher luminosity clump.

If the clustering terms in equations (4.4)-(4.5) are much larger than those due to individual sources (L_m and σ_L^2, respectively), the survey will detect "clumps" rather then individual sources, and I can use $\Psi_{\rm clump}(L_{cl}, z)$ to estimate the corresponding counts.

4.3 Applications

I will apply the above formalism to the case of SCUBA-like galaxies observed at sub-mm wavelengths with

- ▷ the 850 μm channel of the High Frequency Instrument (HFI) of the ESA Planck satellite (FWHM=300$''$; Lamarre et al. 2003);
- ▷ the 500 μm channel of the Spectral and Photometric Imaging REceiver (SPIRE) of the ESA Herschel satellite (FWHM=34.6$''$; Griffin et al. 2000).

4.3.1 Models for the two- and three- point correlation functions

For the evolving two-point spatial correlation function, $\xi(r,z)$, of SCUBA galaxies I adopt *model 2* presented in chapter 2:

$$\xi(r,z) = b^2(M_{\rm eff},z)\xi_{\rm DM}(r,z), \tag{4.14}$$

with $M_{\rm eff} = 1.8 \times 10^{13}\, M_{\odot}/{\rm h}$.

For the amplitude, Q, of the three-point angular correlation function, ζ [equation (4.3)], I consider three models:

(i) $Q(z) = Q(0) = 1$,

(ii) $Q(z) = Q(0)/b(M_{\rm eff},z) = 1/b(M_{\rm eff},z)$,

(iii) $Q(z) = Q(0)/b^2(M_{\rm eff},z) = 1/b^2(M_{\rm eff},z)$,

where any dependence of Q on scale has been neglected. Both calculations based on perturbation theory (e.g. Juszkiewicz, Bouchet & Colombi 1993; Bernardeau 1994) and N-body simulations (e.g. Colombi, Bouchet & Hernquist 1996; Szapudi et al. 1996) suggest that model (i) applies to dark matter. On the other hand, the three-point correlation of luminous objects decreases as the bias factor b increases (Bernardeau & Schaeffer 1992, 1999; Szapudi et al. 2001); the formula (ii), derived from perturbation theory, is expected to hold on scales $\gtrsim 10$ Mpc/h (Fry & Gaztañaga 1993) while for scales smaller than these, Szapudi et al. (2001) quote model (iii) as a phenomenological rule derived from N-body simulations.

A more realistic model should allow for the dependence of Q on the linear scale, induced by the increasing strength of non-linear effects with decreasing scale. The models (i)-(iii) may thus bracket the true behavior of $Q(z)$, which should, however, be not far from model (iii) for the scales of interest here.

4.3.2 Numerical simulations

To test the reliability of our analytical approach, numerical simulations of sky patches were performed using the fast algorithm recently developed by González-Nuevo et al. (2005) which is able to produce realistic two-point distributions of clustered extragalactic point sources. In order to perform such simulations we have directly involved Joaquin González-Nuevo in the present work.

Only SCUBA galaxies were taken into account in the computations. Sources were first randomly distributed over the patch area, with surface densities given, as a function of the flux density, by the model of Granato et al. (2004); we have considered sources down to $S_{\rm min} = 0.01\,{\rm mJy}$. Then, the projected density contrast as a function of position, $\delta(\mathbf{x})$, was derived and its Fourier transform, $\delta(\mathbf{k})$, was computed. Next, in Fourier space, the power spectrum, $P_{cl}(k)$, computed from the two-point angular correlation function, $w(\theta)$, of unresolved SCUBA-like galaxies (see chapter 2, *model 2*), was added to the white noise power spectrum, $P_{Poiss}(k)$, corresponding to the initial spatial distribution. In this way, the transformed density field, $\delta_{corr}(k)$, of spatially correlated sources was obtained:

$$\delta_{corr}(k) = \delta(k)\frac{\sqrt{P_{Poiss}(k) + P_{cl}(k)}}{\sqrt{P_{Poiss}(k)}} \tag{4.15}$$

Finally, the inverse Fourier transform was applied to get the projected distribution of clustered sources in the real space and the fluxes were associated randomly to the simulated sources according to the differential counts predicted by the model of Granato et al. (2004) (for more details, see González-Nuevo et al. 2005).

In the Planck/HFI case, we have simulated sky patches of $12^{\circ}.8 \times 12^{\circ}.8\,{\rm deg}^2$ with pixels of $1.5 \times 1.5\,{\rm arcmin}^2$. In the Herschel/SPIRE case the patches were of $3^{\circ}.28 \times 3^{\circ}.28\,{\rm deg}^2$ and the pixel size was 1/3 of the FWHM.

To check the simulation procedure we have compared the confusion noise, σ,

obtained from it with the analytical results presented in the previous chapter. In the case of Planck/HFI, the simulations give $\sigma_P = 20\,\mathrm{mJy}$ and $\sigma_C = 50\,\mathrm{mJy}$ for Poisson distributed and clustered sources, respectively, in very good agreement with the analytic results, $\sigma_P = 20\,\mathrm{mJy}$ and $\sigma_C = 53\,\mathrm{mJy}$. For the Herschel/SPIRE channel the simulations give $\sigma_P = 6.4\,\mathrm{mJy}$ and $\sigma_C = 1.2\,\mathrm{mJy}$, to be compared with $\sigma_P = 6.0\,\mathrm{mJy}$ and $\sigma_C = 3.2\,\mathrm{mJy}$ (see chapter 2, Table 2). The discrepancy of the results for σ_C actually corresponds to the uncertainty in this quantity, very difficult to determine from the simulations when Poisson fluctuations dominate.

Note that, for the angular resolutions considered here, the very steep counts predicted by the Granato et al. (2004) model determine both Poisson and clustering fluctuations to be essentially independent of the flux limit.

We have also checked that the results obtained from simulations are independent of the pixel size used.

4.3.3 Observations with Planck at 850μm

According to equation (4.4), the mean luminosity of the clump comprises a Poisson term, $\propto \int_V f(\theta)dV$, which accounts for the contributions due to randomly-distributed sources within the resolution (comoving) volume V, and a clustering term, $\propto \int_V \xi(r) f(\theta)dV$, contributed by sources in excess with respect to a Poisson distribution. It is easy to show that

$$\int_V f(\theta)dV = \frac{\pi}{2} r_{\max}[(1+z)d_A(z)\mathrm{FWHM}]^2 \ , \tag{4.16}$$

where $d_A(z)$ is the angular diameter distance [here accompanied by the extra term (1+z) to obtain the transverse *comoving* distance], while $r_{\max}$ represents the maximum (comoving) radius of the clump [assumed to be $> (1+z)d_A(z)\mathrm{FWHM}$]. If, just for illustrative purposes, one adopts the usual power-law model $\xi(r) = (r_0/r)^{1.8}$ cut at $r_{\max}$, the integral of the two-point correlation function in equation (4.4) gives:

$$\int_V \xi(r) f(\theta)dV \simeq 9.3\ r_0^{1.8}\,[(1+z)d_A(z)\mathrm{FWHM}]^{1.2} \ . \tag{4.17}$$

Fig. 4.1 shows the different contributions to the mean luminosity of a clump of SCUBA galaxies as a function of the FWHM, for observations performed at 850μm and for differ-

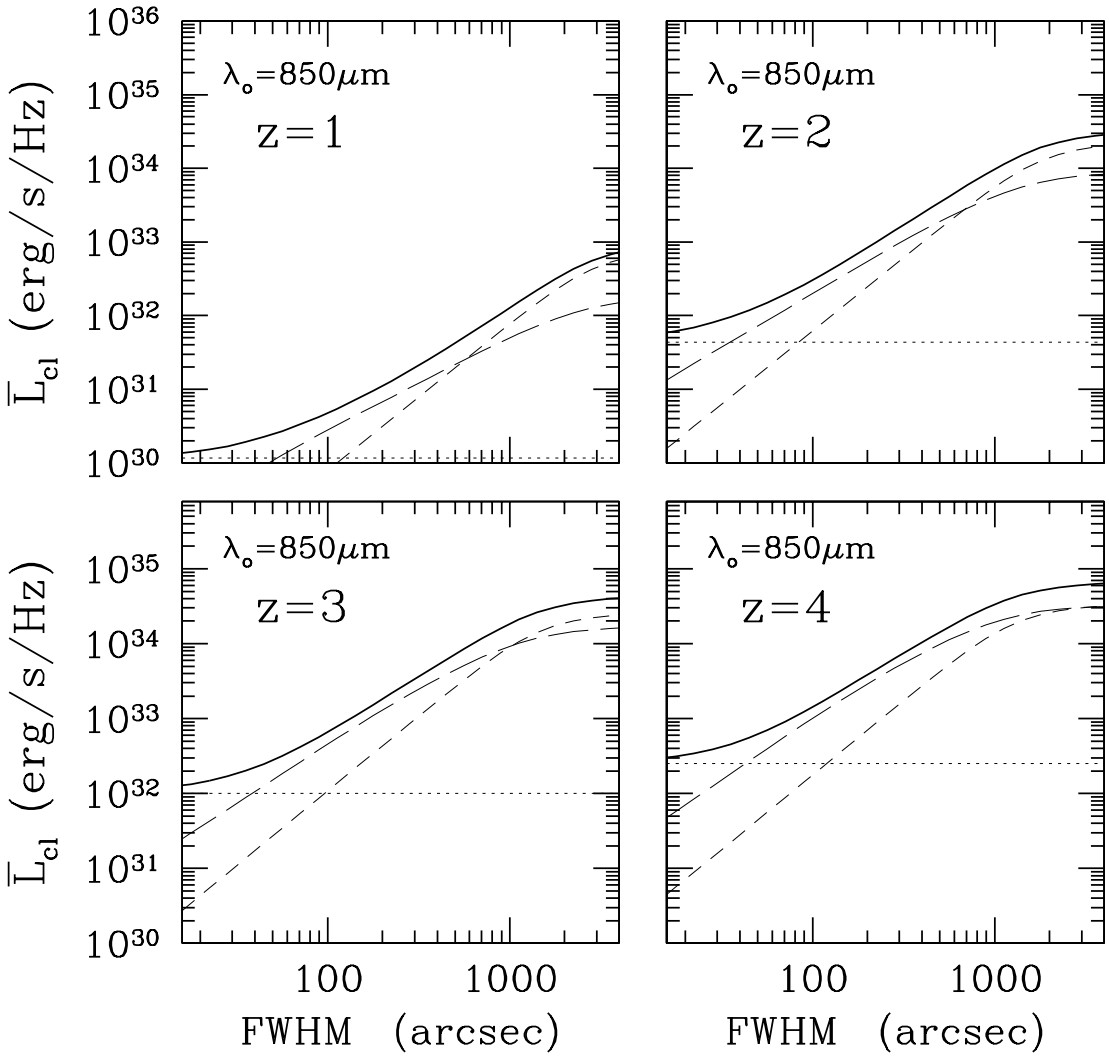

Figure 4.1: Mean luminosity of a clump $\bar{L}_{cl}(z)$ (thick solid curve), as a function of the Full Width at Half Maximum (FWHM) of the telescope, for observations performed at 850μm and for a clump that is located at redshift $z = 1$ (top left-hand panel), $z = 2$ (top right-hand panel), $z = 3$ (bottom left-hand panel) and $z = 4$ (bottom right-hand panel). The thin curves represent the different contributions to $\bar{L}_{cl}$ arising from the mean luminosity of a single source located at redshift z (dotted line), the mean luminosity of sources contained in the volume V ($\propto \int_V f(\theta)dV$; short-dashed curve) and the excess luminosity due to the mean source overdensity ($\propto \int_V \xi(r)f(\theta)dV$; long dashed curve).

ent values of the redshift at which the clump is located. The two-point spatial correlation function adopted here for SCUBA galaxies [equation (4.14)] is flatter on small scales than a power-law model with the standard slope 1.8. As a consequence, the clustering contribution to $\bar{L}_{cl}(z)$, represented by the long dashed curve, is less steep than what predicted by equation (4.17). The mean luminosity of sources within the volume V, provided by the term $\propto \int_V f(\theta)dV$ in equation (4.4) (short-dashed curve) has been computed by assuming $r_{\rm max} = 3r_0$, with $r_0 = 8.3\ h^{-1}$Mpc, according to *model 1* described in chapter 2. I will keep this choice for $r_{\rm max}$ throughout the following analysis.

As expected, at the angular resolution of Planck (FWHM=300$''$), the clustering term dominates over the Poisson one, particularly at high redshift ($z \gtrsim 2$) as an effect of the strong increase of the bias parameter, $b(M_{\rm eff}, z)$, with look-back time. The flattening of the curves at FWHM$\gtrsim$1000$''$ follows from the fact that at those angular scales the resolution volume encompasses the maximum radius of the clump and the integrals over volume in equations (4.16)-(4.17) saturate.

The variance of clump luminosities comprises three distinct terms, as already pointed out in section 4.2. In Fig. 4.2, I show their contributions to $\sigma_{L_{cl}}$ as a function of the FWHM, at 850μm and for different values of the redshift of the clump in the range $z = 1 - 4$. The term which encodes the dependence on the reduced three-point correlation function (whose rms will be denoted as $\sigma^{(3)}_{L_{cl}}$ hereafter) is shown for the three models of $Q(z)$ illustrated in subsection 4.3.1: model (i), long-dashed curve; model (ii), dotted short-dashed curve; model (iii), dotted long-dashed curve. Note that, for those models in which $Q(z)$ decreases with look-back time, the double integration of volume in equation (4.5) is positive only for relatively high values of the FWHM, in particular for high-z clumps.

It can be shown that the condition $(\sigma^{(3)}_{L_{cl}})^2 \geq 0$ is satisfied only if:

$$Q(z) \geq \frac{A^2 - C}{A^2 + 2B}, \tag{4.18}$$

where

$$A = \int_V \xi(r, z) f(\theta) dV, \tag{4.19}$$

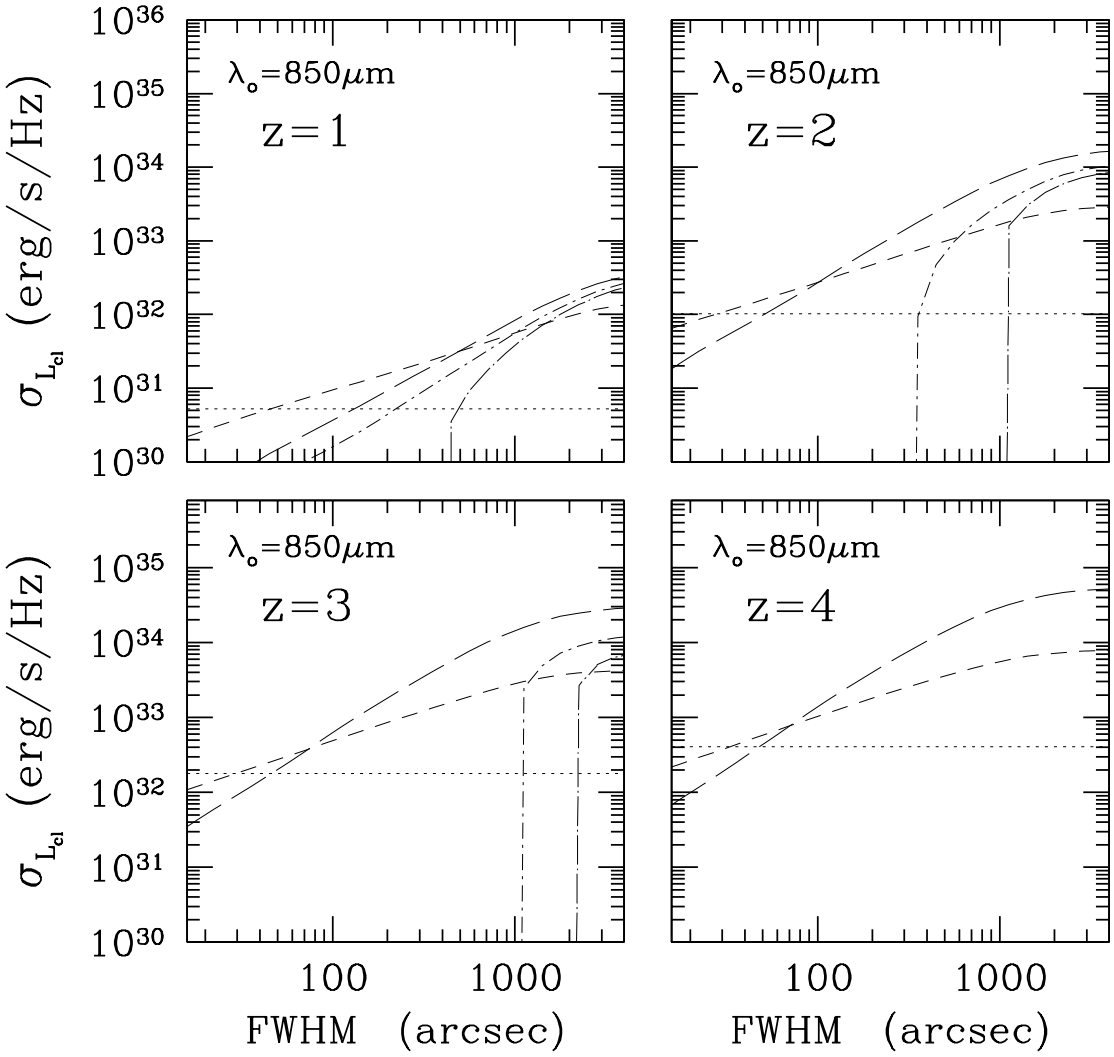

Figure 4.2: Contributions to the rms of the luminosity of a clump $\sigma_{L_{cl}}(z)$, as a function of the Full Width at Half Maximum (FWHM) of the telescope, for observations performed at 850μm and for a clump that is located at redshift $z = 1$ (top left-hand panel), $z = 2$ (top right-hand panel), $z = 3$ (bottom left-hand panel) and $z = 4$ (bottom right-hand panel). The dotted lines show the rms fluctuations around the mean luminosity of a source located at redshift z (σ_L), while the short-dashed curves describe the contribution arising from the fluctuations in the luminosity of the members of the clump. The other curves represent the contribution to $\sigma_{L_{cl}}(z)$ due to fluctuations in the number of the clump members, for three different models for the evolution of the amplitude of the three-point correlation function, $Q(z)$: model (i), long dashed curve; model (ii), dotted short-dashed curve; model (iii), dotted long-dashed curve.

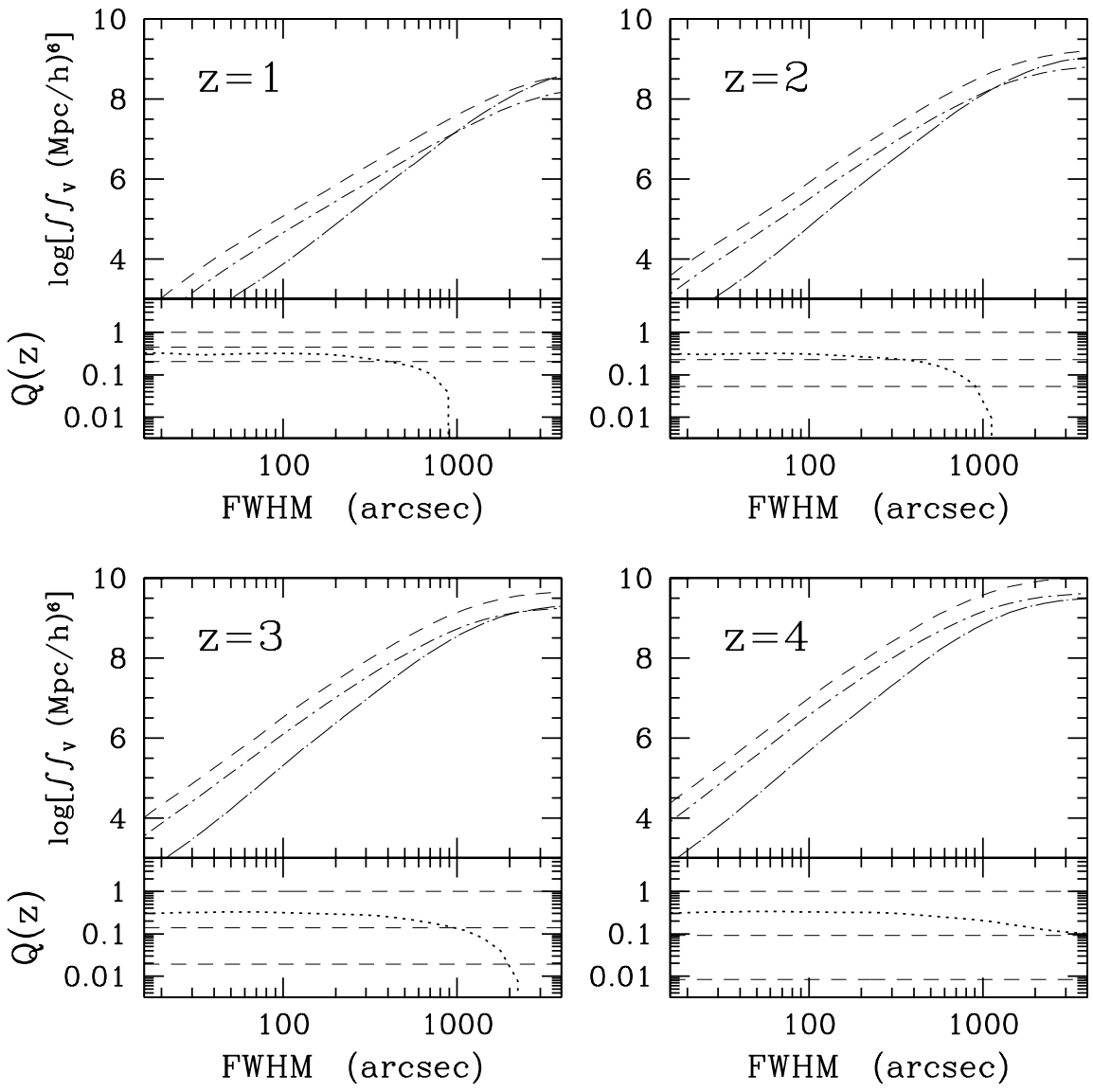

Figure 4.3: *Upper box of each panel*: dependence on the FWHM of the terms A^2 (dotted short-dashed curve), C (dotted long-dashed curve) and A^2+2B (dashed curve) for different values of the redshift of the clumps: $z = 1$ (top left-hand panel), $z = 2$ (top right-hand panel), $z = 3$ (bottom left-hand panel), $z = 4$ (bottom right-hand panel). *Lower box of each panel*: the corresponding value of the ratio $(A^2 - C)/(A^2 + 2B)$ is shown by the dotted line and compared to that of the amplitude of the three point correlation function, $Q(z)$, as predicted by the three models described in subsection 4.3.1: model (i), upper dashed curve; model (ii), middle dashed curve; model (iii), lower dashed curve.

$$B = \int\int_V \xi(r_1, z)\xi(r_{12}, z) f(\theta_1) f(\theta_2) dV_1 dV_2, \quad (4.20)$$

$$C = \int\int_V \xi(r_{12}) f(\theta_1) f(\theta_2) dV_1 dV_2. \quad (4.21)$$

Since the ratio on the right-hand side of equation (4.18) is always lower than 1, model (i) provides non negative values for $(\sigma^{(3)}_{L_{cl}})^2$ for any angular resolution of the instrument. Less trivial is the situation for models (ii) and (iii) since in these cases the satisfaction of the condition (4.18) depends on the relative importance of the terms A^2, C and $A^2 + B$ for any given value of the FWHM and of redshift.

The upper box of each panel of Fig. 4.3 shows the dependence on the FWHM of A^2 (dotted short-dashed curve), C (dotted long-dashed curve) and A^2+2B (dashed curve), for different values of the redshift of the clumps: from $z = 1$ (top left-hand panel) up to $z = 4$ (bottom right-hand panel). In the lower boxes of the same panels the corresponding value of the ratio $(A^2 - C)/(A^2 + 2B)$ (dotted line) is compared to that of the parameter $Q(z)$ for the three models adopted here: model (i), upper dashed curve; model (ii), middle dashed curve; model (iii), lower dashed curve. Compared to A^2, the term C rises steeply for increasing FWHM; such a behavior can be accounted for by a qualitative analysis of the integrals (4.20)-(4.21): the integrations of the spatial correlation function, $\xi(r)$, over the resolution volume V are equivalent to integrations of the corresponding angular correlation function, $w(\theta)$, over the beam of the telescope. If (again for illustrative purpose) one assumes $\xi(r) = (r/r_0)^{-\gamma}$ than the Limber equation implies $w(\theta) \propto \theta^{1-\gamma}$, and by keeping in mind that the solid angle scales like θ^2 one gets:

$$A^2 = \left[\int_{\rm beam} w(\theta) d\Omega\right]^2 \propto (\Theta^{1-\gamma}\Theta^2) \propto {\rm FWHM}^{2(3-\gamma)} \quad (4.22)$$

$$B = \int\int_{\rm beam} w(\theta_1) w(\theta_2) d\Omega_1 d\Omega_2 \propto \Theta^{1-\gamma}\Theta^{1-\gamma}\Theta^2\Theta^2 \propto {\rm FWHM}^{2(3-\gamma)} \quad (4.23)$$

$$C = \int\int_{\rm beam} w(\theta_{12}) d\Omega_1 d\Omega_2 \propto \Theta^{1-\gamma}\Theta^2\Theta^2 \propto {\rm FWHM}^{(5-\gamma)} \quad (4.24)$$

These results, tested for different values of the slope γ by means of direct numerical integrations, provide a qualitatively explanation for the different behaviors of the terms plotted in Fig. 4.3. In particular, due to its steeper dependence on the angular resolution, the term C exceeds A^2 at high values of the FWHM. When this happens the ratio on the right-hand side of equation (4.18) becomes negative and all the adopted models for $Q(z)$ give positive

values for $(\sigma^{(3)}_{L_{cl}})^2$. This accounts for the shape of the term $\sigma^{(3)}_{L_{cl}}$ plotted in Fig. 4.2, in particular for its sharp cut-off at low values of the FWHM. I will set $(\sigma^{(3)}_{L_{cl}})^2 = 0$ when the condition (4.18) is not satisfied.

Fig. 4.4 shows the luminosity function (LF), per unit logarithmic interval, of the clumps at 850 μm as derived from equation (4.10) by assuming the angular resolution of Planck. For comparison, the value of the mean luminosity, $\bar{L}(z)$, of a source located at the same redshift of the clump has been represented by a vertical dotted line. According to the above discussion, the LF predicted by assuming models (ii) and (iii) for the amplitude of the three-point correlation function are indistinguishable for $z \gtrsim 2$, since at these redshifts (and for the angular resolution of Planck) the condition (4.18) does not hold and $(\sigma^{(3)}_{L_{cl}})^2$ is set to zero. The distribution of the clump luminosities comprises a tail of bright "sources" whose luminosities can be hundred times greater than $\bar{L}(z)$; in particular, for the case $Q(z) = 1$, the brightest clumps will fall well above the 5σ detection limit of Planck (i.e. 288 mJy, according to the results obtained in chapter 3), indicated in the same figure by the vertical arrows. The detection and measured abundance of such clumps would then set important constraints on the evolution of the three point correlation function, since the latter quantity, by determining the skewness of the luminosity distribution, influences the extension of the bright tail of the LF.

The effect of clustering on the source counts as derived from the formalism presented here for the Planck/HFI 850 μm channel is illustrated in Fig. 4.5, where the solid line gives the counts of SCUBA galaxies predicted by the model of Granato et al. (2004), and the dotted line gives the summed counts of spiral and starburst galaxies, and of extragalactic radio sources. For the redshift-dependent luminosity functions of spiral and starburst galaxies I have adopted the same phenomenological models illustrated in the previous chapter, while for radio galaxies I have used the model by De Zotti et al. (2005). The short-dashed, dotted short-dashed, and dotted long-dashed lines show the counts of "clumps" expected from our analytic formalism for the three evolution models of the amplitude Q of the three-point correlation function. As expected, at the Planck/HFI resolution the counts of "clumps"

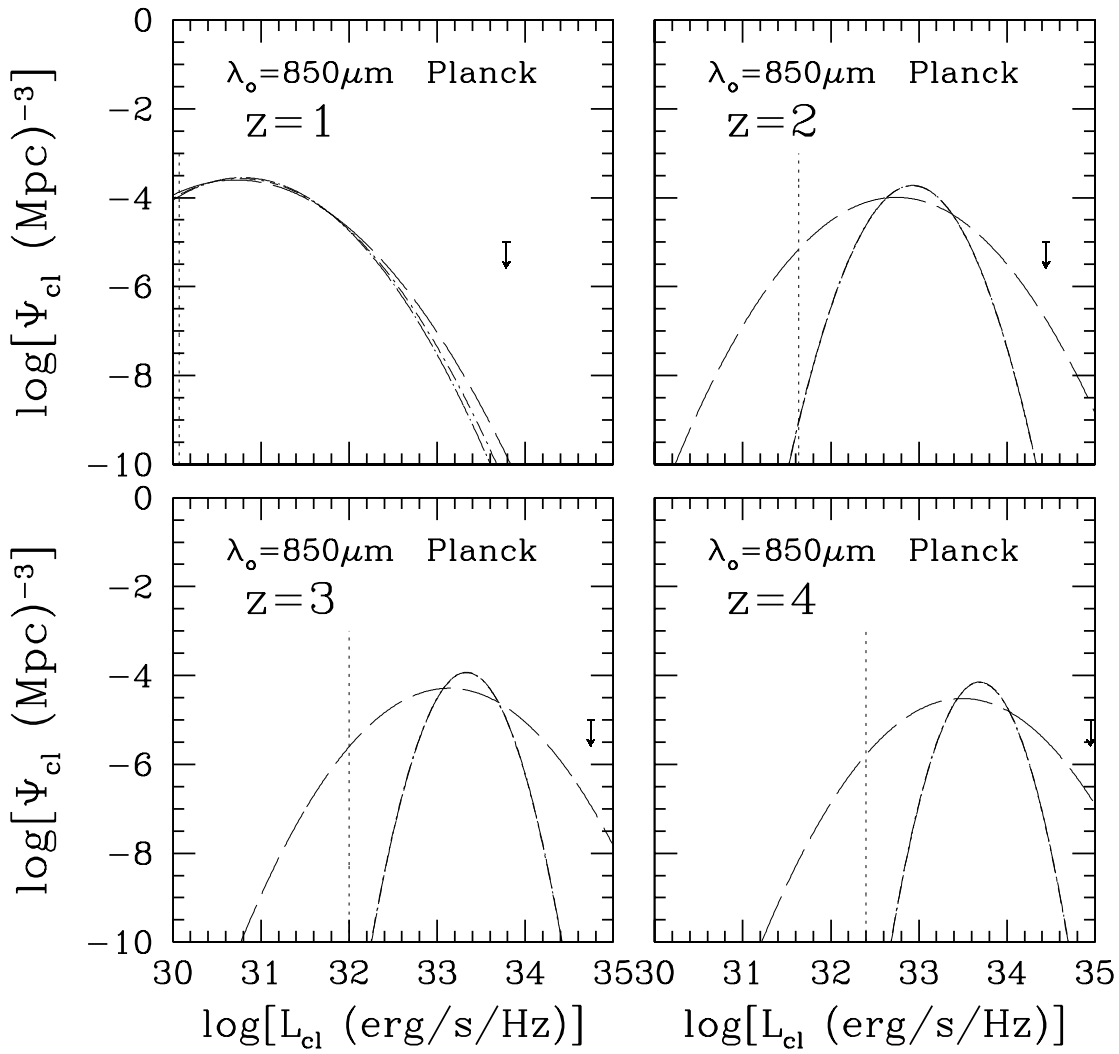

Figure 4.4: Luminosity function of the clumps (per unit logarithmic interval of L_{cl}) as a function of the luminosity of the clump, L_{cl}, for observations performed by Planck/HFI at 850μm and for different clump redshifts: $z = 1$ (left-hand top panel), $z = 2$ (right-hand top panel), $z = 3$ (left-hand bottom panel) and $z = 4$ (right-hand bottom panel). The curves show the LF obtained for three different models for the evolution of the amplitude of the three-point correlation function, $Q(z)$: model (i), long dashed curve; model (ii), dotted short-dashed curve; model (iii), dotted long-dashed curve. In the latter two cases the condition (4.18) is not satisfied for $z \gtrsim 1$ and $(\sigma^{(3)}_{L_{cl}})^2$ is set to zero; as a consequence, the corresponding curves are indistinguishable. The vertical dotted lines show, for comparison, the mean luminosity, $\bar{L}(z)$, of a source located at redshift z. The arrows indicate the minimum luminosity detectable by Planck at 850 μm for a 5σ detection limit of 288 mJy, as estimated in chapter 3.

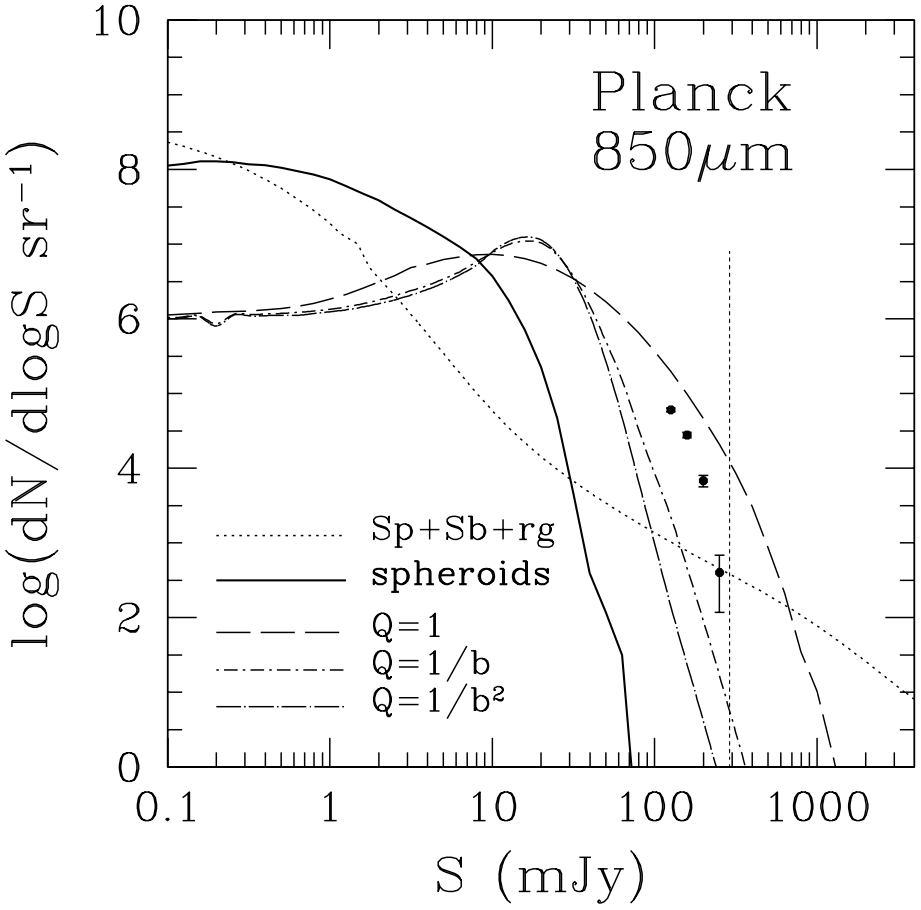

Figure 4.5: Differential source counts of SCUBA galaxies at 850 μm (solid line) compared with counts expected in the case of observations performed with the angular resolution of Planck/HFI (FWHM=300$''$) for the three models for the evolution of the amplitude of the three-point correlation function, $Q(z)$, (model (i): short dashed curve; model (ii): dotted short-dashed curve; model (iii): dotted long-dashed line). The summed contributions from (unclustered) spiral galaxies, starburst galaxies, and extragalactic radio sources is represented by the dotted curve. The filled circles with (1-σ Poisson) error bars show the counts estimated from the simulations (see text). The vertical dotted line shows the Planck/HFI 5σ detection limit ($S_d = 288$ mJy) estimated in the previous chapter by allowing for clustering fluctuations.

are sensitive to the evolution of the three-point correlation function. Clearly the predicted counts below $\simeq 50\,\mathrm{mJy}$, where Poisson fluctuations become important, are of no practical use; they are shown just to illustrate how the formalism accounts for the disappearance of lower luminosity objects which merge into the "clumps".

The filled circles with 1σ Poisson error bars in Fig. 4.5 are obtained by filtering the simulated maps with a Gaussian response function of $5'$ FWHM to mimic Planck/HFI observations. The lower flux limit of the estimated counts is set by Poisson fluctuations. It should be noted that the procedure used for the simulations only takes into account the two-point angular correlation function and does not allow us to deal with the three-point correlation function and its cosmological evolution, ingredient which is however included in the analytic model. In principle it is possible to go the other way round, i.e. to evaluate from the simulations the reduced angular bispectrum, b_r, by applying the standard Fourier analysis (González-Nuevo et al. 2005; Argüeso et al. 2003) and infer from it an estimate of the three-point correlation function weighted over the redshift distribution. However, the relationship of the three-point correlation function with the angular bispectrum involves a six dimensional integral which is really difficult to deal with in practice (Szapudi 2004). An alternative possibility consists in computing the number of triplets (above a fixed flux threshold) and in using the estimator developed by Szapudi & Szalay (1998) to derive an estimate of the three-point angular correlation function. On the whole, these methods turn out to be impractical if one also wants to take into account the effect of the evolving three-point correlation function when comparing simulations with analytic results. On the other hand, it is very reassuring that the counts obtained from simulations are within the range spanned by analytic models.

4.3.4 Observations with Herschel at 500μm

In the Herschel case (FWHM$\sim 35''$), the beam encompasses only a small fraction of the "clump" and therefore the observed flux is generally dominated by the single brightest source in the beam as it can be inferred from Fig. 4.1. Thus, the analytic model described in Section 4.2 is no longer applicable. As illustrated by the left-hand panel of Fig. 4.6, such formalism would strongly over-predict the observed counts at bright flux densities (and the

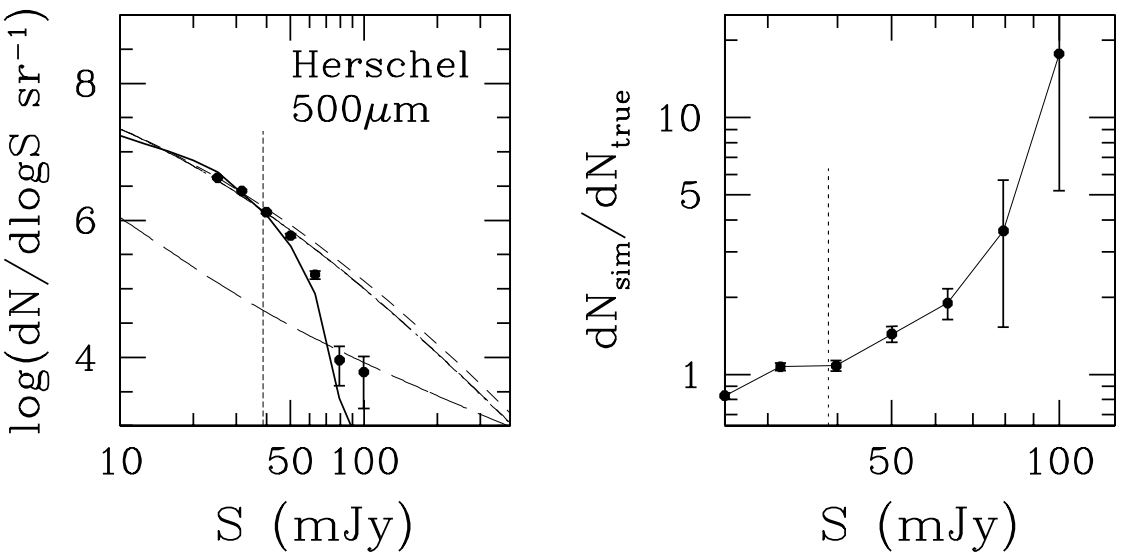

Figure 4.6: *Left-hand panel*: same as in Fig. 4.5 but for the 500 μm channel of Herschel/SPIRE (FWHM=34.6″). The results for models (ii) and (iii) for the evolution of $Q(z)$ overlap, while model (i) is only slightly higher. *Right-hand panel*: ratio between the differential counts of SCUBA galaxies estimated from the simulations for the Herschel/SPIRE resolution and those predicted by the model of Granato et al. (2004). The dotted vertical line, in both panels, corresponds to the 5σ detection limit (S_d = 38.6 mJy) estimated in chapter 2 also accounting for clustering fluctuations.

results are essentially independent of the three-point correlation function). On the other hand, the simulations (filled circles with error bars) show that neighbor sources appreciably contribute to the observed fluxes, hence to the counts at bright flux density levels, as more clearly illustrated by the right-hand panel of Fig. 4.6. Such count estimates were obtained filtering the simulated maps with a Gaussian response function of FWHM=34.6″, appropriate for the Herschel 500 μm channel; again, the lower flux limit of the estimated counts is set by Poisson fluctuations.

4.4 High-z proto-clusters detectable with Planck/HFI

The formalism presented here, supported by numerical simulations, suggests that Planck/HFI will be able to detect hundreds of clumps of SCUBA-like sources at high red-

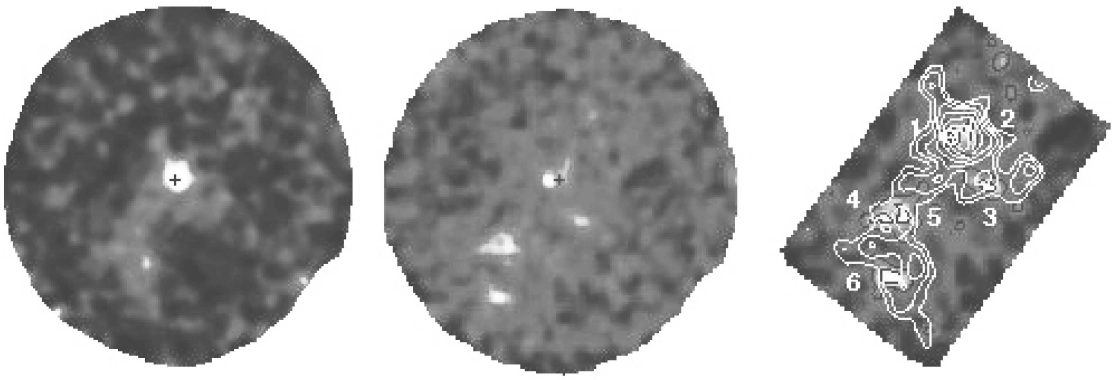

Figure 4.7: Submillimeter imaging of the field around an X-ray selected QSO obtained by Stevens et al. (2004). The left-hand panel shows the SCUBA 850 μm image (diameter $\sim 150''$, resolution $14.8''$). The middle panel shows the corresponding 450 μm image (diameter $\sim 120''$, resolution $8.5''$). The right-hand panel shows a signal-to-noise ratio image ($1.5' \times 1.0'$) at 450 μm (grey scale with back contours at 2, 3, 4 and 5 σ) overlaid with the 850 μm signal-to-noise ratio contours at 2, 3, 4 5, 6, 7 and 8 σ. The extent of the contoured region is ~ 400 kpc. Numbers on the right-hand panel identify 450 μm sources with peak signal-to-noise ratio greater than 3. The optical position of the QSO is marked with a plus sign on the left-hand and middle panels. (figure from Stevens et al. 2004).

shift, although they will probably show up as fluctuations just below the estimated 5σ detection limit. It is interesting to note that evidences of the existence of clumps of SCUBA-like galaxies have been obtained from sub-mm observations of the region surrounding high-z powerful radio galaxies and AGNs (Ivison et al. 2000; Stevens et al. 2003; 2004; Greve et al. 2006); in fact, these objects are generally used to find out proto-clusters in the distant Universe. The most significant example is that provided by Stevens et al. (2004) who found a filamentary structure of six massive star-forming proto-spheroids associated to an X-ray selected QSO at $z = 1.8$ (see Fig. 4.7). This clump exhibits a total flux of several tens of mJy at 850 μm and of few hundreds mJy at 450 μm and quite certainly represents the core region of a forming cluster. The areas mapped at 450 and 850 μm are of few arcmin^2 (equivalent to a linear size of ~ 400 kpc at $z = 2$), about 10 times smaller than the Planck beam at 850 μm. This means that the beam of Planck will encompass a much larger fraction of the clump, that is expected to extend over a clustering diameter ($2r_0 \sim 16$ Mpc comoving). Therefore, the flux measured by Planck should be much higher then the sum

of the fluxes of the sources detected by Stevens et al. (2004).

The counts and the redshift distribution of the high-z *proto-clusters* detectable by Planck will be extremely useful. They can be used to put independent constraints on the cosmological model and in particular on the presence and possible evolution of the dark energy component of the Universe (see e.g. Bartelmann et al. 2006). In fact, due to its influence on the clustering pattern, different evolutionary models for the dark energy can lead to different distributions of proto-clusters at redshift $z \gtrsim 1.5$. The abundance of high-z proto-clusters may also contain precious information on the statistical properties of the initial density perturbations, in particular for what concerns any possible deviation of their distribution from the Gaussian behavior; in fact the counts of rare high-redshift massive objects are determined by the high-density tail of the primordial density distribution function which is generally assumed to be close to a Gaussian. Since the Gaussian tail decays exponentially at high densities, even a small deviation from Gaussianity can lead to huge enhancements in the number densities (see e.g. Matarrese et al. 2000; Verde et al. 2001; Scoccimarro & Sefusatti 2004). Therefore the proto-clusters detectable by Planck should be powerful probes of primordial non-Gaussianity. Finally, the counts of the clumps could be used to constrain the time evolution of the three-point correlation function ζ, quantity which is very poorly constrained by the available data.

Obviously, Planck/HFI will also detect other populations of extragalactic sources (see Fig. 4.5), and in particular, relatively nearby dusty galaxies (starburst and normal late-type galaxies) that are likely to dominate the Planck counts, and flat-spectrum radio sources. These populations, however, are easily singled out since they are very bright at far-IR or radio frequencies and must therefore be included either in the IRAS or in radio catalogs.

A follow up with Herschel/SPIRE of previously uncatalogued HFI-detected "sources" could give the opportunity to understand the nature of individual galaxies within the selected proto-clusters. In fact, the higher resolution and sensitivity of SPIRE will probably allow us to resolve each proto-cluster into its members. As an example the members of

the protocluster detected by Stevens et al. (2004) have 450μm-fluxes in the range 30−45 mJy, comparable to the 5σ detection limits estimated in chapter 3 for the channels of Herschel/SPIRE. In addition, the clumps detectable by Planck will be typically more luminous than the one reported by Stevens et al. and therefore many components of the protoclusters are expected to have fluxes well above several tens of mJy in the wavelength-range covered by SPIRE.

Herschel data will then determine the sub-mm fluxes of the brighter active star-forming galaxies making up the proto-clusters and precisely locate them for further studies. Follow-up spectroscopy of just the brightest galaxy in each clump will provide the distances of all cluster members. This could be a very efficient way to determine the evolution of the sub-mm luminosity function, hence of the star-formation rate, and to investigate many other astrophysical properties of high-z galaxies, up to $z \sim 5$.

4.5 Conclusions

In the presence of strong clustering, low-resolution surveys measure the summed contributions of groups of sources within the beam. The counts of bright intensity peaks are therefore shifted to higher flux levels compared to the counts of individual sources detected with high-resolution instruments. If the beam-width corresponds to a sizable fraction of the clustering size, as in the case of Planck/HFI, one actually detects the fluxes of clumps of sources. In the Planck/HFI case the summed fluxes of physically correlated sources within the beam are generally much higher than the luminosity of the brightest source in the beam, so that the outcome of the surveys will be counts of "clumps" of sources rather than of individual sources. I have argued that the luminosity distribution of such "clumps" at any redshift can be modeled with a log-normal function, with a mean determined by the average source luminosity and by the average of summed luminosities of neighbors, and a variance made of three contributions (the variances of source luminosities, of neighbor luminosities, and of neighbor numbers). This latter contribution depends on the three-point correlation function, so that the counts of "clumps" can be used to get information on this elusive quantity and on its cosmological evolution. Under the, rather extreme, assumption that the

coefficient, Q, of the three-point correlation function is independent of redshift, the counts of "clumps" extend beyond the formal HFI 5σ detection limit. In the more likely cases of Q decreasing as b^{-1} or b^{-2}, b being the bias factor, the "clumps" will only show up in Planck maps as $< 5\sigma$ fluctuations. Nevertheless still a substantial number of them will show up at $\geq 3\sigma$ in all high frequency (≥ 350 GHz) HFI channels, so that highly significant detections can be obtained by combining data at different frequencies and using appropriate detection techniques (e.g. the Spherical Mexican Hat wavelet; see e.g. González-Nuevo et al. 2006).

The rich catalog of candidate proto-clusters at substantial redshifts (typically at $z \simeq 2$–3) that Planck/HFI could provide will be very important to investigate the formation of large scale structure and, particularly, to probe primordial non-Gaussianity and constrain the evolution of the dark energy thought to control the dynamics of the present day universe. Detailed numerical simulations carried out by using the fast algorithm recently developed by González-Nuevo et al. (2005) are fully consistent with the analytic results, although a full comparison would require an upgrade of the algorithm to include the effect of the evolving three-point correlation function.

As the ratio of the beam-width to the clustering angular size decreases, the observed fluxes approach those of the brightest sources in the beam and the "clump" formalism no longer applies. However, simulations show that also in the case of the Herschel/SPIRE $500\,\mu$m survey the contribution of neighbors to the observed fluxes enhances the bright tail of the observed counts. Due to the extreme steepness of such a tail, as predicted by the model of Granato et al. (2004), even a modest addition to the fluxes of the brightest sources may lead to counts at flux densities $\simeq 50 - 100$ mJy substantially higher than what would be observed with a higher resolution instrument. It should be noted that, in the case of strong clustering, the canonical 5σ detection limit (shown by the vertical dotted line in both panels of Fig. 4.6) does not free the observed counts from the confusion bias.

Finally, I have suggested that combining Planck and Herschel data will give the unprecedented opportunity of observing at the same time both the cosmological evolution of large scale structure and the astrophysical evolution of proto-cluster members up to very high redshifts. In particular, given the spectral properties of high-z proto-spheroidals and the sensitivity of the various channels of Herschel, I expect observations with SPIRE to be

well suited for identifying members of each protocluster.

Chapter 5

Clustering contribution to arcminute-scale CMB anisotropies

5.1 Introduction

In recent years different experiments (BIMA: Dawson et al. 2002; CBI: Mason et al. 2003, Readhead et al. 2004; ACBAR: Kuo et al. 2004), aimed at measuring the anisotropies of the cosmic microwave background (CMB) on arcmin angular scales, have detected signals at multipoles $\ell > 2000$ in excess of the expected primordial CMB anisotropies. The origin of this excess signal, in the range $16\,\mu\mathrm{K} \lesssim \Delta T \lesssim 26\,\mu\mathrm{K}$, is not well understood yet, although several possibilities have been discussed in the literature.

All experimental groups argue that it cannot be due to point-source contamination. If so, the most likely candidate is the thermal Sunyaev-Zeldovich (SZ) effect, which is expected to dominate CMB anisotropies on angular scales of a few arcminutes (Gnedin & Jaffe 2001). However, an interpretation based on SZ effects from clusters of galaxies (Bond et al. 2005; Komatsu & Seljak 2002) or due to the inhomogeneous plasma distribution during the formation of large scale structure (Zhang et al. 2002) would require values of σ_8 significantly higher ($\gtrsim 1$) than what indicated by current data ($\sigma_8 \sim 0.7 - 0.8$; Spergel et al. 2006). SZ effects associated with the formation and the early evolutionary phases of massive spheroidal galaxies could account for the BIMA signal, although some parameters need to

be stretched to their boundary values (De Zotti et al. 2004). Alternative interpretations of the excess signal advocate non-standard inflationary models (Cooray & Melchiorri 2002; Griffiths et al. 2003).

In this chapter I analyze the contributions of extragalactic point sources to the power spectrum on arcminute scales at 30 and 150 GHz, the frequencies relevant for BIMA, CBI and ACBAR experiments, including the clustering contribution from high-z proto-spheroidal galaxies. The outline of the chapter is as follows. In Section 5.2 I briefly resume the basic formalism concerning the power spectrum of temperature fluctuations; in Section 5.3 I describe the different source populations which give the dominant contributions to the number counts at cm and mm wavelengths. In Section 5.4 I present estimates for arcminute-scale CMB anisotropies due to extragalactic sources, while in Section 5.5 I summarize the main conclusions.

5.2 Power spectrum of temperature fluctuations: formalism

It is convenient to express the CMB temperature fluctuations, δT, in terms of spherical harmonics:

$$\delta T(\theta,\phi) = \sum_{\ell=0}^{\infty} \sum_{m=-\ell}^{\ell} a_\ell^m Y_\ell^m(\theta,\phi). \tag{5.1}$$

Within such a formalism, the angular correlation function of temperature anisotropies

$$C(\theta) = \langle \delta T(\theta',\phi') \delta T(\theta'',\phi'') \rangle \ , \tag{5.2}$$

θ being the separation between two generic positions in the sky, (θ',ϕ') and (θ'',ϕ''), takes on the following form

$$C(\theta) = \frac{1}{4\pi} \sum_{\ell=1}^{\infty} \sum_{m=-\ell}^{\ell} |a_\ell^m|^2 P_\ell(\cos\theta) \tag{5.3}$$

with

$$|a_\ell^m|^2 = 2\pi \int_0^\pi C(\theta) P_\ell(\cos\theta) \sin\theta d\theta \ , \tag{5.4}$$

where P_ℓ are the Legendre polynomials. These are exact relations, governing the actual correlation structure of the observed sky. However the sky we see is only one of infinitely many

possible realizations of the statistical process that yield the temperature perturbations; therefore we are interested in the *ensemble average power*. The angular power spectrum of temperature fluctuations, C_ℓ, is thus defined as the expectation value of $|a_\ell^m|^2$:

$$C_\ell \equiv \langle |a_\ell^m|^2 \rangle = \langle |a_\ell^0|^2 \rangle = 2\pi \int_0^\pi C(\theta) P_\ell(\cos\theta) \sin\theta d\theta \ , \tag{5.5}$$

and the angular correlation function writes

$$C(\theta) = \frac{1}{4\pi} \sum_{\ell=1}^{\infty} (2\ell+1) C_\ell P_\ell(\cos\theta) \ . \tag{5.6}$$

In order to estimate the C_ℓ for a clustered population of sources which fall below the detection limit S_d I first need to compute the autocorrelation function of intensity fluctuations, $C^{(I)}(\theta, S_d)$ due to the unresolved population. To this aim, I adopt the approximated expression for their angular correlation function, $w(\theta, S_d)$, derived in chapter 2 [equation (2.15)] and multiply it for the square of the mean intensity, $I(S_d)$, contributed by the sources fainter than S_d:

$$C^{(I)}(\theta, S_d) = w(\theta, S_d) I^2(S_d) \ . \tag{5.7}$$

The angular power spectrum of intensity fluctuations, $C_\ell^{(I)}$, is then obtained by inserting $C^{(I)}(\theta, S_d)$ into equation (5.5) and then converting to the power spectrum of temperature fluctuations, $C_\ell^{(T)}$, by means of the following relation

$$C_\ell^{(T)} = \left[\frac{\lambda^2}{2k_b} \frac{(e^x - 1)^2}{e^x x^2} \right]^2 C_\ell^{(I)} \tag{5.8}$$

where $x = h\nu / k_b T$, T being the average temperature of the CMB ($T \sim 2.73$ K).

The contribution to the power spectrum due to randomly-distributed sources (not dependent on angular scale) is easily computed from their differential source counts dN/dS:

$$\sigma^2(S_d) = \frac{1}{4\pi} \int_0^{S_d} S^2 \frac{dN}{dS}(S) dS \tag{5.9}$$

and converted to temperature fluctuations via equation (5.8), where $C_\ell^{(I)}$ is now replaced by σ^2.

The theoretical predictions derived in this chapter will be quoted as

$$\delta T_\ell = \sqrt{\frac{\ell(2\ell+1)}{4\pi} C_\ell^{(T)}} \ . \tag{5.10}$$

which is a measure of the power spectrum per unit interval in $\log \ell$.

5.3 Extragalactic sources at cm and mm wavelengths

The estimated contributions of the various populations of extragalactic sources to the counts at 30 GHz (the frequency of BIMA and CBI experiments) and at 150 GHz (ACBAR experiment) are shown in Fig. 5.1 and have been obtained from the model of De Zotti et al. (2005), which updates that of Toffolatti et al. (1998). The model takes into account the canonical flat- and steep-spectrum radio sources, and star-forming galaxies with their complex spectra including both radio (synchrotron plus free-free) and dust emission. The model includes also a treatment of the sources characterized by spectra peaking at high radio frequencies, such as:

- *extreme GHz Peaked Spectrum (GPS) sources*: they are powerful ($\log P_{1.4\mathrm{GHz}} \gtrsim 25$ W Hz^{-1}), compact ($\lesssim 1$ kpc) radio sources with a convex spectrum peaking at GHz frequencies (see O'Dea 1998, for a review). They are believed to represent the early stages of the evolution of powerful radio sources, when the radio emitting region grows and expands within the interstellar medium of the host galaxy, before plunging in the intergalactic medium and becoming an extended radio source (Fanti et al. 1995; Readhead et al. 1996; Snellen et al. 2000). The convex shape of the spectrum of the GPS sources is expected to arise from the synchrotron self-absorption.

- *early-type galaxies hosting an almost inactive supermassive black hole*: in these sources the accretion onto the central black hole may occur via Advection-Dominated Accretion Flows (ADAF) with low-radiative efficiency (Rees et al. 1982; Fabian & Rees 1995); if this is the case, then their radio emission at cm and mm wavelengths is explained as due to strongly self-absorbed thermal cyclo-synchrotron radiation coming from the inner parts of the accretion flows. However, the ADAF model is not the only possible explanation of the radio emission from early-type galaxies. And in fact, for a number of these objects, the high frequency nuclear emission is substantially below the predictions of the standard ADAF scenario (Di Matteo et al. 1999, 2001), while it is better accounted for by the Adiabatic Inflow-Outflow Solution (ADIOS) developed by Blandford & Begelman (1999). According to this alternative model, the energy liberated by the accretion onto the central black hole drives an outflow at the polar

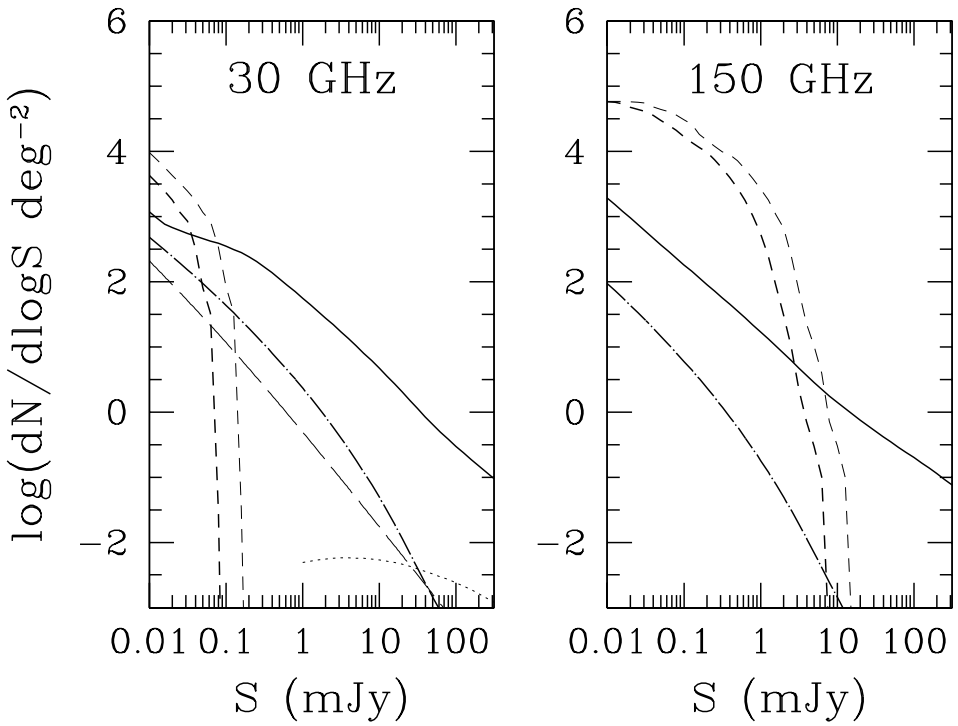

Figure 5.1: Differential counts, $dN/d\log S$, of different populations of extragalactic objects at 30 and 150 GHz, based on the De Zotti et al. (2005) evolution model. Solid lines: canonical flat– plus steep-spectrum sources; dot-dashed lines: starburst+spiral galaxies; short-dashed lines: dusty proto-spheroidal galaxies with (upper curve) and without the mm excess (see text). The left-hand panel also show the estimated counts of GPS sources (dotted line) and of ADAF/ADIOS sources (long-dashed line).

region which carry a considerable fraction of the mass, energy and angular momentum available in the accretion flow. As a consequence the radio emission from the inner regions is significantly reduced.

An additional contribution to the counts at the frequencies probed by the experiments considered here is expected from dusty proto-spheroidal galaxies whose counts at 850 μm and 1.2mm appear to fall very rapidly at flux densities above several mJy (Scott et al. 2002; Borys et al. 2003; Greve et al. 2004). The poor knowledge of the millimeter emission of these sources, however, makes estimates of their contribution to the 30 GHz counts quite

uncertain. The two short-dashed lines in Fig. 5.1 show the counts obtained by using the physical evolutionary model by Granato et al. (2004) with two choices for the spectral energy distribution (SED). The lower (thicker) line refers to the SED produced by the code GRASIL (originally described by Silva et al. 1998). An excess emission by a factor $\simeq 2$ at $\lambda \gtrsim 1\,\mathrm{mm}$ was however detected in several Galactic clouds by combining Archeops with WMAP and DIRBE data (Bernard et al. 2003; Dupac et al. 2003), and in NGC1569 (Galliano et al. 2003). The origin of the excess is still not understood. Possibilities discussed in the literature are that the grain sizes or composition change in dense environments or that there is an intrinsic dependence of the dust emissivity index on temperature (Dupac et al. 2004). If the excess is due to very cold grains (Reach et al. 1995; Galliano et al. 2003) it cannot be present in the high-z proto-spheroids. But if it is a general property of the SED of dusty galaxies, the predicted counts of dusty proto-spheroids shift to the upper (thin) short-dashed curve.

5.4 Contributions of extragalactic sources to arcminute scale anisotropies

5.4.1 Observations with the Cosmic Background Imager (CBI)

The Cosmic Background Imager (CBI; Padin et al. 2002) is an interferometer array located in the Chilean Andes that was designed to measure the power spectrum of CMB fluctuations in the 26-36 GHz band and for multipoles in the range $400< \ell <3500$.
The results produced by CBI are presented in Readhead et al. (2004) and refer to the analysis of four separated fields in low-dust regions of the sky, covering a total area of ~ 90 deg^2. The measured power spectrum in the highest multipole bin, $\ell_{\rm eff} = 2530$, is $\delta T = 18.6 \pm 3.0\ \mu$K (see Fig. 5.2).
CBI measurements are expected to be strongly contaminated by point sources for $\ell \gtrsim 1500$ since the power spectrum, δT_ℓ, of the CMB fluctuations falls off rapidly with ℓ while the point source contribution increases as ℓ (if the sources are randomly distributed). The strategy of the CBI group (Readhead et al. 2004; but see also Mason et al. 2003) to

remove the point source contamination comprises pointed 31 GHz observations with the 40m telescope of the Owens Valley Radio Observatory (OVRO) of all NVSS sources with 1.4 GHz flux density $\geq 6\,\mathrm{mJy}$, and direct counts at 31 GHz using the CBI deep and mosaic maps. Although the 4σ threshold of OVRO observations is 6 mJy, the survey is 99% complete only at $S_{31\mathrm{GHz}} > 21\,\mathrm{mJy}$. The limiting flux density ranges from 6 to 12 mJy in the deep CBI maps, and from 18 to 25 mJy in the mosaic maps. Subtraction of OVRO detected sources removes two-thirds of the observed power level.

Furthermore, Readhead et al. (2004) have adopted the constraint matrix approach to remove from their dataset all NVSS sources with flux densities greater than 3.4 mJy at 1.4 GHz , and have estimated the contribution to fluctuations due to sources below the NVSS cutoff by using the observed OVRO-NVSS distribution of spectral indices and adopting a rather shallow power-law slope for the counts ($N(>S) \propto S^{-0.875}$); for comparison, Richards (2000) finds $N(>S) \propto S^{-1.4\pm0.1}$ for $40\mu\mathrm{Jy} < S_{1.4} < 1\,\mathrm{mJy}$ (see also Windhorst et al. 1993).

At the flux-density levels relevant for the CBI experiment, apart from SZ effects, the dominant contribution to fluctuations due to extragalactic sources is expected to come from the classical steep- and flat–spectrum radio sources. However, an accurate determination of the 30 GHz fluctuations due to sources with $S_{1.4} \leq 3.4\,\mathrm{mJy}$ is very difficult because of the effect of sources with inverted spectra (in fact, Readhead et al. 2004 report the detection of a source, NGC 1068, with $S_{30\mathrm{GHz}} \simeq 400\,\mathrm{mJy}$, not removed by the constraint matrix), and of variability. This difficulty is illustrated by the results of high-frequency radio surveys. Ricci et al. (2004) and Sadler et al. (2006) found that the 18 GHz flux densities of extragalactic sources detected by the ATCA pilot survey are not significantly correlated with the SUMSS flux densities at 0.84 GHz (i.e. at a frequency not far from that of the NVSS survey). Waldram et al. (2003) also reported a large spread (about a factor of 10) of the 15 to 1.4 GHz flux density ratios of sources detected in their 9C survey at 15 GHz, although the flux densities at the two frequencies are correlated. They also noted that pointed 15 GHz observations of the NVSS sources with $S_{1.4} \geq 25\,\mathrm{mJy}$ in the area covered by their survey would have detected 434 sources above the 9C survey limit of 25 mJy but would have missed 31 sources having $S_{15} \geq 25\,\mathrm{mJy}$ but $S_{1.4} < 25\,\mathrm{mJy}$. The distribution of spectral indices has

a systematic drift toward flatter values with decreasing low-frequency flux density down to $S_{1.4} \simeq 1\,\mathrm{mJy}$ (Windhorst et al. 1993), so that the fraction of sources with inverted spectra is expected to be higher at the fainter flux density levels of interest here.

High frequency surveys emphasize flat-spectrum sources. The dominant flat-spectrum population is made of blazars, which are highly variable on timescales of years and whose variability amplitude increases with frequency (Impey & Neugebauer 1988; Ciaramella et al. 2004). The monitoring campaigns at 22, 37 and 87 GHz by the Metsähovi group (Teräsranta et al. 1998) have shown that intensity variations by factors of several are common at these frequencies, so that a substantial fraction of such sources may have had, at the moment of the CBI observations, 30 GHz fluxes higher, even by a considerable factor, than 3.4 mJy. Variability could indeed account, to a large extent, for the lack of a correlation between the ATCA 18 GHz and the SUMSS 0.84 GHz flux densities (Ricci et al. 2004) and for the large spread of the 15 to 1.4 GHz flux density ratios (Waldram et al. 2003).

To appraise residual fluctuations at 30 GHz due to unsubtracted sources we have adopted the analytical description of the counts below a few mJy by Richards (2000) at 1.4 GHz:

$$\frac{dN}{dS}_{1.4}(S_{1.4}[\mathrm{Jy}]) = AS_{1.4}^{-\gamma} \ \ \mathrm{sr}^{-1}\mathrm{Jy}^{-1} \tag{5.11}$$

with $A = 8.3 \pm 0.4$ and $\gamma = 2.4 \pm 0.1$ and computed the 30GHz Poisson fluctuations, σ_{30}^2, contributed by those sources with $S_{1.4} < 3.4\,\mathrm{mJy}$:

$$\sigma_{30}^2(S_{1.4} < 3.4\mathrm{mJy}) = \int_0^{+\infty} S_{30}^2 \frac{dN}{dS_{30}}(S_{30}|S_{1.4} < 3.4\mathrm{mJy})dS_{30}. \tag{5.12}$$

In order to extrapolate the 1.4GHz source counts to the frequency of the CBI experiment a Gaussian distribution, $p(\alpha)$, of spectral indices was assumed

$$p(\alpha)d\alpha = \frac{1}{\sqrt{2\pi}\sigma} \exp\left[-\frac{(\alpha - \bar{\alpha})^2}{2\sigma^2}\right] \tag{5.13}$$

with mean $\bar{\alpha} = 0.4$ (Fomalont et al. 1991; Windhorst et al. 1993) and two values of the dispersion ($\sigma = 0.3$ or 0.4), based on the width of the distribution of $\alpha_{1.4}^{15.2}$ of Waldram et al. (2003, their Fig. 9). The 30 GHz differential counts of sources with $S_{1.4} < 3.4\,\mathrm{mJy}$ are

then given by

$$\frac{dN}{dS_{30}}(S_{30}|S_{1.4} < 3.4\mathrm{mJy}) = \int_{-\infty}^{\alpha_{\max}} \frac{dN}{dS_{1.4}}(S_{30} \cdot (1.4/30)^{-\alpha}) \cdot (1.4/30)^{-\alpha} p(\alpha) d\alpha \qquad (5.14)$$

where $\alpha_{\max} = \log_{10}(3.4/S_{30})/\log_{10}(1.4/30)$.

A comparison with the 30 GHz counts yielded by the De Zotti et al. (2005) model, which takes into account the available information from high-frequency surveys, shows that, in the 30 GHz flux density range relevant to estimate fluctuations, the counts extrapolated using the upper values of A and γ are somewhat too high if $\sigma = 0.4$; more consistent counts (only slightly above the model predictions) are obtained with the central values $A = 8.3$, $\gamma = 2.4$. To bound the plausible range of residual fluctuations I have therefore considered the cases $A = 8.3$, $\gamma = 2.4$, $\sigma = 0.4$ (upper dotted line in the left-hand panel of Fig. 5.2) and $A = 7.9$, $\gamma = 2.3$, $\sigma = 0.3$ (lower dotted line).

The additional contribution to CMB fluctuations given by correlated positions in the sky of canonical steep- and flat-spectrum radio sources has been recently analyzed by González-Nuevo et al. (2005). Their outcomes indicate that the extra power due to the clustering of radio sources cannot, by itself, explain the excess signal detected by CBI (and BIMA). Using the $w(\theta)$ estimated by Blake & Wall (2002) from sources in the NVSS survey down to $S \simeq 10$ mJy - which can represent a realistic approximation to the clustering properties of faint undetected sources in the CBI fields - Gonzalez-Nuevo et al. (2005) found that clustered radio sources at $S_{30\mathrm{GHz}} < 3.4$ mJy can give an extra power $\delta T \simeq$ 3-4 μK, which has to be summed up - in quadrature - to the Poisson term, $\delta T \simeq 20$ μK.

GPS and ADAF/ADIOS sources are potentially worrisome for observations with CBI because of their inverted low-frequency spectra.

However GPS sources are rare (see Fig. 5.1, dotted line) and the analysis made by De Zotti et al. (2000) implies that they likely have very flat counts and therefore are minor contributors to small scale fluctuations. Furthermore, the repeated multifrequency measurements by Tinti et al. (2005) have demonstrated that most GPS candidates identified with quasars in the sample of Dallacasa et al. (2000) are in fact flaring blazars, so that the surface densities of bona-fide GPS sources is probably substantially lower than that

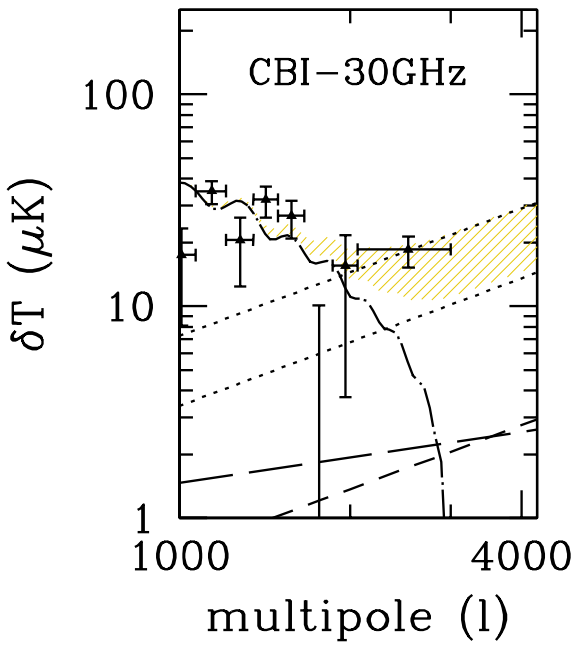

Figure 5.2: Angular power spectrum (δT_ℓ) measured at 30 GHz by CBI (data points from Readhead et al. 2004). The primordial CMB angular power spectrum is overplotted and represented by the dot-dashed-line. Also indicated is the estimated range of contributions of unsubtracted canonical radio sources (dotted lines; see text), and of Poisson distributed (short-dashed line) and clustered (long-dashed line) protospheroidal galaxies. The contributions of the latter sources are insensitive to the adopted flux limit because of the very steep counts. The shaded areas show the ranges spanned by the quadratic sum of the different contributions.

estimated by De Zotti et al. (2000), a conclusion further supported by an examination, carried out by De Zotti et al. (2005), of GPS candidates in the WMAP sample (Bennett et al. 2003).

ADAF/ADIOS sources are far more numerous than GPS sources, but have a low radio power. The estimate by De Zotti et al. (2005) of their counts is well below that by Perna & Di Matteo (2000), whose results are probably affected by a numerical error, and implies that also these sources do not contribute significantly to the fluctuations measured by the CBI experiment. On the other hand, Pierpaoli & Perna (2004; model A) pointed out that if the standard ADAF model (Narayan & Yi 1994) is used, these sources could make up to 40–50% of the BIMA and CBI excesses. However, the standard ADAF scenario faces a number of serious difficulties, some of which are summarized in Sec. 4.3 of De Zotti et al. (2005), suggesting that radio emission is suppressed by massive outflows. It is therefore likely that the results of model A by Pierpaoli & Perna (2004) should be regarded as, probably generous, upper limits.

As for starburst galaxies, the slope α of their differential counts ($dN/dS \propto S^{\alpha}$) can exceed three, if these objects have to account for the very steep ISOCAM 15μm counts below a few mJy as implied by recent analyses (Gruppioni et al. 2003; Franceschini et al. 2003; Pozzi et al. 2004; Silva et al. 2005). In this case, their main contribution to small scale fluctuations comes from weak sources, at μJy levels, far fainter than those removed from CBI maps. On the other hand, the counts of such sources are tightly constrained by μJy counts at 1.4 GHz (Richards 2000), 5 GHz (Fomalont et al. 1991), and 8.4 GHz (Fomalont et al. 2002). Taking such constraints into account and applying an average spectral index $\alpha = 0.8$, appropriate for this class of sources, I find that they can only provide a minor contribution to the excess power detected by CBI: $\sim 5.0\,\mu$K (to be compared with the observed excess of 18.6 μK) at $\ell \simeq 2500$ for a detection limit $S_d = 3.4$ mJy.

The fluctuations due to high-z protospheroids give comparable contributions from both the Poisson and the clustering terms. Adopting the standard expression for the two-point correlation function, $\xi(r) = (r/r_0)^{-1.8}$ with a constant comoving clustering length $r_0 = 8.3\ \mathrm{h}^{-1}\,\mathrm{Mpc}$, in agreement with what inferred in chapter 2, I get $\delta T \sim 1\mu$K at $\ell_{\mathrm{eff}} = 2530$, for both Poisson and clustering fluctuations. Clearly these contributions, to be summed in quadrature to the contribution from canonical radio sources, have a negligible effect.

5.4.2 Observations with the Berkeley-Illinois-Maryland Association Array (BIMA)

The Berkeley-Illinois-Maryland Association Array (BIMA) is an interferometer composed by 6.1m-diameter antennas with $6'.6$ beams at 28.5 GHz (Holzapfel et al. 2000), which is used to investigate CMB anisotropies on arcminute scales.

Analysis of 11 fields selected for lying in regions with low dust content and observed with BIMA during the summers of 1997, 1998 and 2000 gave indications for an excess power compared to primordial CMB anisotropies (Dawson et al. 2001). Dawson et al. (2002) have continued the project in summer 2001 with a subset of eight fields from the original survey in an effort to achieve uniform sensitivity and selection criteria across the sample. Moreover,

two new fields were added to the survey for a total of 10, covering approximately 0.1 deg^2. Thier estimates of the power spectrum of CMB fluctuations in the higher multipoles bins are: $\delta T = 16.6^{+5.3}_{-5.9}$ μK for $\ell_{\rm eff} = 5237$ and $\delta T < 26.5$ μK for $\ell = 8748$.

To remove point source contamination, the BIMA group (Dawson et al. 2002) have carried out a VLA survey at 4.8 GHz of the observed fields. These observations reached a rms flux $\sigma \simeq 25\,\mu{\rm Jy\,beam}^{-1}$ for a $9'$ FWHM region centered at the center of the corresponding BIMA field. Sources with flux densities $> 6\sigma \sim 150$ μJy within $8'$ of the pointing center were identified and removed. On the other hand, point sources with flux densities $S_{4.8} > 150$ μJy, lying at an angular distance θ from the BIMA field center, cannot be detected (and removed) by VLA observations if $S_{4.8} < S_{lim}(\theta) = 150\mu{\rm Jy}/f(\theta)$, where $f(\theta)$ is the VLA response function, assumed to be Gaussian:

$$f_{\rm VLA}(\theta) = e^{-(\theta/\sigma_{\rm VLA})^2/2}, \tag{5.15}$$

with

$$\sigma_{\rm VLA} = \frac{\rm FWHM_{VLA}}{2\sqrt{2\ln 2}} \sim 3.82'. \tag{5.16}$$

As a consequence, sources with flux $S_{4.8} < S_{lim}(\theta)$ which lie within a ring of radius θ (from the BIMA field center) and thickness $d\theta$ produce a fluctuation

$$d\sigma^2_{4.8}(\theta) = 2\pi\theta d\theta \int_0^{S_{lim}(\theta)} S^2_{4.8} \frac{dN}{dS}(S_{4.8}) dS_{4.8}. \tag{5.17}$$

The fluctuations contributed by *all* the un-subtracted sources can be computed by integrating $d\sigma^2_{4.8}(\theta)$ over θ from 0 to $0.5 \times {\rm FWHM_{BIMA}} (= 3.3')$ and dividing the result by the area of the BIMA field:

$$\sigma^2_{4.8} = \frac{1}{\pi(0.5 \times {\rm FWHM_{BIMA}})^2} \int_0^{0.5\times{\rm FWHM_{BIMA}}} d\sigma^2_{4.8} \tag{5.18}$$

I have made this computation by adopting the integrated number counts at 4.8 GHz of Fomalont et al. (1991):

$$N_{4.8}(S_{4.8}[\mu{\rm Jy}]) = (23.2 \pm 2.8) S_{4.8}^{-1.18\pm0.19} \ \ {\rm arcmin}^{-2}. \tag{5.19}$$

The value of $\sigma_{4.8}$ has been then extrapolated to 30 GHz by assuming a mean spectral index $\alpha = 0.4$, appropriate for the relevant flux-density range (Fomalont et al. 1991; Windhorst

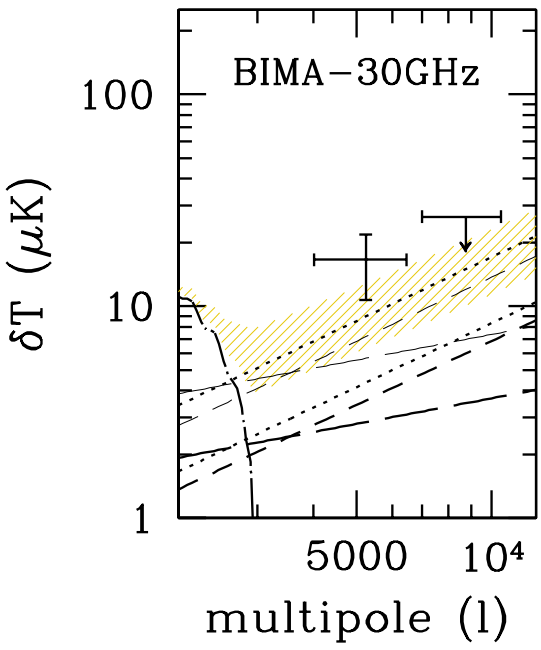

Figure 5.3: Angular power spectrum (δT_ℓ) measured at 30 GHz by BIMA (data points from Dawson et al. 2002). The primordial CMB angular power spectrum is overplotted and represented by the dot-dashed-line. Also indicated is the estimated range of contributions of unsubtracted canonical radio sources (dotted lines; see text), and of Poisson distributed (short-dashed line) and clustered (long-dashed line) proto-spheroidal galaxies. The upper pair of long- and short-dashed lines refers to proto-spheroidal galaxies with the submillimetre excess mentioned in Sec. **??**. The shaded areas show the ranges spanned by the quadratic sum of the different contributions.

et al. 1993):

$$\sigma_{30} = \sigma_{4.8} \left(\frac{30}{4.8} \right)^{-0.4} . \tag{5.20}$$

The resulting power spectrum of temperature fluctuations contributed by un-subtracted radio sources is shown in Fig. 5.3, where the shaded area reflects the range of values corresponding to the uncertainties in the counts of Fomalont et al. (1991) and in the dust emission spectrum of high redshift spheroids (see below).

The contribution from star forming galaxies is estimated to be $\sim 4.3\,\mu$K at $\ell \simeq 6880$, using the nominal 6σ detection limit, $S_d = 150\,\mu$Jy, while the contribution from GPS and ADAF/ADIOS sources, according to the considerations made in the previous section, is completely negligible.

High-z protospheroids, which are not represented in the 4.8 GHz counts, give at $\ell_{\rm eff} = 6864$, a Poisson contribution of $\simeq 5\mu$K and a clustering contribution of $\simeq 3\mu$K. If these

sources show the mm excess mentioned in Sect. 2, their contribution to fluctuations would be approximately doubled (see Fig. 5.3) and, when summed in quadrature to the above estimates for the contribution of radio sources, could account for the reported excess signal.

5.4.3 Observations with the Arcminute Cosmology Bolometer Array Receiver (ACBAR)

The Arcminute Cosmology Bolometer Array Receiver (ACBAR) is a 16-element bolometer array designed to make use of the Viper telescope at the South Pole to produce detailed images of the CMB in three millimeter-wavelength bands: 150, 220 and 280 GHz, with high sensitivity and high angular resolution ($\sim 4'$-$5'$).

The ACBAR measurements in the 150 GHz band[1], relative to two low-dust regions of the sky covering a total of 24 deg^2, have been reported by Kuo et al. (2004): in the highest multipoles bins, characterized by $\ell_{\rm eff} = 2081$ and $\ell_{\rm eff} = 2507$, the estimated power spectrum of CMB fluctuations is respectively $\delta T = 18.4 \pm 3.0$ μK and $\delta T = 17.5 \pm 7.8$ μK. These results are consistent with the excess detected by the CBI experiment. However, fluctuations due to extragalactic radio sources in the ACBAR band are quite small (a few μK at $\ell_{\rm eff} = 2507$).

Quoting results by Blain et al. (1998), Kuo et al. (2004) conclude that dusty proto-galaxies are also not expected to contribute significantly to the observed signal. However, the Blain et al. (1998) estimate actually refers to Poisson fluctuations only, while, as already pointed out before, the strong positional correlation of SCUBA galaxies implies that the main contribution on ACBAR scales could come from source clustering. I have estimated such a contribution by assuming a 5σ flux limit of 24 mJy. The latter value has been computed for the angular resolution of ACBAR (FWHM=$5'$) using the formalism presented in chapter 3 for the source confusion noise. Moreover, if dusty proto-spheroidal galaxies have the excess emission (compared to model expectations) discussed in Sec. **??** (Fig. 5.4, right-hand panel), the power measured in the highest multipole bin can be easily explained in terms of fluctuations due to undetected high-z galaxies (in this case the estimated flux limit for source detection is $S_d = 43$ mJy). In either case, dusty proto-spheroids are found to give a relevant contribution to the measured power, even without the excess mm-emission

[1] An analysis of the 220 and 280 GHz data has not been published yet.

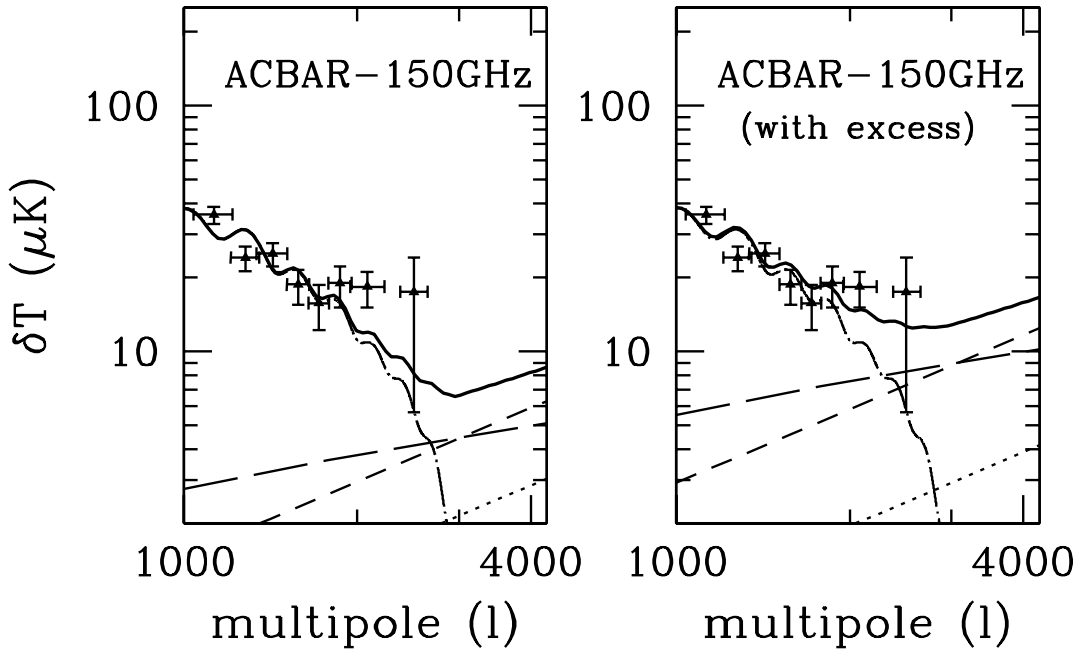

Figure 5.4: Angular power spectrum ($\delta T = \sqrt{\ell(\ell+1)C_\ell/2\pi}$) as measured by ACBAR at 150 GHz (data points are from Kuo et al. 2004). The dotted, long- and short-dashed, and dot-dashed curves have the same meaning as in Fig. 2; the solid lines are the quadratic sum of all the contributions. The contribution given by undetected Poisson distributed and clustered proto-spheroidal galaxies has been calculated without (left-hand panel) and with (right-hand panel) the excess mm emission discussed in the text. In this case I adopted $S_{\rm lim} \simeq 24$ mJy (left-hand panel) and $S_{\rm lim} \simeq 43$ mJy (right-hand panel) for source detection. These limits correspond to the 5σ source detection threshold estimated as in chapter 2 for the $5'$ FWHM of ACBAR.

(Fig. 5.4, left-hand panel).

5.5 Conclusions

In this chapter I have discussed the possible contributions of the various classes of extragalactic sources (including, in addition to the canonical radio sources, GHz Peaked Spectrum sources, advection-dominated sources, starburst galaxies and high-redshift proto-spheroidal galaxies) to the arcminute scale fluctuations measured by the CBI, BIMA, and

ACBAR experiments.

Contamination from extragalactic point sources is a likely candidate to account for a large fraction, perhaps for most of the excess power on arcminute scales detected by the CBI and BIMA experiments. The fluctuations due to radio sources undetected by the ancillary low-frequency surveys may in fact be higher than estimated by the CBI and BIMA groups. On the other hand, extreme GHz Peaked Spectrum sources and advection dominated sources, potentially worrisome because of their spectra peaking at high microwave/mm-wave wavelengths, should only provide a minor contribution to the CBI and BIMA signals.

Although the very steep $15\,\mu$m counts of starburst galaxies below a few mJy imply a very strong cosmological evolution, radio surveys down to μJy levels constrain the contribution of their *radio* emission to fluctuations at 30 GHz to be relatively small. On the other hand, the *dust* emission at rest-frame mm wavelengths from star-forming galaxies at high-redshifts, such as those detected by SCUBA and MAMBO surveys, can be redshifted down to 30 GHz. Using the spectral energy distributions given by the Granato et al. (2004) model, I find that these sources yield fluctuations of a few to several μK on arcminute scales. Their rest-frame spectral energy distribution at mm wavelengths, however, is poorly known, and may well be higher than what implied by the adopted model.

Furthermore, observational indications and theoretical arguments converge in suggesting that these sources are highly clustered so that their fluctuations may be strongly super-Poissonian for multipoles $\ell \lesssim 3000$ (the clustering-to-Poisson ratio increases with the angular scale, i.e. with decreasing multipole number, De Zotti et al. 1996). Clustering fluctuations of the high-z galaxies detected by (sub)-mm SCUBA and MAMBO surveys may indeed provide the dominant contribution to the signal measured by the ACBAR experiment at 150 GHz at the highest multipoles.

Because the dust emission spectrum rises very steeply with frequency, lower frequency surveys cannot be used to remove their effect from 30 GHz maps. In the present data situation, they therefore set an *unavoidable* limit to the determination of the primordial CMB angular power spectrum at high multipoles, even at frequencies as low as ~ 30

GHz.

I stress that the present results are fully compatible with the estimated contributions of Sunyaev-Zeldovich effects in clusters of galaxies to the arcminute scale anisotropies, as shown by Douspis et al. 2006. In fact, while an interpretation of the *full* CBI and BIMA signals in terms of SZ fluctuations would require a density fluctuation amplitude (measured by the parameter σ_8) at or above the limit allowed by current data (Bond et al. 2005), our analysis leaves room for an SZ contribution corresponding to the σ_8 values favoured by analyses of CMB, cosmic shear, and large scale structure data (Spergel et al. 2003, 2006; Pierpaoli et al. 2003; Van Waerbecke et al. 2005).

New interesting constraints on the CMB angular power spectrum up to $\ell \sim 2500$ at 34 GHz should be provided in the near future by the VSA experiment (see e.g. Rebolo et al. 2004). The reduced noise level of the new configuration and an effective cleaning of deep fields down to ~ 5 mJy – achieved by dedicated observations with the Ryle Telescope at 15 GHz – will shed new light on the nature of the excess at high multipoles and on the point source populations mainly contributing to the number counts at $S_{34} \sim$ a few mJy. Moreover, *Planck* HFI data as well as the forthcoming surveys by the *Herschel* telescope – probing frequencies where the emission due to cold dust grains is the dominant one – will be unique in determining the cosmological evolution, the emission and the clustering properties of high-redshift dusty galaxies.

Chapter 6

The large scale clustering of radio sources

6.1 Introduction

Extragalactic radio sources are well suited to probe the large scale structure of the Universe since they are detected over large cosmological distances (up to $z \sim 6$), are unaffected by dust extinction, and can thus provide an unbiased sampling of volumes larger than those usually probed by optical surveys. On the other hand, their 3D-space distribution can only be recovered in the very local Universe ($z \lesssim 0.2$; see Peacock & Nicholson 1991; Magliocchetti et al. 2004) as the majority of radio galaxies detected in the available surveys have very faint optical counterparts, so that measurements of their redshifts are a difficult task.

Even the detection of clustering in the 2D distribution of radio sources proved to be extremely difficult (see Webster 1976, Seldner & Peebles 1981, Shaver & Pierre 1989) since, when projected onto the sky, the space correlation is significantly diluted because of the broad redshift distribution. It was only with the advent of deep radio surveys covering large areas of the sky, such as the Faint Images Radio Sky at Twenty centimeters (FIRST; Becker, White & Helfand 1995), Westerbork Northern Sky Survey (WENSS; Rengelink et al. 1997), NRAO VLA Sky Survey (NVSS; Condon et al. 1998), and Sydney University Molonglo Sky

Survey (SUMSS; Bock, Large & Sadler 1999; Mauch et al. 2003), that the angular clustering of this class of objects has been detected with a high statistical significance down to flux density limits of few mJy (see Cress et al. 1997 and Magliocchetti et al. 1998, 1999 for the FIRST survey; Blake & Wall 2002a,b and Overzier et al. 2003 for NVSS; Rengelink & Röttgering 1999 for WENSS and Blake, Mauch & Sadler 2004 for SUMSS). Amongst all the above surveys, NVSS is characterized by the most extensive sky coverage and can thus take advantage of high statistics despite being less deep than the FIRST survey (flux limit: $\sim 3\,$mJy vs $\sim 1\,$mJy of FIRST). The two-point angular correlation function, $w(\theta)$, measured for NVSS sources brighter than 10 mJy is well described by a power-law, extending from ~ 0.1 degrees up to almost 10 degrees. A signal of comparable amplitude and shape was detected in the FIRST survey at the same flux density limit, on scales of up to 2-3 degrees (see e.g. Magliocchetti et al. 1999), while on larger angular separations any positive clustering signal - if present - was hidden by the noise.

Most analyses of radio source clustering performed so far (see e.g. Blake & Wall 2002a,b; Overzier et al. 2003) assume a two-point spatial correlation function of the 'standard' form $\xi_{\rm rg}(r) = (r/r_0)^{-\gamma}$. The power-law shape is in fact preserved when projected onto the sky (see Limber 1953), so that the observed power-law behaviour of the angular correlation is well recovered. The studies summarized by Overzier et al. (2003) typically found correlation lengths r_0 in the range 5–$15\,h^{-1}\,$Mpc. Such wide range on one hand may reflect real differences in the correlation properties of radio sources of different classes/luminosities, while, on the other hand, mirrors the large uncertainties associated to both the redshift distribution of the sources and the time-evolution of clustering, which are necessary ingredients to estimate $\xi_{\rm rg}(r)$ from the observed $w(\theta)$.

A deeper examination of the power-law behaviour of the NVSS angular two-point correlation function up to scales of the order of $\sim 10^\circ$ highlights some interesting issues. In fact, within the Cold Dark Matter paradigm of structure formation, the spatial correlation function of matter displays a sharp cut-off around a comoving radius of $r \sim 100\,$Mpc[1] (see

[1] I assume a flat universe with a cosmological constant and $\Omega_{0,m} = 0.27$, $\Omega_b = 0.045$, $\sigma_8 = 0.9$, $n = 1$,

e.g. Matsubara 2004, Fig. 1) which, at the average redshift for radio sources $\langle z \rangle \sim 1$, corresponds to angular separations of only a few ($\sim 1^\circ - 2^\circ$) degrees, in clear contrast with the observations. This opens the question of how to reconcile the clustering properties of these sources with the standard scenario of structure formation.

In this chapter I investigate in more detail this issue and provide a self-consistent explanation for such a puzzling behaviour. I will exploit the available spectroscopic information on local radio sources to limit the uncertainties on their total redshift distribution and will also focus on the time evolution of their clustering properties via the bias parameter. In this way interesting constraints on the typical mass of dark matter halos hosting the population of radio sources can be derived. The dependence of the predicted angular correlation function on cosmological parameters will be also investigated.

The layout of the chapter is as follows. A short description of the NVSS survey is presented in Section 6.2. Section 6.3 illustrates the adopted model for the redshift distribution of mJy radio sources, while in Section 6.4 I describe the calculations of the two-point angular correlation function. Results and discussions are presented in Section 6.5. In Section 6.6 I summarize the main conclusions.

6.2 The NRAO VLA Sky Survey

The NVSS (Condon et al. 1998) is the largest radio survey that currently exists at 1.4 GHz. It was constructed between 1993 and 1998 and covers ~ 10.3 sr of the sky north of $\delta = -40^\circ$. The survey was performed with the Very Large Array (VLA) in the D configuration and the full width at half-maximum (FWHM) of the synthesized beam is 45 arcsec. The source catalogue contains 1.8×10^6 sources down to a flux density of 2.5 mJy and it is claimed to be 99 per cent complete above the integrated flux density $S_{1.4\mathrm{GHz}} = 3.5$ mJy.

The two-point angular correlation function, $w(\theta)$, of NVSS sources has been measured by Blake & Wall (2002a,b) and Overzier et al. (2003) for different flux-density thresholds between 3 mJy and 500 mJy. The overall shape of $w(\theta)$ is well reproduced by a double

and $h = 0.72$, in agreement with the first-year WMAP results (Spergel et al. 2003).

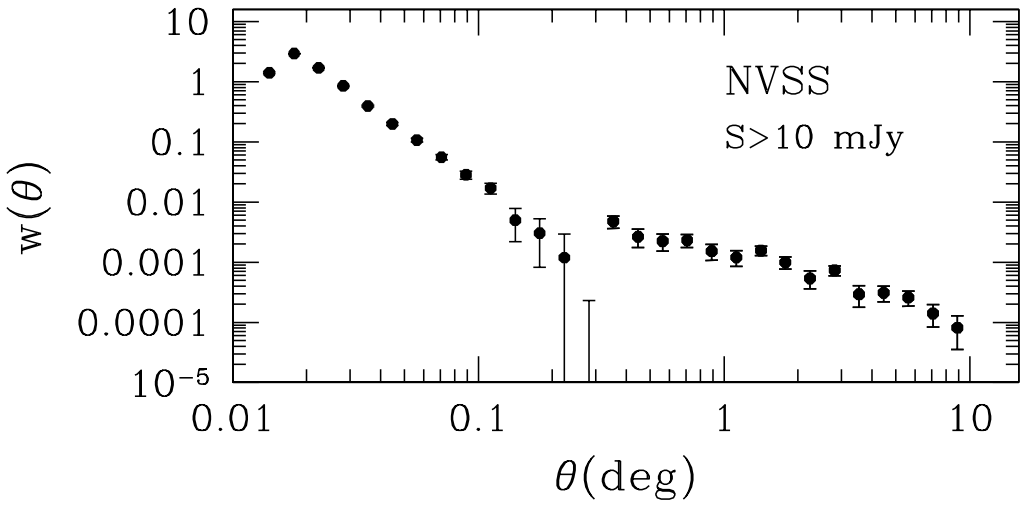

Figure 6.1: Two-point angular correlation function, $w(\theta)$, of NVSS sources with $S_{1.4\mathrm{GHz}} \geq$ 10 mJy, as measured by Blake & Wall (2002b).

power-law (see Fig. 6.1). On scales below $\sim 0.1^\circ$, the steeper slope reflects the distribution of the resolved components of single giant radio sources (i.e. radio galaxies with lobes extending up to Mpc scales). The shallower power-law on larger scales describes the correlation between distinct radio sources. Since the behaviour on small scales is mainly determined by the joint effect of the astrophysical properties of the sources and of the resolution of the VLA in the various configurations, while that on larger scales is of cosmological origin, throughout this chapter I will only concentrate on the latter aspect. In fact, the clustering behaviour on scales $\gtrsim 0.1^\circ$ provides insights on both the nature of the radio sources, through the way in which they trace the underlying dark matter distribution, and on the cosmological framework which determines the distribution of dark matter at each epoch.

In order to get more information on the cosmological evolution of radio sources, I will concentrate the attention on the two-point angular correlation function as measured by Blake & Wall (2002b) for sources with $S_{1.4GHz} \geq 10$ mJy, which is shown in Fig. 6.1. In fact, such a flux limit represents the deepest flux-density for which systematic surface density gradients are approximately negligible (Blake & Wall 2002a). The NVSS source surface density at this threshold is 16.9 deg^{-2}.

The data corresponding to separations in the range $0.1^\circ \lesssim \theta \lesssim 0.3^\circ$ most likely suffer from a deficit of pairs probably due to an imperfect cleaning of bright side lobes (see Blake, Mauch & Sadler, 2004). Therefore in the following I will only consider scales $\theta > 0.3^\circ$. In this range of scales, the measured angular correlation function is found to be described as a power law, $w(\theta) = 1.49 \cdot 10^{-3} \times \theta^{-1.05}$, with θ in degrees (see Blake, Mauch & Sadler 2004).

6.3 Redshift distribution of millijansky radio sources

In order to provide theoretical predictions for the angular two-point correlation function of a given class of objects it is necessary to know their redshift distribution, $\mathcal{N}(z)$. Unfortunately, the redshift distribution of mJy radio sources is not yet accurately known as the majority of radio sources powered by Active Galactic Nuclei (AGN) – which dominate the mJy population – are located at cosmological distances ($< z > \sim 1$) and are in general hosted by galaxies which are optically extremely faint.

A large set of models for the epoch-dependent Radio Luminosity Function (hereafter RLF) are available in literature (see e.g. Dunlop & Peacock 1990, Rowan-Robinson et al. 1993, Toffolatti et al. 1998, Jackson & Wall 1999, Willot et al. 2001), but they all suffer from the fact that they are mainly based on, and constrained by, data sets which include only bright sources ($S_{1.4GHz} \gtrsim 100\,\mathrm{mJy}$) so that any extrapolation of their predictions to lower fluxes is quite uncertain. Amongst all the available RLFs, those provided by Dunlop & Peacock (1990, hereafter DP90) are the most commonly used to infer the redshift distribution of radio sources at the mJy level. DP90 derived their set of RLFs on the basis of spectroscopically complete samples from several radio surveys at different frequencies. By using a 'maximum entropy' analysis they determined polynomial approximations to the luminosity function and its evolution with redshift which were all consistent with the data available at that time. In addition, they also proposed two models of a more physical nature, assuming either Pure Luminosity Evolution (hereafter PLE) or Luminosity/Density Evolution.

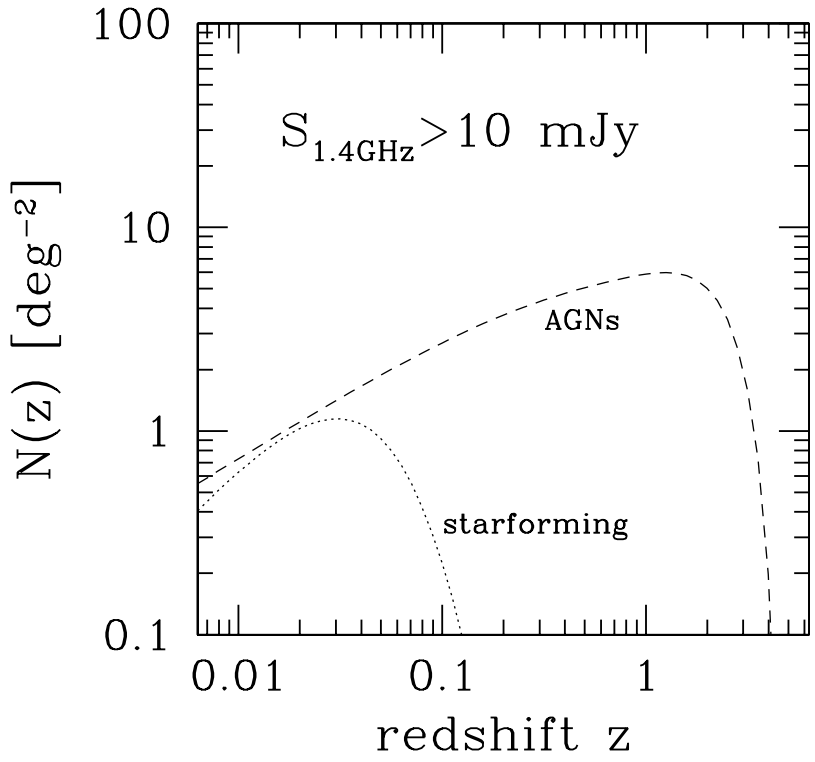

Figure 6.2: Adopted redshift distribution per unit redshift interval, $\mathcal{N}(z)$, for the radio source population with $S_{1.4\mathrm{GHz}} \geq 10\,\mathrm{mJy}$. The dashed line represents the contribution of AGN-powered radio sources according to the PLE model of DP90, while the dotted line shows the contribution from star-forming galaxies obtained by Magliocchetti et al. (2002).

Recently, with the aim of determining the photometric and spectroscopic properties for at least the population of local (i.e. $z < 0.2$) radio sources at the mJy level, a number of studies have concentrated on samples obtained by combining radio catalogues like FIRST and NVSS with optical ones like SDSS and 2dFGRS (Sadler et al. 2002, Ivezić et al. 2002, Magliocchetti et al. 2002, 2004). The radio/optical samples obtained in this way provide a crucial constraint at $z \sim 0$ for any theoretical model aiming at describing the epoch-dependent RLF.

For instance, Magliocchetti et al. (2002, hereafter M02) have shown that the RLF at 1.4 GHz derived from all the objects in their spectroscopic sample having $S \geq 1$ mJy and $b_J \leq 19.45$, is well reproduced at radio luminosities $P_{1.4\mathrm{GHz}} > 10^{20.5}\,\mathrm{W\,Hz^{-1}\,sr^{-1}}$ by

the DP90's PLE model for steep-spectrum FRI-FRII sources. At lower radio luminosities, where the radio population is dominated by star-forming galaxies, the measured RLF is better described by the one proposed by Saunders et al. (1990) for IRAS galaxies (see also Rowan-Robinson et al. 1993), although with a small adjustment of the parameters.

Following M02, I adopt the DP90 PLE model to derive the redshift distribution of AGN-powered radio sources with $S_{1.4\mathrm{GHz}} \geq 10\,\mathrm{mJy}$ (see Fig. 6.2, dashed line). I will not take into account the other DP90 models, since they are inconsistent with the local RLF. In fact, while the model assuming density/luminosity evolution over-predicts the number of steep-spectrum radio galaxies below $P_{1.4\mathrm{GHz}} \lesssim 10^{22}\,\mathrm{W\,Hz^{-1}\,sr^{-1}}$, models using polynomial approximations for the RLF give an unrealistic overestimate of the number of local sources at all luminosities.

I will also use the fit provided by M02 to the local RLF in order to estimate the redshift distribution of star-forming radio galaxies with $S_{1.4\mathrm{GHz}} \geq 10\,\mathrm{mJy}$ (see Fig. 6.2, dotted line). Note that star-forming galaxies comprise less than 30% of the $z \lesssim 0.1$ population of radio sources with $S_{1.4\mathrm{GHz}} \geq 10\,\mathrm{mJy}$, and only $\simeq 0.5\%$ of the total counts at this flux limit. As I will show in the next Section, this result implies that the contribution of star-forming galaxies to the large scale angular clustering of NVSS sources is entirely negligible.

6.4 The model for the angular correlation function

I will use the Limber equation introduced in chapter 2 [equation (2.6)] to predict the angular correlation function of radio sources. To this end, I need, in addiction to the redshift distribution of both AGN-powered and star-forming radio galaxies described in the previous Section, a suitable model for the spatial two-point correlation function.

6.4.1 The spatial correlation function

On sufficiently large linear scales (e.g. $r \gtrsim 3\,\mathrm{Mpc}$), such as those typically sampled by radio galaxies at angular separations $\theta \gtrsim 0.3^\circ$, the clustering signal is produced by galaxies residing in distinct dark matter halos; therefore, I will assume for the spatial two-

point correlation function of radio galaxies the standard form

$$\xi(r,z) = b^2(M_{\rm eff},z)\xi_{\rm DM}(r,z) \ , \tag{6.1}$$

under the assumption of a one-to-one correspondence between radio galaxies and their host halos. Again, $M_{\rm eff}$ represents the effective mass of the dark matter haloes in which the sources reside. Calculations will be performed within a 'concordance cosmology' with $\Omega_{0,m} = 0.27$, $\Omega_{0,\Lambda} = 0.73$, $h = 0.72$ and further assuming a scale-invariant initial power spectrum with a slope $n = 1$ and a normalization $\sigma_8 = 0.9$. Note that the value of σ_8 favoured by the recent 3-year WMAP data (Spergel et al. 2006) is lower than the one assumed here; however I have tested that the predicted angular correlation function is almost insensitive to the normalization of the power spectrum ('cosmic conspiracy', Peacock 1997).

In the range of scales of interest here the clustering evolves in the linear regime, so that $\xi_{\rm DM}(r,z) = D^2(z)\xi_{DM}(r,0)$, $D(z)$ being the linear density growth-rate (Carroll, Press & Turner 1992).

According to the adopted redshift distribution (see Fig. 6.2), the majority of radio sources are located at cosmological distancies, (i.e. $z \sim 1$) so that angular separations of few degrees in the sky typically correspond to comoving linear scales $r \gtrsim 100$ Mpc, for which $\xi_{\rm DM}(r)$ takes on negative values. From equation (6.1), it follows that even the spatial correlation function of radio galaxies would be negative in the same range of scales. However this conclusion is not straightforward since the analytic prescription of $\xi(r)$ given in equation (6.1) has only been tested by N-body simulations on scales $r \lesssim 100$ Mpc, for which $\xi_{\rm DM} \gtrsim 0$.
Therefore, before proceeding with the analysis of the angular clustering of NVSS sources, I have exploited the 'Hubble volume' simulations to test equation (6.1) in the regime of negative clustering.

6.4.2 The issue of bias at large scales

The N-body simulations with the largest volume extention, useful to investigate clustering on very large scales, are those carried out in 1997 and 1998 on 512 processors of

the CRAY T3E at the Garching Computer Centre of the Max Planck Society. Also referred to as 'Hubble volume' simulations, they are made of 10^9 particles and were derived for a $(2000\ h^{-1}\mathrm{Mpc})^3$ volume of a τCDM universe (that corresponds to a flat universe filled with cold dark matter but with a null cosmological constant) and a $(3000\ h^{-1}\mathrm{Mpc})^3$ volume of a ΛCDM universe (cf. e.g Colberg et al. 2000). I have analysed only the ΛCDM simulation which has been performed assuming $\Omega_{0,m} = 0.3$, $\Omega_{0,\Lambda} = 0.7$ and $\sigma_8 = 0.9$. The matter trasfer function was computed using CMBFAST (Seljak & Zaldarriaga 1996), with $h = 0.7$ and $\Omega_{0,b} = 0.040$. The slope of the primordial power spectrum was taken to be unity. The mass of a single particle in the simulation is $M_{\mathrm{par}} = 2.24 \times 10^{12}\ h^{-1}\ \mathrm{M}_{\odot}$.

A catalogue of dark matter haloes at $z = 0$ has been produced and made available to the international community by the VIRGO consortium (see http://www.mpa-garching.mpg.de/Virgo/). Haloes were identified in the simulation using a friends-of-friends algorithm (Davies et al. 1985) with a linking length of 0.164. I have used such a catalogue to study the large scale clustering properties of dark matter haloes. Therefore the following analysis is necessarily restricted to the case $z = 0$.

For each halo, the catalogue provides both the position within the simulated volume and the number, n_{par}, of particles which concur to define the halo, so that its mass can be estimated directly as $M_{\mathrm{halo}} = n_{\mathrm{par}} \times M_{\mathrm{par}}$.

I have tested the ST99 fitting formula by constructing mass-limited samples of haloes from the given catalogue and comparing the spatial correlation function as measured from these samples with that derived from equation 6.1, with the factor b^2 replaced by the square of the *effective* bias factor of all haloes with masses greater than a chosen threshold mass M_{min}, that is:

$$b_{\mathrm{eff}} = \int_{M_{\mathrm{min}}}^{\infty} b(M,z)n(M,z)dM \times \left[\int_{M_{\mathrm{min}}}^{\infty} n(M,z)dM\right]^{-1}, \qquad (6.2)$$

where $n(M,z)$ is the number density of haloes with masses in the range $M, M + dM$. The approximate formula for $n(M,z)$ provided by ST99 is assumed in the present analysis.

It is worth noting that a technical problem arises when comparing analytic for-

mulae with simulations: it is unclear how to define the boundaries of simulated haloes so that their mass corresponds to the mass M in equation 6.2. A simple way to overcome this problem is that of using the analytic expression for the halo mass function, $n(M,z)$, to estimate the mean halo separation, d_c, of haloes with $M \geq M_{\rm min}$:

$$d_c = \left[\int_{M_{\rm min}}^{\infty} n(M,z)dM\right]^{-1/3}. \quad (6.3)$$

The analytic correlation function can then be compared to that of a mass-limited sample of simulated haloes with the same mean separation.

I have constructed four mass-limited samples of dark matter haloes by assuming d_c = 30, 70, 120 and 170 h^{-1} Mpc, which correspond, respectively, to $M_{\rm min} = 9.4 \times 10^{13}$, 4.5×10^{14}, 9.0×10^{14} and 1.1×10^{15} $M_{\odot}$, as derived from equation 6.3. The four samples contains respectively 1002010, 77866, 15610 and 5507 simulated haloes.

Since $\xi(r)$ quantifies the excess/deficit of pairs of sources at a given separation r with respect to the number of pairs expected in the case of a Poisson distribution, I have first generated a catalogue of points by randomly distributing them within the (3000 h^{-1}Mpc)^3 volume of the simulation. The number of random points used here is 10 times higher than that of the haloes in each sample. I have then computed the spatial correlation function by means of the Landy-Szalay operator (Landy & Szalay 1993):

$$\xi(r) = \frac{DD(r) - 2DR(r) + RR(r)}{RR(r)}, \quad (6.4)$$

where $DD(r)$, $DR(r)$ and $RR(r)$ are the (normalized) halo-halo, halo-random and random-random pairs. Estimates of $\xi(r)$ are provided in logaritmic bins of dlogr=0.1 for the two samples characterized by the lower halo separation (i.e. d_c = 30 and 70 h^{-1} Mpc) and in logaritmic bins of dlogr=0.2 for the other two samples, in order to improve the statistics on large scales. The results are shown in Fig. 6.3 as points with Poisson error bars. The solid curves represent the analytic estimates of correlation functions of dark matter haloes and have been computed for the cosmological model used for the simulation. The matter transfer function was calculated from the fitting formulae of Eisenstein & Hu (1998). Fig. 6.3 also compares the analytic value of the effective bias parameter [$b^2_{\rm eff}(M_{\rm min}, z = 0)$, shown as a dashed-line] with the ratio between the measured halo correlation function and the

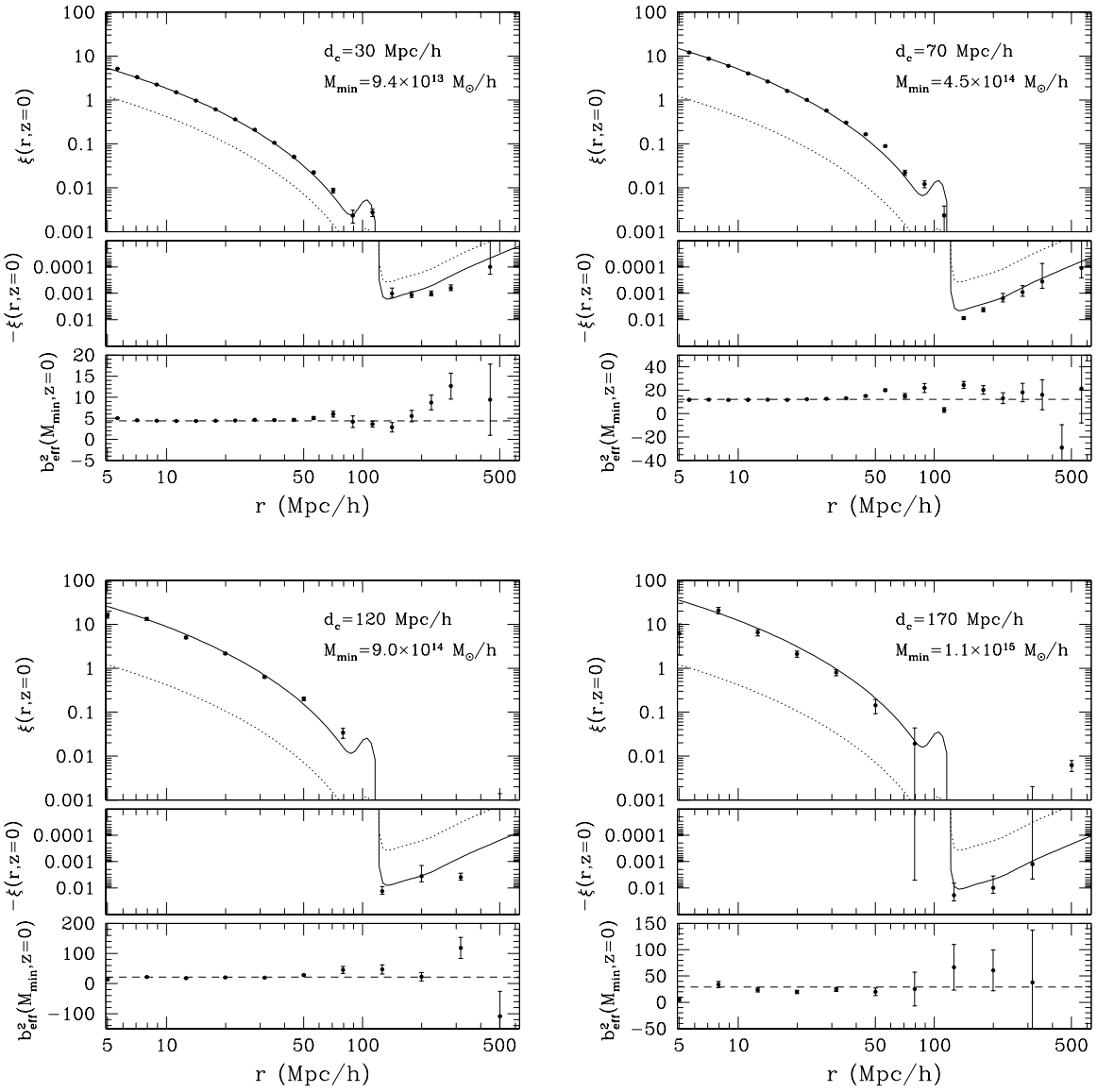

Figure 6.3: The two-point spatial correlation function, at $z = 0$, of four mass-limited samples of dark matter haloes identified in the ΛCDM 'Hubble volume' simulation. Poisson error bars are associated to the estimates. The values of the mean halo separation, d_c, in each sample and those of the corresponding minimum halo mass, $M_{\rm min}$, as derived from equation 6.3, are reported. The solid curves show the analytic correlation function of dark matter haloes computed from equation 6.1 with the ST99 prescription for the effective bias parameter $b_{\rm eff}$ (equation 6.2). The dotted curve represents the analytic correlation function of dark matter. In the lower panel of each figure the ratio between the measured correlation function of the haloes and that of the dark matter is compared with the analytic value (dashed-line) of $b^2_{\rm eff}(M_{\rm min}, z)$.

correlation function of dark matter ($\xi_{\rm DM}$, shown by the dotted curve). Note that, within 3σ uncertainties, there is a good agreement between measurements and analytic prescriptions.

I can thus conclude that, at least for $z = 0$, the linear bias parameter computed from the ST99 fitting formula provides a good description of the clustering properties of dark matter haloes even on scales above 100 h^{-1} Mpc.

6.4.3 Angular correlation function of the radio source population

Since the population of radio sources with $S_{1.4\rm GHz} \geq 10$ mJy is composed of two different types of objects, i.e. AGNs and star-forming galaxies, which display different clustering properties (see e.g. Saunders, Rowan-Robinson & Lawrence 1992, Madgwick et al. 2003), I write the angular correlation function of the whole NVSS sample as follows (cf. e.g. Wilman et al. 2003, equation 9):

$$w(\theta) = f^2_{\rm AGN} w_{\rm AGN}(\theta) + f^2_{\rm SF} w_{\rm SF}(\theta) + 2 f_{\rm AGN} f_{\rm SF} w_{\rm cross}(\theta) \tag{6.5}$$

where $f_{\rm AGN}$ and $f_{\rm SF}$ are, respectively, the fractions of AGNs and star-forming galaxies in the sample, that is

$$f_{\rm AGN/SF} = \frac{\int_{\mathcal{Z}} dz \mathcal{N}_{\rm AGN/SF}(z)}{\int_{\mathcal{Z}} dz \mathcal{N}(z)}, \tag{6.6}$$

$\mathcal{N}(z)$ being the total AGN+SF redshift distribution.

In equation (6.5), $w_{\rm AGN}$ and $w_{\rm SF}$ are the angular correlation functions of the two classes of radio sources, while $w_{\rm cross}$ accounts for the cross-correlation between the two populations:

$$\begin{aligned} w_{\rm cross}(\theta) &= \int_{z_{\rm min}}^{z_{\rm max}} dz \mathcal{N}_{\rm AGN}(z) \mathcal{N}_{\rm SF}(z) \times \int_{z_{\rm min}-z}^{z_{\rm max}-z} d(\delta z) \xi_{\rm cross}[r(\delta z, \theta), z] \\ &\times \left[\int_{z_{\rm min}}^{z_{\rm max}} dz \mathcal{N}_{\rm AGN}(z) \int_{z_{\rm min}}^{z_{\rm max}} dz \mathcal{N}_{\rm SF}(z) \right]^{-1}. \end{aligned} \tag{6.7}$$

I model $\xi_{\rm cross}$ as (cf. e.g. Magliocchetti et al. 1999, equation (31)):

$$\begin{aligned} \xi_{\rm cross}(r, z) &= \sqrt{\xi_{\rm AGN}(r, z) \xi_{\rm SF}(r, z)} \\ &= b(M^{\rm AGN}_{\rm eff}, z) b(M^{\rm SF}_{\rm eff}, z) \xi_{\rm DM}(r, z); \end{aligned} \tag{6.8}$$

where $\xi_{\rm AGN}$ and $\xi_{\rm SF}$ are, respectively, the spatial correlation functions of AGNs and star-forming galaxies, while $M^{\rm AGN}_{\rm eff}$ and $M^{\rm SF}_{\rm eff}$ denote the effective masses of the corresponding

dark matter halos (cf. equation 6.1). Note that this definition likely overestimates the cross-correlation term, which may be close to zero or negative since AGN-powered radio sources are normally found in clusters while star-forming galaxies preferentially reside in the field.

The angular correlation function of radio galaxies can be computed once the values of both $M_{\rm eff}^{\rm AGN}$ and $M_{\rm eff}^{\rm SF}$ are provided.

The observationally determined spatial correlation length of star-forming galaxies, that is $r_0(z = 0) \sim 3$–4 Mpc/h (Saunders, Rowan-Robinson & Lawrence 1992; see also Wilman et al. 2003), is consistent with an effective halo mass not exceeding $M_{\rm eff}^{\rm SF} = 10^{11}$ $M_\odot$/h. I will adopt this value in the following analysis. Any dependence of $M_{\rm eff}^{\rm SF}$ on redshift can be ignored because of the small redshift range probed by star-forming galaxies with $S_{1.4\rm GHz} \geq 10$ mJy. Less obvious is the value of $M_{\rm eff}^{\rm AGN}$ and also its dependence on redshift. Therefore, I will compare the predicted angular correlation function of radio sources with the one that is observationally determined in order to get constaints on both the effective mass of the haloes in which radio AGNs reside and on its cosmic evolution.

6.5 Results

6.5.1 A redshift-dependent halo mass for radio AGNs?

As a first step, I obtain estimates of the angular two-point correlation function, $w(\theta)$, by assuming a redshift-independent effective mass for the host halos of AGN-powered radio sources, $M_{\rm eff}^{\rm AGN}$. This is in agreement with the clustering properties of optically selected quasars (Porciani, Magliocchetti & Norberg 2004; Croom et al. 2005). The value of $M_{\rm eff}^{\rm AGN}$ is taken as a free parameter.

The top panel of Fig. 6.4 shows the contributions to $w(\theta)$ of NVSS sources with $S_{1.4\rm GHz} \geq 10\,$mJy arising from the clustering of AGNs with $M_{\rm eff}^{\rm AGN} = 10^{13}$, 10^{14}, and $10^{15}\,M_\odot$/h (short-dashed curves) and star-forming galaxies (long-dashed curve), as well as from the cross-correlation between these two populations (dotted curves). As noted above, the cross correlation term, computed from equation (6.8) for the three values of $M_{\rm eff}^{\rm AGN}$, is

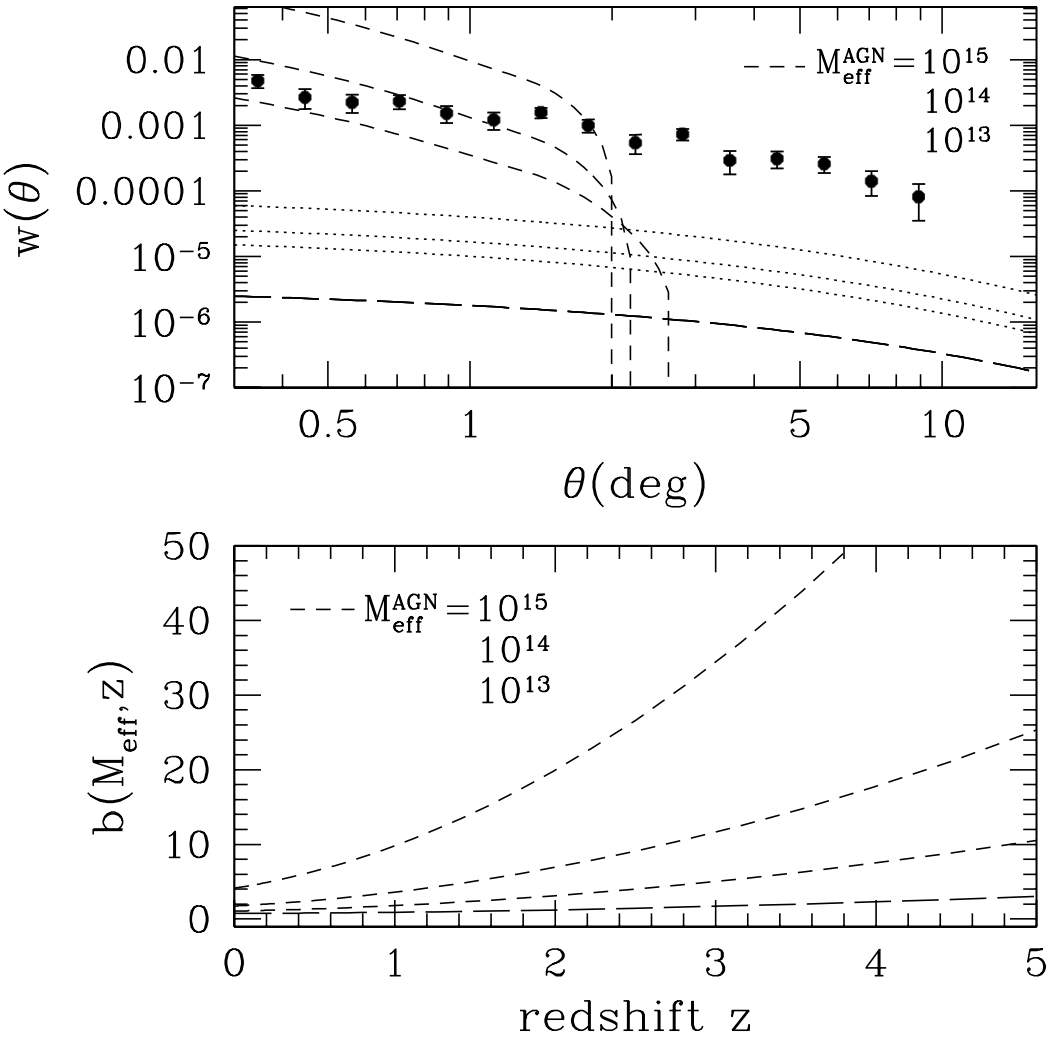

Figure 6.4: *Top panel*: contributions to the two-point angular correlation function of NVSS sources with $S_{1.4\mathrm{GHz}} \geq 10$ mJy from AGNs (short-dashed curves), star-forming galaxies (long-dashed curve), and their cross-correlation (dotted curves). The effective halo mass of AGN-powered radio galaxies is assumed to be constant with redshift. The three short-dashed and dotted curves correspond, from bottom to top, to $M_{\mathrm{eff}}^{\mathrm{AGN}} = 10^{13}$, 10^{14} and $10^{15}\,M_\odot/h$, respectively. The effective mass of the haloes in which star-forming galaxies reside is $M_{\mathrm{eff}}^{\mathrm{SF}} = 10^{11}\,M_\odot/h$ (long-dashed curve). Points with error bars represent the angular two-point correlation function of NVSS sources as measured by Blake & Wall (2002b). *Lower panel*: Evolution of the bias parameter for AGNs (short-dashed curves) and star-forming galaxies (long-dashed curve).

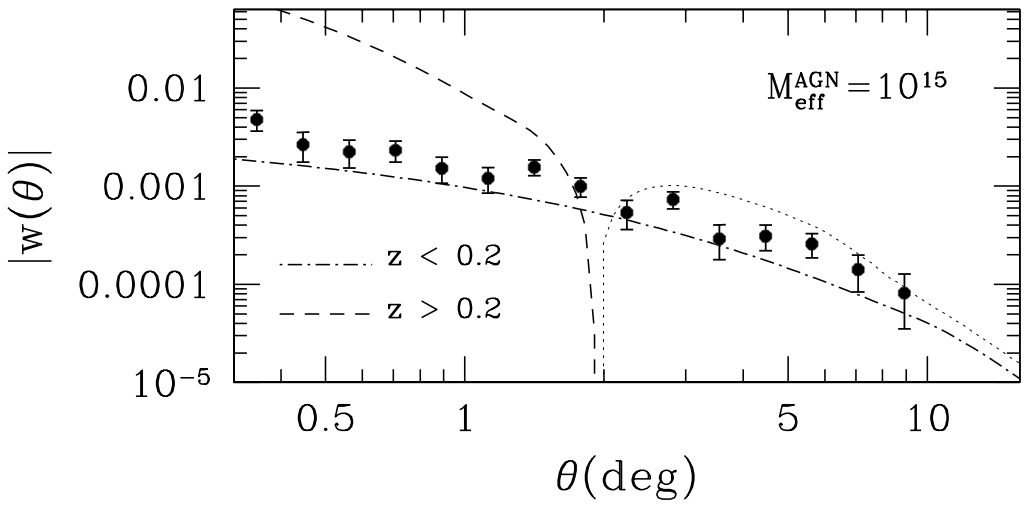

Figure 6.5: Contributions to the two-point angular correlation function of NVSS sources with $S_{1.4\mathrm{GHz}} \geq 10$ mJy from radio sources above (dashed and dotted lines) and below (dot-dashed line) $z = 0.2$, for $M_{\mathrm{eff}}^{\mathrm{AGN}} = 10^{15}\, M_{\odot}/\mathrm{h}$ and $M_{\mathrm{eff}}^{\mathrm{SF}} = 10^{11}\, M_{\odot}/\mathrm{h}$. Star-forming galaxies contribute (yet marginally) only at $z < 0.2$. The contribution of higher redshift sources (AGNs only) is positive for $\theta \lesssim 2^{\circ}$, and becomes negative on larger scales (the dotted line shows its absolute value).

likely overestimated. The above contributions are then compared with the observational determination of Blake & Wall (2002b). In the lower panel of the same Figure the redshift-evolution of the bias parameter is represented.

Figure 6.4 shows that the contribution of star-forming galaxies to the observed angular correlation function is negligible. This is because their contribution to the $S_{1.4\mathrm{GHz}} \geq 10$ mJy counts is small, implying $f_{\mathrm{SF}} \sim 5 \times 10^{-3}$ [see equation (6.5)], compared with $f_{\mathrm{AGN}} \sim 1$. This conclusion is in disagreement with that of Cress & Kamionkowsky (1998), which relies on the adoption of a local RLF of star-forming galaxies strongly exceeding the direct estimates of M02.

Clearly, models in which the effective mass of the haloes hosting radio AGNs is constant in redshift badly fail at reproducing the overall shape of the observed angular correlation function. This is because contributions to $w_{\mathrm{AGN}}(\theta)$ on a given angular scale come from both local and high-redshift sources. For a redshift-independent halo mass, on scales $\theta \gtrsim 2^{\circ}$ the

positive contribution of local sources is overcome by the negative contribution of distant AGNs which dominate the source redshift distribution and whose bias parameter rapidly increases with look-back time [see equation (6.1) and Fig. 6.4].

The situation is illustrated by Fig. 6.5 which shows that the contribution to $w_{\rm AGN}(\theta)$ from local AGNs ($z < 0.2$, dot-dashed line) with $M_{\rm eff}^{\rm AGN} = 10^{15}\,M_{\odot}/{\rm h}$ comes close to accounting for the observed angular correlation function (the dot-dashed line also includes the contribution of star-forming galaxies with $M_{\rm eff}^{\rm SF} = 10^{11}\,M_{\odot}/{\rm h}$, which however turns out to be almost negligible). But if the same value of $M_{\rm eff}^{\rm AGN}$ also applies to high-redshift AGNs, $w_{\rm AGN}(\theta)$ turns out to be too high on small scales and negative on large scales. Therefore, the only way to account for the behaviour of the data on large scales is to weight down the high-z contribution by decreasing the bias factor at such redshifts. A similar result – which drastically rules out models featuring a bias function strongly increasing with z – was obtained by Magliocchetti et al. (1999) via their counts in cells analysis of the FIRST data.

Having shown that the contribution of star-forming galaxies to the clustering signal is negligible, hereafter I will only consider AGNs and will drop the 'AGN' index from the effective mass.

6.5.2 The clustering evolution of radio AGNs

The only way to cancel the increment of the bias parameter with look-back time is to assume that the typical mass of the halo hosting AGN-powered radio sources decreases with redshift. A mass that behaves in such a way is the characteristic mass $M_{\star}(z)$, defined in chapter 1 (subsection 1.2.4) by the condition:

$$\sigma[M_{\star}(z), z] = \delta_c(z)\ . \tag{6.9}$$

$M_{\star}(z)$ represents the typical mass-scale at which the matter density fluctuations collapse to form bound structures and therefore it is associated to the massive virialized systems which collapse at each redshift. In the bottom-up scenario of structure formation envisaged by the CDM paradigm, $M_{\star}(z)$ is a decreasing function of redshift. Provided that AGN-powered radio galaxies are mainly found in very dense environments such as groups or clusters of

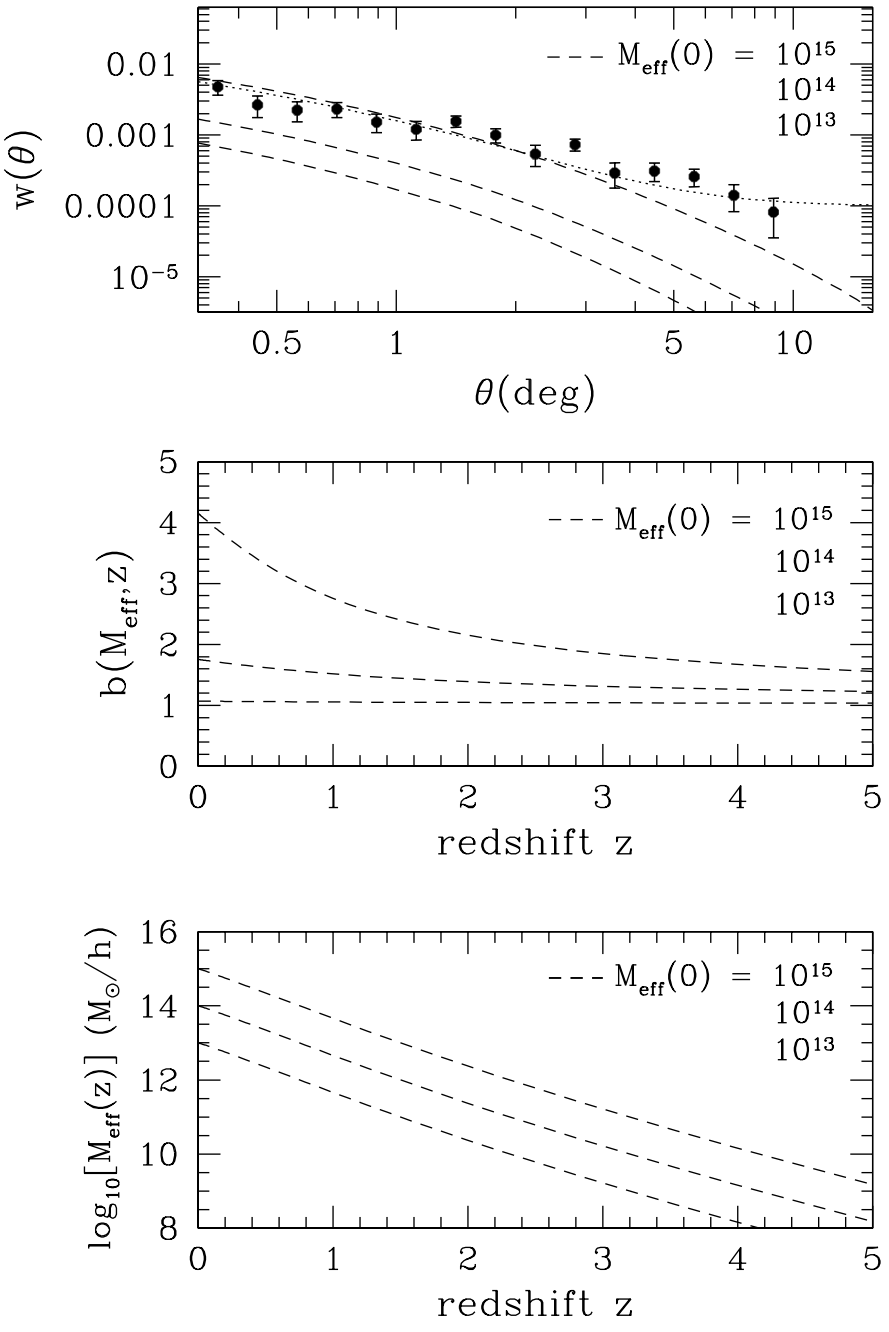

Figure 6.6: Two-point angular correlation function (top panel), bias parameter (central panel), and effective mass of the host dark matter haloes (bottom panel) for radio sources with $S_{1.4\mathrm{GHz}} \geq 10\,\mathrm{mJy}$ in a model in which $M_{\mathrm{eff}} \propto M_{\star}(z)$ (see text for details). The three dashed curves correspond, from bottom to top, to different local values of the effective mass: $\mathrm{M_{eff}}(z=0) = 10^{13}$, 10^{14} and $10^{15}\,M_{\odot}/\mathrm{h}$. The dotted line in the top panel represents the prediction obtained for $M_{\mathrm{eff}}(z=0) = 10^{14.9}\,M_{\odot}/\mathrm{h}$ by adding a constant offset $\epsilon = 0.0001$ to $w(\theta)$ in order to account for the effect of possible spurious density gradients in the survey. Points with error bars show the two-point angular correlation function of NVSS sources as measured by Blake & Wall (2002b).

galaxies, it looks resonable to assume that the epoch-dependent effective mass controlling their clustering properties, $M_{\rm eff}$ is proportional to $M_\star(z)$.

As required by the data, this choice for $M_{\rm eff}$ (whose redshift dependence is shown in the bottom panel of Fig. 6.6) leads to an almost redshift-independent bias factor (central panel of Fig. 6.6) except for the highest value of $M_{\rm eff}(0)$ for which one finds a moderate decrease of b for increasing z.

As shown by the top panel of Fig. 6.6, this model successfully reproduces the observed $w(\theta)$ up to scales of at least $\simeq 4^\circ$. The best fit is obtained for $M_{\rm eff}(z=0) = 10^{14.96\pm0.04}\, M_\odot/{\rm h}$. On the largest angular scales ($\theta \gtrsim 5^\circ$), the model correlation function still falls below the data. However, small systematic variations in the source surface density due to calibration problems at low flux densities may spuriously enhance the estimates of $w(\theta)$ (Blake & Wall 2002a). As a matter of fact, an offset as small as $\epsilon = 10^{-4}$ would be enough to remove the discrepancy between the model and the data (dotted line in the top panel of Fig. 6.6).

6.5.3 Dependence on cosmological parameters

If the measured $w(\theta)$ is indeed unaffected by spurious density gradients in the survey, it could be possible to reconcile the model with the observed signal by exploiting the dependence of the model predictions on the cosmological parameters, such as the matter density parameter, $\Omega_{0,m}$, the baryon density parameter, $\Omega_{0,b}$, and the Hubble constant, h (see Matsubara 2004, Fig. 1). In fact, decreasing $\Omega_{0,m}$ shifts the cut-off of the dark matter spatial correlation function $\xi_{\rm DM}$ to larger scales, while a non-null value of $\Omega_{0,b}$ generates a peak in the spatial correlation function just below the cut-off scale. The amplitude of this peak is an increasing function of $\Omega_{0,b}$.

A change in the value of h has an effect which is qualitatively similar to that induced by changing $\Omega_{0,m}$, but of a significantly smaller amplitude; for this reason, in the following analysis, this parameter is kept fixed to the reference value $h = 0.72$. The dependence of the clustering pattern on the rms mass fluctuation, σ_8, is also ignored: in principle this quantity contributes to the overall normalization of the spatial clustering, but

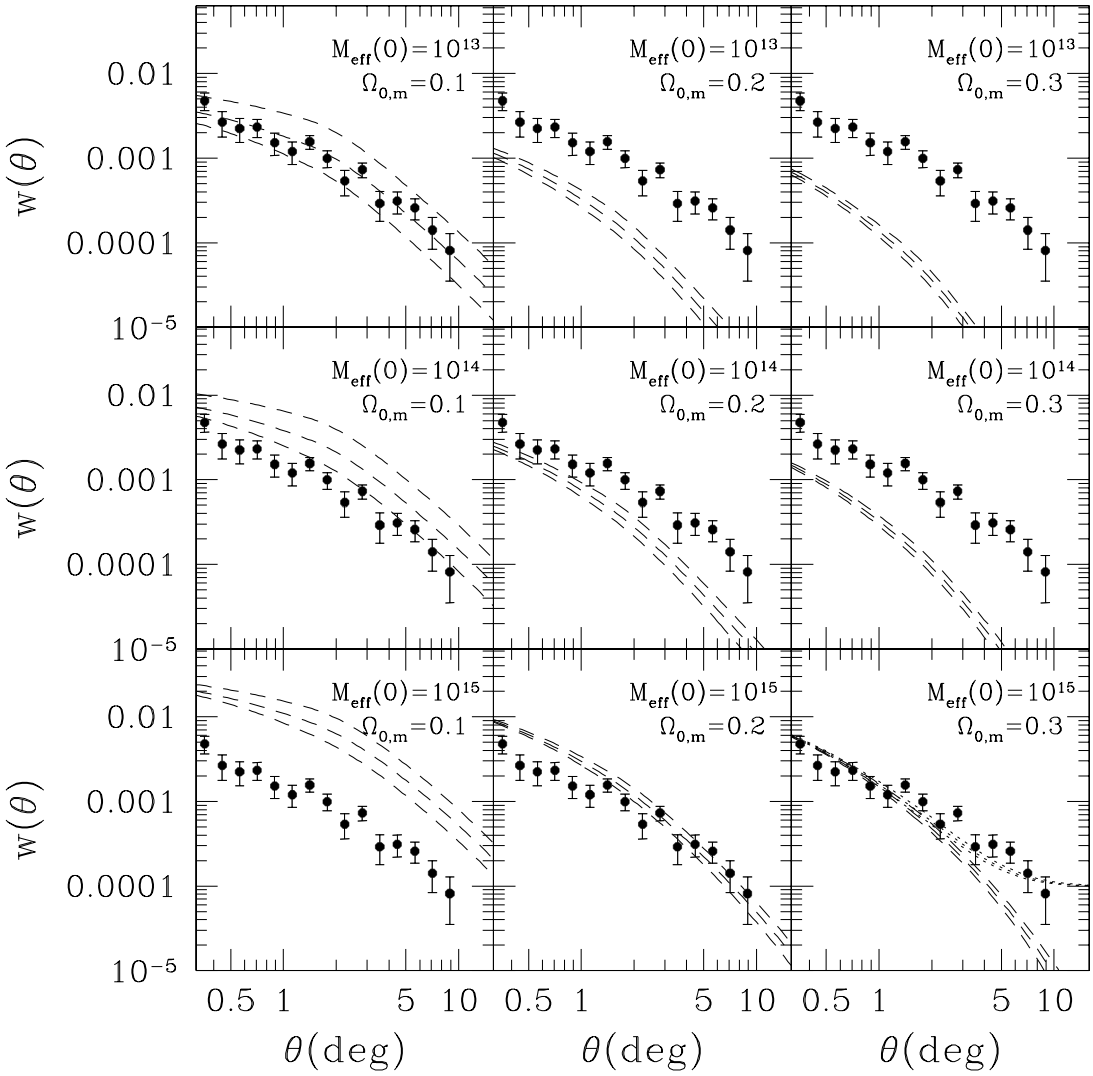

Figure 6.7: Dependence on cosmological parameters of the two-point angular correlation function of radio sources with $S_{1.4\mathrm{GHz}} \geq 10$ mJy. The effective mass of the dark matter haloes in which the sources reside is assumed to be proportional to $M_\star(z)$. In each panel, the adopted values of $M_{\rm eff}(0)$ (in solar units) and of the matter density parameter, $\Omega_{0,m}$ are indicated: the former increases from top to bottom panels while the latter increases from left-hand to right-hand panels. In each panel, the three dashed curves correspond to different choices for the baryonic mass density parameter: $\Omega_b = 0.03$, 0.045 and 0.06 from the lower to the upper curves, respectively. In the bottom right-hand panel the dotted curves (almost indistinguishable from each other) represent the two-point correlation function obtained by adding to the dashed curves a constant offset $\epsilon = 10^{-4}$ (see text for details).

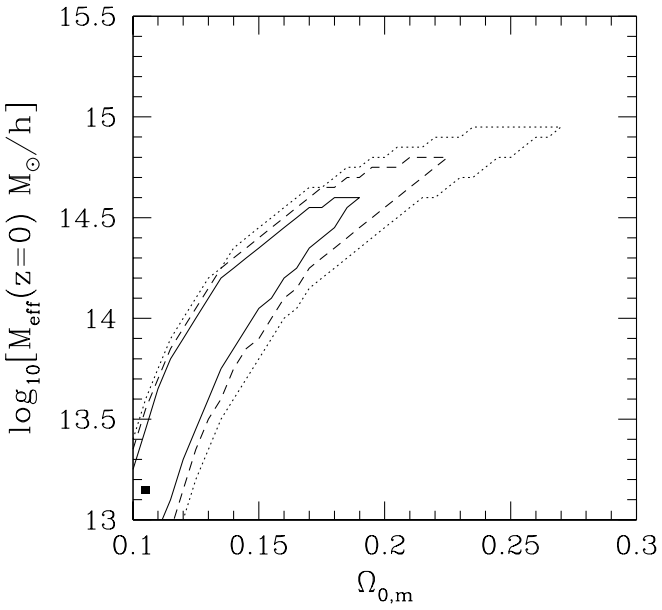

Figure 6.8: Confidence contours derived from a χ^2 analysis on the $\Omega_{0,m}$-$\log_{10}[M_{\rm eff}(z=0)]$ plane, having assumed $\Omega_b = 0.045$. The curves, from the inner to the outer one, correspond to the 68.3, 95.4 and 99.7 per cent confidence intervals. The filled square corresponds to the best-fit set of parameters $\Omega_{0,m} = 0.105$, $M_{\rm eff}(z=0) = 10^{13.15}\,M_\odot/{\rm h}$.

I have checked that in our case the effect is almost negligible. This is because the decrement of b with increasing σ_8 is compensated by the corresponding increment of both the dark matter spatial correlation function and of the effective mass (assumed to be proportional to $M_\star(z)$). Therefore also σ_8 is kept to the reference value 0.9.

The free parameters we are left with in our analysis are then: $M_{\rm eff}(0)$, $\Omega_{0,m}$ and $\Omega_{0,b}$. Fig. 6.7 shows the predicted two-point angular correlation function for different choices of these parameters. In each panel, the dashed curves correspond (from bottom to top) to $\Omega_{0,b} = 0.03$, 0.045 and 0.06. The values adopted for both $M_{\rm eff}(0)$, and $\Omega_{0,m}$ are given in each panel: $M_{\rm eff}(0)$ increases from the top to the bottom panels, while $\Omega_{0,m}$ increases from the left-hand to the right-hand panels.

Note that variations of these parameters within the allowed ranges mainly translate into changes of the normalization of $w(\theta)$, although varying $\Omega_{0,b}$ also affects the $w(\theta)$ slope

on scales $\theta \lesssim 2^\circ$, while changes in $\Omega_{0,m}$ modify its slope on larger scales. In general, the amplitude of $w(\theta)$ increases with increasing $M_{\rm eff}(0)$ or $\Omega_{0,b}$, and decreases for increasing $\Omega_{0,m}$. Fig. 6.7 then suggests that, given the observed $w(\theta)$, smaller values of $M_{\rm eff}(0)$ are favoured when combined with lower values of $\Omega_{0,m}$.

Fixing the baryonic content to the reference value $\Omega_{0,b} = 0.045$, I have then investigated the $\Omega_{0,m}$–$M_{\rm eff}(0)$ interdependence by constructing χ^2 contours on the $\Omega_{0,m}$-$M_{\rm eff}(0)$ plane. The results are shown in Fig. 6.8 where the curves represent, from the innermost to the outermost, contours corresponding to the 68.3, 95.4 and 99.7 per cent confidence intervals, respectively. The filled square corresponds to the best-fit set of parameters: $\Omega_{0,m} = 0.105$, $M_{\rm eff}(z=0) = 10^{13.15}\, M_\odot/{\rm h}$. The effect of a change in the baryonic content is just that of smearing the relation between $\Omega_{0,m}$ and $M_{\rm eff}(0)$ (in particular for $\Omega_{0,m} \lesssim 0.2$) since there is a whole set of $\Omega_{0,m}$–$M_{\rm eff}(0)$ pairs which can provide the same best-fit to the data.

Under the hypothesis of a zero offset, one finds that the fit obtained with the above combination of parameters is extremely good, although it is obtained for a local matter density parameter $\Omega_{0,m}$ which is smaller than indicated by other data sets (see e.g. Spergel et al. 2006). Note however that this difference is only significant to about a 2σ level.

As a last comment, I stress that the degeneracy between the host halo mass and the matter density parameter indicates that large area radio surveys without redshift information can hardly provide significant constraints on cosmological parameters, unless independent information on $M_{\rm eff}$ is available. On the other hand, for a given set of cosmological parameters, such surveys yield important information on the masses of the hosting halos.

6.6 Conclusions

In this chapter I have presented a theoretical analysis of the angular two-point correlation function of NVSS radio sources with $S_{1.4GHz} \geq 10$ mJy, which exhibits the puzzling feature of a power-law behaviour up to very large ($\sim 10^\circ$) angular scales. I have

found that standard models for clustering, which successfully account for the clustering properties of optically selected quasars, turn out to be unable to explain the long positive tail of the $w(\theta)$, even when 'extreme' values for the parameters are invoked. This is because – according to the standard scenario for biased galaxy formation in which extragalactic sources are more strongly clustered at higher redshifts – the clustering signal of radio sources at $z \gtrsim 1$, which is negative on large scales, overwhelms that of more local sources, and therefore determines a sharp cut-off in the angular two-point correlation function on scales of $\sim$ 1–2 degrees.

The only possible way to overcome this problem is to assume that the clustering strength of radio sources was weaker in the past. The data can then be accounted for if the characteristic mass of the halos in which these objects reside, $M_{\rm eff}(z)$, is proportional to $M_{\star}(z)$, the typical mass-scale at which the matter density fluctuations collapse to form bound structures (see Mo & White 1996).

A good fit of the observed $w(\theta)$ up to scales of at least 4° degrees is obtained for $M_{\rm eff}(z=0) = 10^{14.96 \pm 0.04}\, M_{\odot}/{\rm h}$. The data on larger scales can be accurately reproduced if the measured values of $w(\theta)$ are slightly enhanced by small systematic variations in the source surface density due to calibration problems at low flux densities, as envisaged by Blake & Wall (2002a).

In the absence of such a systematic offset, the data point towards a value for the mean cosmic matter density which is lower than what indicated by other data sets. In fact, the best fit in this case is obtained for $\Omega_{0,m} = 0.105$ and $M_{\rm eff}(z=0) = 10^{13.15}\, M_{\odot}/{\rm h}$, with rather large uncertainties on both parameters, as shown in Fig. 6.8. In particular, the best fit value of $\Omega_{0,m}$ is less than 3σ away from the 'concordance' value. This shows that current large scale radio surveys without redshift measurements cannot provide strong constraints on cosmological parameters, but are nevertheless informative on the evolution history of the dark matter halos hosting radio sources.

Taken at face value, the above results point to different evolutionary properties for different types of AGNs as the decreasing trend for the effective mass ruling the clustering properties of radio sources found in this work strongly differs from the behaviour of that

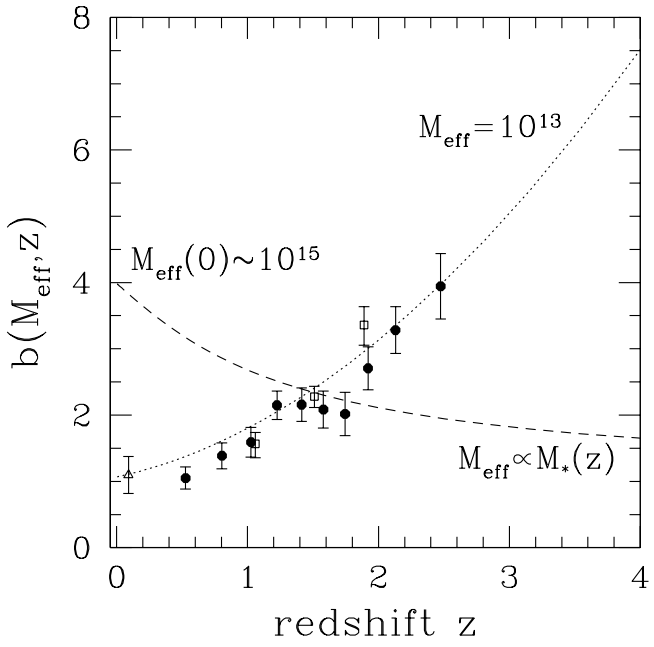

Figure 6.9: Bias factor as a function of redshift. The data points are from observations of optically selected quasars (open squares from Porciani et al. 2004, filled dots from Croom et al. 2005, open triangle from Grazian et al. 2004; the values of b derived by these authors have been scaled to the values of σ_8 and $\Omega_{0,m}$ used here), while the dashed line represents the functional form derived in this work for the mJy population of radio sources. The dotted curve shows the bias function obtained for a characteristic halo mass constant in time and equal to $\sim 10^{13}\,M_{\odot}/\mathrm{h}$.

associated to optically selected quasars. For the latter sources, the data are in fact consistent with a constant $M_{\rm eff} \sim 10^{13}\,M_{\odot}/\mathrm{h}$, at least up to the highest probed redshift, $z \simeq 2.5$ (see e.g. Grazian et al. 2004; Porciani et al. 2004; Croom et al. 2005). This different behaviour is illustrated in Fig. 6.9, where the values of the bias inferred for optically selected quasars have been scaled to the values of σ_8 and $\Omega_{0,m}$ used here.

It must be noted, however, that the available data provide very weak constraints on the clustering properties of radio sources at $z \gtrsim 1.5$. For example, I have directly checked that the predicted $w(\theta)$ does not change significantly over the range of angular scales considered

here if I assume $M_{\rm eff} \propto M_\star(z)$ for $z \lesssim 1.5$ and $M_{\rm eff} \sim$ const $\sim 10^{13}\, M_\odot$/h at higher redshifts. It is thus possible that the difference in the clustering evolution between AGN-powered radio sources and optically selected quasars is limited to $z \lesssim 1.5$, consistent with the observational indications that, at higher redshifts (i.e. $2.5 \lesssim z \lesssim 4.5$), the environment of radio-quiet and radio-loud QSOs is almost the same (Russel, Ellison & Benn 2005).

Interestingly, our analysis indicates that, at $z \simeq 1.5$, the effective halo mass associated to radio sources is consistent with being essentially equal to that of optical quasars (Croom et al. 2005). This suggests that, at least in this narrow redshift range, the bias parameter for radio-loud and radio-quiet AGNs is similar.

On the other hand, our findings suggest that, for $z \lesssim 1.5$ and at variance with what found for optical quasars, the clustering of radio sources reflects that of the largest halos which collapse at any given cosmic epoch. This conclusion is in keeping with results of previous studies showing that, locally, radio sources are preferentially associated with groups and clusters of galaxies (e.g. Peacock & Nicholson 1991; Magliocchetti et al. 2004) and, at higher redshift, are often associated with very massive galaxies and very massive galaxy environments (e.g. Carilli et al. 1997; Best, Longair & Röttgering 1998; Venemans et al. 2002; Best et al. 2003; Croft et al. 2005; Overzier et al. 2006).

Chapter 7

Conclusions

Observations at sub-mm and radio wavelengths are very informative on the large-scale structure of the Universe at high redshift. While the radio band is suited for detecting distant powerful AGNs, the sub-mm band can probe the earliest and most dramatic stages of the evolution of galaxies in which most of the mass in stars present in the Universe today was assembled.

Investigation of the sub-mm Universe has been possible only in recent years thanks to the advent of the SCUBA facility. By observing at both 450 and 850 μm, SCUBA have reveled tens of bright sub-mm sources in sub-degree areas of the sky, whose peculiar features (a very high star-formation above all) make them to be identified with the high-z progenitors of local massive elliptical galaxies. This implies that SCUBA sources are highly biased tracers of the matter distribution and therefore should strongly cluster in space with a strength at least comparable to that of bright ellipticals at low-redshift. And indeed, some hints for a significant clustering of the sub-mm population emerge from the small sample of sources detected by SCUBA at 850μm.

Definitive constraints on the large scale distribution of high-z protospheroids will be provided by the new wide-area extragalactic surveys which will be carried out at far-IR to sub-mm wavelengths with both space satellites (e.g. NASA/Spitzer, ESA/Herschel, ESA/Planck) and ground-based instruments (e.g. SCUBA-2).

As a consequence of the small primary aperture of the telescopes operating from space in the far-IR/sub-mm waveband, most of these forthcoming surveys are expected to be strongly contaminated by source confusion. Clustering contributes to enhance the confusion by increasing the probability of having close pairs of objects falling within the telescope beam. This effect depends on the spatial two-point correlation function of the sources which is determined, on large scales, by the effective mass of the halo, $M_{\rm eff}$, in which the sources reside. SCUBA-like galaxies are the only sub-mm population for which clustering can significantly affect the confusion noise; I have shown that, for this class of objects, a dark halo mass of $M_{\rm eff} \sim 10^{13}\ h^{-1}\ {\rm M}_{\odot}$ is consistent with the result of Peacock et al. (2000) on the angular correlation function of the 850-μm background population in the *Hubble Deep Field* North and with the mass of the halo inferred for local bright elliptical galaxies and other related classes of sources (e.g. EROs).

By exploiting this constraint, clustering is found to increase the confusion noise - when compared to the case of purely Poisson fluctuations - by 10-25 per cent for the lowest frequency (i.e. the lowest angular resolution) Spitzer and Herschel channels while it is expected to dominate the source confusion noise in the case of Planck/HFI channels at $\nu \geq$ 143 GHz. These implies that the surveys performed by HFI will be strongly contaminated by clustering, while a minor contribution is expected for those carried out with Herschel.

In the same way in which it enhances the source confusion, clustering can also affect the estimates of the extragalactic source counts. In fact, in low-resolution surveys what the instrument measures is not the flux of individual objects but the sum of all physically related sources in a resolution element. As a consequence, the estimated source counts provide the abundance of *clumps of sources* rather than that of *individual sources* detected with high-resolution instruments. If, on one hand, this can be seen as a problem for low-resolution surveys performed in the far-IR/sub-mm waveband because of the strong clustering of SCUBA-like galaxies, on the other hand it can provide indirect information on the clustering properties of the sub-mm source population and can be exploited to find out protoclusters at high redshift in shallow wide-area surveys.

I have analyzed the effect of clustering on extragalactic source counts in the survey that will be carried out by Planck at 850 μm. To this aim I have developed a detailed formalism that is able to provide the counts of clumps once the luminosity function and the clustering properties of the sources under exam have been specified. The estimates of the distribution of clump luminosities indicate that, except under rather extreme assumptions, the clumps will show up, in the Planck maps, as fluctuations in the range $2\sigma - 5\sigma$. Since the effect is sensitive to both the two- and three-point correlation functions, the surface density of such clumps could provide a wealth of information on the clustering properties of SCUBA-like galaxies. Moreover, the catalog of candidate proto-clusters at substantial redshifts (typically at $z \sim 2 - 3$) that Planck is expected to provide will offer the unique opportunity to investigate the formation of large scale structure, to constrain the evolution of the dark energy and to probe primordial non-Gaussianity.

The reliability of the theoretical approach has been confirmed by detailed numerical simulations of sky patches performed using the fast algorithm recently developed by Gonzalez-Nuevo et al. (2004).
Numerical simulations have been performed also for the Herschel/SPIRE 500 μm survey (the one with the lowest resolution among those that will be carried out by SPIRE). In this case the "clump" formalism no longer applies since the smallness of the ratio of the beam-width to the clustering angular size makes the observed fluxes to approach those of the brightest sources. The simulations have shown that the contribution of neighbors to the observed fluxes may lead to counts, at flux densities $\simeq 50 - 100$ mJy, several times higher than would be observed with a high resolution instrument. This means that even the sub-mm surveys of Herschel will encode indirect information on the clustering of SCUBA-like galaxies through its effect on the source counts estimates.

Although the availability of a complete sample of individual SCUBA-like galaxies would offer the most easy and efficient way to analyze the large scale structure sampled by these sources, a powerful complement is offered by the study of the statistical properties of the far-IR/sub-mm background light contributed by unresolved sources. The wide-area surveys that will be carried out by Planck/HFI will be relatively shallow, so that a wealth of

complementary information on the clustering properties of high-z protospheroids will be encoded in the power spectrum of fluctuations on sub-degree scales, as a confirmed by a number of theoretical works.

A signal in excess of that expected for primordial CMB anisotropies, on arcminute scales, has been recently found by a number of experiments like CBI and BIMA at 30GHz and ACBAR at 150 GHz. Although a non negligible fraction of this signal can be contributed by the thermal Sunyaev-Zeldovich (SZ) effect, we have shown that at 30 GHz, fluctuations due to unsubtracted radio sources are higher than estimated by the CBI and BIMA groups. Within the uncertainties due to the extrapolation of the radio source counts from lower to higher frequencies, they can account for the whole excess signal measured by CBI and for a significant fraction of it in the case of BIMA. High-z protospheroids are instead predicted to dominate the fluctuations due to extragalactic sources at 150 GHz, thus accounting for most of the power measured by ACBAR in the highest multipole bin where clustering dominates over Poisson fluctuations.

Once the contribution from unresolved/unsubtracted is taken into account, there is room for a contribution from the Sunyaev-Zeldovich effect within clusters of galaxies, with a density fluctuation amplitude parameter, σ_8, consistent with the values preferred by current data (i.e. σ_8 ~0.7-0.9).

The sub-mm astronomy is still at its beginning and better constraints on the statistical properties of the source in this waveband awaits the next generation of dedicated instruments. In the meantime, information on the the large scale structure of the high-redshift Universe and its cosmic evolution can be obtained by exploiting the existing data sets in order to provide a coherent scenario of structure formation in which sub-mm galaxies could then be located.

Observations in the radio band are the best suited to provide an unbiased sample of large volumes of the Universe up to very high redshifts. Many large-area radio samples are already available. Among all, that provided by the NVSS is the most extended: it covers more than half of the whole-sky and counts $\sim 10^6$ sources down to fluxes of few mJy at 1.4 GHz.

According to the phenomenological model of Dunlop & Peacock (1990), the most of the objects with $S_{1.4\mathrm{GHz}} > 10$ mJy in the NVSS sample are powered by an AGN and have a mean redshift $\langle z \rangle \sim 1$. Interestingly, the angular correlation function $w(\theta)$ of these sources exhibits a power-law behavior up to very large (~ 10 degrees) angular scales that is difficult to explain within the standard scenario for biased structure formation, in which extragalactic sources are more strongly clustered at high redshift. After having discarded the possibility that the angular clustering signal can be explained by a high-density local ($z \lesssim 0.1$) source population, I have found no alternatives to assuming that - at variance with all the other extragalactic populations studied so far, and in particular optically selected quasars - the radio sources responsible for the large-scale clustering signal were increasingly *less* clustered with increasing look-back time, up to at least $z \sim 1.5$.

The data are accurately accounted for in terms of a bias function which decreases with increasing redshift, mirroring the evolution with cosmic time of the characteristic halo mass, $M_\star$, entering the non-linear regime. In the framework of the standard concordance model (the one emerging from WMAP data), the effective halo mass controlling the bias parameter is found to decrease from about $10^{15}\ h^{-1}\ \mathrm{M}_\odot$ at $z \sim 0$ to the value appropriate for optically selected quasars, $\sim 10^{13}\ h^{-1}\ \mathrm{M}_\odot$, at $z \sim 1.5$. This suggests that, in the redshift range probed by the data, the clustering evolution of radio sources - and probably the triggering of radio activity - is ruled by the growth of large-scale structure, and that they are associated with the densest environments virializing at any cosmic epoch.

The data provide only loose constraints on the radio source clustering at $z \gtrsim 1.5$ so that the possibility that at these redshifts the clustering evolution of radio sources enters a different regime, perhaps similar to that found for optically selected quasars, cannot be ruled out.

Bibliography

[1] Abazajian K., Zheng Z., Zehavi I. et al., 2005, ApJ, **625**, 613

[2] Argüeso F., González-Nuevo J., Toffolatti L., 2003, ApJ, **598**, 86

[3] Bardeen J. M., Bond J. R., Kaiser N., Szalay A. S., 1986, ApJ, **304**, 15

[4] Barger A. J., Cowie L. L., Sanders D. B., 1999, ApJ, 518, L5

[5] Barger A. J., Cowie L. L., Sanders D. B., Fulton E., Taniguchi Y., Sato Y., Kawara K., Okuda H., 1998, Nat, **394**, 248

[6] Bartelmann M., Doran M., Wetterich C., 2006, A&A, 454, 27

[7] Baugh C. M., Lacey C. G., Frenk C. S., Granato G. L., Silva L., Bressan A., Benson A. J., Cole S., 2005, MNRAS, **356**, 1191

[8] Becker R.H., White R.L., Helfand D.J., 1995, ApJ, **450**, 559

[9] Bennett C. L., Hill R. S., Hinshaw G. et al., 2003, ApJS, **148**, 97

[10] Benson A. J., Cole S., Frenk C. S., Baugh C. M., Lacey C. G., 2000, MNRAS, **311**, 793

[11] Berlind A. A. et al., 2003, ApJ, **593**, 1

[12] Bernard J.-Ph, Meny C., Dupac X., et al. 2003, paper presented at the Planck WG7 meeting, Jodrell Bank

[13] Bernardeau F., 1994, A&A, **291**, 697

[14] Bernardeau F., Schaeffer R., 1992, A&A, **255**, 1

[15] Bernardeau F., Schaeffer R., 1999, A&A, **349**, 697

[16] Bertoldi F., Menten K. M., Kreysa E., Carilli C. L., Owen, F., 2001,in 'Highlights of Astronomy', Edited by H. Rickman. San Francisco, CA: PASP, Vol. 12

[17] Best P. N., Lehnert M. D., Miley G. K., Röttgering H. J. A., 2003, MNRAS, **343**, 1

[18] Best P. N., Longair M. S., Röttgering H. J. A., 1998, MNRAS, **295**, 549

[19] Blain A. W., 2001, in Cristiani S., Renzini A., Willians R. E., eds, Proc. ESO7ECF/STScI workshop, Deep Fields. Springer, Berlin, p.129

[20] Blain A. W., Chapman S. C., Smail I., Ivison R., 2004, ApJ, **611**, 725

[21] Blain A. W., Ivison R. J., Smail I., 1998, MNRAS, **296**, L29

[22] Blain A. W., Kneib J-P., Ivison R. J., Smail I., 1999, ApJ, **512**, L87

[23] Blain A. W., Longair M. S., 1993, MNRAS, **264**, 509

[24] Blain A. W., Smail I., Ivison R. J., Kneib J.-P., Frayer D. T., 2002, PhR, 369, 111

[25] Blake C., Mauch T., Sadler E.M., 2004, MNRAS, **347**, 787

[26] Blake C., Wall J., 2002a, MNRAS, **329**, L37

[27] Blake C., Wall J., 2002b, MNRAS, **337**, 993

[28] Blandford R. D., Begelman M. C., 1999, MNRAS, **303**, L1

[29] Bock D.C.-J., Large M.I., Sadler E.M., 1999, ApJ, **117**, 1578

[30] Bond J.R., Contaldi C.R., Pen U.L., et al., 2005, ApJ, **626**, 12

[31] Borys C., Chapman S., Halpern M., Scott D. 2002, MNRAS, **330**, L63

[32] Borys C., Chapman S., Halpern M., Scott D. 2003, MNRAS, **344**, 385

[33] Calzetti D., Armus L., Bohlin R. C., Kinney A. L., Koornneef J., Storchi-Bergmann, 2000, ApJ, **533**, 682

[34] Carilli C. L., Röttgering H. J. A., van Ojik R., Miley G. K., van Breugel W. J. M., 1997, ApJS, **109**, 1

[35] Carroll S. M., Press W. H., Turner E. L. 1992, ARA&A, **30**, 499

[36] Chapman S. C., Blain A. W., Ivison R. J., Smail I. R., 2003a, Nature, **422**, 695

[37] Chapman S. C. et al., 2001, ApJ, **548**, L17

[38] Chapman S. C. et al., 2003b, ApJ, **585**, 57

[39] Chapman S. C., Blain A. W., Smail I., Ivison R. J., 2005, ApJ, **622**, 772

[40] Chapman S. C., Scott D., Borys C., Fahlman G. G., 2002, MNRAS, **330**, 92

[41] Ciaramella A., Bongardo C., Aller H. D., et al. 2004, A&A, **419**, 485

[42] Cirasuolo M., Shankar F., Granato G. L., De Zotti G., Danese L., 2005, ApJ, **629**, 816

[43] Colberg J. M. et al., 2000, MNRAS, **319**, 209

[44] Cole S. et al., 2005, MNRAS, **362**, 505

[45] Cole S., Lacey C. G., Baugh C. M., Frenck C. S., 2000, MNRAS, **319**, 168

[46] Coles P., Jones B., 1991, MNRAS, **248**, 1

[47] Coles P., Lucchin F., 1995, *Cosmology: The origin and evolution of cosmic structure*, Chichester: Wiley, 1995

[48] Colombi S., Bouchet F. R., Hernquist L., 1996, ApJ, **465**, 14

[49] Condon J. J., 1974, ApJ, **188**, 279

[50] Condon J. J., Cotton W. D., Greisen E. W., Yin Q. F., Perley R. A., Taylor G.B., Broderick J. J., 1998, AJ, **115**, 1693

[51] Cooray A., Melchiorri A., 2002, PhRvD, **66**, 083001

[52] Cress C. M., Helfand D. J., Becker R. H., Gregg M. D., White R. L., 1997, ApJ, **473**, 7

[53] Cress C. M., Kamionkowski M., 1998, MNRAS, **297**, 486

[54] Croft S., Kurk J., van Breugel W., Stanford S. A., de Vries W., Pentericci L., Röttgering H., 2005, AJ, **130**, 867

[55] Croom S.M., Boyle B.J., Loaring N.S., Miller L., Outram P.J., Shanks T., Smith R.J., 2002, MNRAS, **335**, 459

[56] Croom S.M., Shanks T., Boyle B.J., Smith R.J., Miller L., Loaring N.S, Hoyle F., 2001, MNRAS, **325**, 483

[57] Croom S. M., et al., 2005, MNRAS, **356**, 415

[58] Daddi E., Broadhurst T., Zamorani G., Cimatti A., Rottgering H., Renzini A., 2001, A&A, **376**, 825

[59] Daddi E. et al., 2001, A&A, **361**, 535

[60] Daddi E. et al., 2003, ApJ, **588**, 50

[61] Dallacasa D., Stanghellini C., Centonza M., Fanti R., 2000, A&A, **363**, 887

[62] Dautcourt G., 1977, Astronomische Nachrichten, **298**, 141

[63] Davis M., Efstathiou G., Frenk C. S., White S. D. M., 1985, ApJ, **292**, 371

[64] Dawson K. S., Holzapfel W. L., Carlstrom J. E., Joy M., LaRoque S. J., Reese E. D., 2001, ApJ, **553**, L1

[65] Dawson K. S., Holzapfel W. L., Carlstrom J. E., Joy M., LaRoque S. J., Miller A. D., Nagai, D., 2002, ApJ, **581**, 86

[66] De Breuck et al., 2004, A&A, 424, 1

[67] Dekel A., Lahav O., 1999, ApJ, **520**, 24

[68] Devriendt J. E. G., Guiderdoni B., 2000, A&A, **363**, 851

[69] De Zotti G., Burigana C., Cavaliere A., Danese L., Granato G.L., Lapi A., Platania P., Silva L., 2004, in Proc. Int. Symp. Plasmas in the Laboratory and in the Universe: new insights and new challenges, eds. G. Bertin, D. Farina & R. Pozzoli, AIP Conf. Proc., 703, 375

[70] De Zotti G., Franceschini A., Toffolatti L., Mazzei P., Danese L., 1996, ApL&C, **35**, 289

[71] De Zotti G., Granato G.L., Silva L., Maino D., Danese L., 2000, A&A, **354**, 467

[72] De Zotti G., Ricci R., Mesa D., Silva L., Mazzotta P., Toffolatti L., González-Nuevo J., 2005, A&A, **431**, 893

[73] De Zotti G., Shankar F., Lapi A., Granato G. L., Silva L., Cirasuolo M. Salucci P. Danese L., 2006, MmSAI, **77**, 661

[74] Di Matteo T., Carilli C. L., Fabian A. C., 2001, ApJ, **547**, 731

[75] Di Matteo T., Fabian A. C., Rees M. J., Carilli C. L., Ivison R. J., 1999, MNRAS, **305**, 492

[76] Dole H. et al., 2001, A&A, **372**, 364

[77] Dole H., Lagache G., Puget J.-L., 2003, ApJ, **585**, 617

[78] Dole H. et al., 2004, ApJSS, **154**, 93

[79] Douspis M., Aghanim N., Langer M., 2006, submitted to A&A, (astro-ph/0601597)

[80] Dressler A., 1980, ApJ, **236**, 351

[81] Dunlop J. S., 2001, NewAR, **45**, 609

[82] Dunlop J. S., Peacock J.A., 1990, MNRAS, **247**, 19

[83] Dupac X., Bernard J.-P., Boudet N., et al. 2003, A&A, **404**, L11

[84] Dupac X., Bernard J.-P., Boudet N., Giard M., Lamarre J.M., Mény C., Pajot F., Ristorcelli I., 2004, in The Dense Interstellar Medium in Galaxies, Proc. 4th Cologne-Bonn-Zermatt Symp., ed. Pfalzner S., Kramer C., Straubmeier C., Heithausen A. (Springer Proc. Phys.), 91, 419

[85] Eales S., Lilly S., Gear W., Dunne L., Bond R. J., Hammer F., Le Fevre O., Crampton D., 1999, ApJ, **515**, 518

[86] Eales S., Lilly S., Webb T., Dunne L., Gear W., Clements D., Yun M., 2000, AJ, **120**, 2244

[87] Eisenstein D. J. et al., 2005, ApJ, **633**, 560

[88] Eisenstein D. J., Hu W., 1998, ApJ, **496**, 605

[89] Eddington A. S., 1913, MNRAS, **73**, 359

[90] Fabian A. C., Rees M. J., 1995, MNRAS, **277**, L55

[91] Fanaroff B. L., Riley J. M, 1974, MNRAS, **167**, 31

[92] Fanti C., Fanti R., Dalla Casa D. et al., 1995, A&A, **302**, 317

[93] Farrah D. et al., 2006, ApJ, **641**, 17, erratum **643**, 139

[94] Fixen D. J., Dwek E., Mather J. C., Bennet C. L., Shafer R. A., 1998, ApJ, **508**, 123

[95] Fomalont E. B., Kellermann K. I., Partridge R. B., Windhorst R. A., Richards E. A., 2002, AJ, **123**, 2402

[96] Fomalont E. B., Windhorst R. A., Kristian J.A., Kellerman K.I. 1991, AJ, **102**, 1258

[97] Fox M. J. et al., 2002, MNRAS, **331**, 839

[98] Fisher K.B.; Davis M., Strauss M.A., Yahil A., Huchra J., 1994, MNRAS, **266**, 50

[99] Franceschini A., 2003, In: Galaxies at high redshift. XI Canary Islands Winter School of Astrophysics, Santa Cruz de Tenerife, Spain, November 15 - 26, 1999, edited by I. Prez-Fournon, M. Balcells, F. Moreno-Insertis and F. Snchez. Cambridge, UK: Cambridge University Press, 2003, p. 69-129

[100] Franceschini A., Aussel H., Cesarsky C.J., Elbaz D., Fadda D., 2001, A&A, **378**, 1

[101] Franceschini A., Berta S., Rigopoulou D., et al., 2003, A&A, **403**, 501

[102] Frith W. J., Outram P. J., Shanks T., 2005, MNRAS, **364**, 593

[103] Fry J. N., 1984, ApJ, **279**, 499

[104] Fry J. N., Gaztañaga E., 1993, ApJ, **413**, 447

[105] Fry J. N., Melott A., Shandarin S.F., 1993, ApJ, **412**, 504

[106] Fry J. N., Seldner M., 1982, ApJ, **259**, 474

[107] Galliano F., Madden S. C., Jones A. P., Wilson C. D., Bernard J. P., Le Peintre F., 2003, A&A, **407**, 159

[108] Gaztañaga E., Bernardeau F., 1998, A&A, **331**, 829

[109] Genzel R., Cesarsky C., 2000, ARA&A, **38**, 761

[110] Giavalisco M., Dickinson M., 2001, **ApJ**, 550, 177

[111] Gnedin N. Y., Jaffe A. H., 2001, ApJ, **551**, 3

[112] González-Nuevo, J., Argüeso F., López Caniego M., Toffolatti L., Sanz J. L., Vielva P., Herranz D., 2006, MNRAS, **369**, 1603

[113] González-Nuevo J., Toffolatti L., & Argüeso F., 2005, ApJ, **621**, 1

[114] Granato G.L., Silva L., Monaco P., Panuzzo P., Salucci P., De Zotti G., Danese L., 2001, MNRAS, **324**, 757

[115] Granato G.L., De Zotti G., Silva L., Bressan A., Danese L., 2004, ApJ, **600**, 580

[116] Grazian A., Negrello M., Moscardini L., Cristiani S., Haehnelt M. G., Matarrese S., Omizzolo A., Vanzella E., 2004, AJ, **127**, 592

[117] Greve T.R., Ivison R.J., Bertoldi F., Stevens J.A., Dunlop J.S., Lutz D., Carilli C.L., 2004, MNRAS, **354**, 779

[118] Greve T. R., Ivison R. J., Stevens J. A., 2006, Astron. Nachr, **327**, 208

[119] Griffin M. J., Swinyard B. M., Vigroux L. G., 2000, Proc. SPIE, **4013**, 184

[120] Griffiths L.M., Kunz M., Silk J., 2003, MNRAS, **339**, 680

[121] Grossan B., Smoot G. F., 2006, submitted to A&A (astro-ph/0604512)

[122] Gruppioni C., Lari C., Pozzi F., Zamorani G., Franceschini A., Oliver S., Rowan-Robinson M., Serjeant S., 2002, MNRAS, **335**, 831

[123] Gruppioni C., Pozzi F., Zamorani G., Ciliegi P., Lari C., Calabrese E., La Franca F., Matute I., 2003, MNRAS, **341**, L1

[124] Guzzo L., 2000, Nuclear Physics B Proceedings Supplements, Vol. 80, Proceedings of the Texas Symposium on Relativistic Astrophysics and Cosmology held in Paris, France, 14-18 December, 1998 (astro-ph/9911115)

[125] Guzzo L., Strauss M.A., Fisher K.B., Giovanelli R., Haynes M., 1997, ApJ, **489**, 37

[126] Haiman Z., Knox L., 2000, ApJ, **530**, 124

[127] Hauser M. G. et al., 1998, ApJ, **508**, 25

[128] Hill G. J., Lilly S. J., 1991, ApJ, 367, 1

[129] Hogg D. W., 2001, AJ, **121**, 1207

[130] Hogg D. W., Turner E. L., 1998, PASP, **110**, 727

[131] Holland W. S. et al., 1999, MNRAS, **303**, 659

[132] Holzapfel W. L., Carlstrom J. E., Greco L., Holder G., Joy M., Reese E. D., 2000, **539**, 57

[133] Hughes D. et al., 1998, Nat, **394**, 241

[134] Hughes D.H., Gaztañaga E., 2001, in Lowenthal J.D. & Hughes D.H., eds, Proc. of the conference Deep millimeter surveys: implications for galaxy formation and evolution. World Scientific Publishing, Singapore, p. 207

[135] Impey C. D., Neugebauer G., 1988, AJ, **95**, 307

[136] Ivezić Z. et al., 2002, ApJ, **124**, 2364

[137] Ivison R. J., Dunlop J. S., Smail I., Dey A., Liu M. C., Graham J. R., 2000, ApJ, **542**, 27

[138] Ivison R. J. et al., 2002, MNRAS, **337**, 1

[139] Ivison R. J. et al., 2005, MNRAS, **364**, 1025

[140] Jackson C. A., Wall J. V., 1999, MNRAS, **304**, 160

[141] Jeong W.-S., Pearson C. P., Lee H. M., Pak S., Nakagawa T., 2006, MNRAS, **369**, 281

[142] Jing Y.P., Boerner G., 1997, A&A, **318**, 667

[143] Jing Y.P., Boerner G., 1998, ApJ, **503**, 37

[144] Jing Y.P., Boerner G., 2004, ApJ, **607**, 140

[145] Juszkiewicz R., Bouchet F.R., Colombi S., 1993, ApJ, **412**, L9

[146] Kaiser N., 1984, ApJ, **264**, L9

[147] Kampen E. et al., 2005, MNRAS, **359**, 469

[148] Kayo I., Taruya A., Suto Y., 2001, ApJ, **561**, 22

[149] Kawakatu N., Umemura M., 2002, MNRAS, **329**, 572

[150] Kawakatu N., Umemura M., Mori M., 2003, ApJ, **583**, 85

[151] Kessler M. F., Steinz J. A., Anderegg M. E., Clavel J., Drechsel G. et al., 1996, A&A, **315**, 27

[152] Kiss Cs., Abraham P., Klaas U., Juvela M., Lemke, D., 2001, A&A, **379**, 1161

[153] Knox L., Cooray A., Eisenstein D., Haiman Z., 2001, ApJ, **550**, 7

[154] Knudsen K.K, van der Werf P.P., 2003, in Plionis M. ed., Proc. Conf. Multiwavelength Cosmology, preprint (astro-ph/0309184)

[155] Kofman L., Bertschinger E., Gelb J.M., Nusser A., Dekel A., 1994, ApJ, **420**, 44

[156] Komatsu E., Seljak U., 2002, MNRAS, **336**, 1256

[157] Kormendy J., Richstone D., 1995, ARA&A, **33**, 581

[158] Kuo C.L., Ade P.A.R., Bock J.J. et al., 2004, ApJ, **600**, 32

[159] Lagache G., Dole H., Puget J.-L., 2003, MNRAS, **338**, 555

[160] Lagache G., Puget J.-L., 2000, A&A, **355**, 17

[161] Lahav O., et al. (2dFGRS Team), 2002, MNRAS, **333**, 961

[162] Lamarre J.-M. et al., 2003, Proc. SPIE, **4850**, 730

[163] Landy S. D., Szalay A. S., 1993, ApJ, **412**, 64

[164] Lapi A. Shankar F., Mao J., Granato G. L., Silva L., De Zotti G., Danese L., 2006, ApJ in press (astro-ph/0603819)

[165] Larson R. B., 1998, MNRAS, 301, 569

[166] Limber D. N., 1953, ApJ, **117**, 134

[167] Lonsdale C.L. et al., 2003, PASP, **115**, 897

[168] Loveday J., Maddox S.J., Efstathiou G., Peterson B.A., 1995, ApJ, **442**, 457

[169] Lutz D. et al., 2001, A&A, 378, 70

[170] Madgwick D. S. et al., 2003, MNRAS, **344**, 847

[171] Madau P., Ferguson H. C., Dickinson M. E., Giavalisco M., Steidel C. C., Fruchter A., 1996, MNRAS, **283**, 1388

[172] Magliocchetti M., 2006, proceedings of the XLIst Rencontres de Moriond 'From Dark Halos to Light', L.Tresse, S.Maurogordato and J. Tran Than h Van editors (astro-ph/0606007)

[173] Magliocchetti M. et al., 2002, MNRAS, **333**, 100 (M02)

[174] Magliocchetti M. et al., 2004, MNRAS, **350**, 1485

[175] Magliocchetti M., Maddox S. J., Lahav O., Wall J. V., 1998, MNRAS, **300**, 257

[176] Magliocchetti M., Maddox S. J., Lahav O., Wall J. V., 1999, MNRAS, **306**, 943

[177] Magliocchetti M., Moscardini L., Panuzzo P., Granato G.L., De Zotti G., Danese L., 2001, MNRAS, **325**, 1553

[178] Magorrian J., et al. 1998, AJ, **115**, 2285

[179] Mason B.S., Pearson T.J., Readhead A.C.S., et al., 2003, ApJ, **591**, 540

[180] Matarrese S., Verde L., Jimenez R., 2000, ApJ, **541**, 10

[181] Matsubara T., 2004, ApJ, **615**, 573

[182] Mauch T., Murphy T., Buttery H. J., Curran J., Hunstead R. W., Piestrzynski B., Robertson J. G., Sadler E. M., 2003, MNRAS, **342**, 1117

[183] Menci N., Cavaliere A., Fontana A., Giallongo E., Poli F., 2002, ApJ, **575**, 18

[184] Mészáros P., 1974, A&A, **37**, 225

[185] Mo H. J., White S. D. M., 1996, MNRAS, **282**, 347

[186] Mortier A. M. J. et al., 2005, MNRAS, **363**, 563

[187] Moscardini L., Coles P., Lucchin F., Matarrese S., 1998, MNRAS, **299**, 95

[188] Moustakas L. A., Somerville R. S., 2002, ApJ, **577**, 1

[189] Murakami H., 1998, in Bely P. Y., Breckinridge J. B., eds, Proc. SPIE Vol. 3356, IR Space Telescopes and Instruments. SPIE, Bellingham, WA, p.471

[190] Murdoch H. S., Crawford D. F., Jauncey D. L., 1973, ApJ, **183**, 1

[191] Narayan R., Yi I., 1994, ApJ, **428**, L13

[192] Norberg P. et al., 2002, MNRAS, **332**, 827

[193] O'Dea C. P., 1998, PASP, **110**, 493

[194] Outram P. J., Hoyle F., Shanks T., Croom S. M., Boyle B. J., Miller L., Smith R. J., Myers A.D., 2003, MNRAS, **342**, 483

[195] Overzier R. A. et al., 2006, ApJ, 637, 58O

[196] Overzier R. A., Röttgering H. J. A., Rengelink R. B., Wilman R. J., 2003, A&A, **405**, 53

[197] Padin S. et al., 2002, PASP, **114**, 83

[198] Peacock J. A., 1997, MNRAS, **284**, 885

[199] Peacock J. A., 1999, *Cosmological Physiscs*, Cambridge University Press

[200] Peacock J. A., Dodds S. J., 1996, MNRAS, **280**, L19

[201] Peacock J.A. et al., 2000, MNRAS, **318**, 535 (P00)

[202] Peacock J. A., Nicholson D., 1991, **253**, 307

[203] Peebles P. J. E., 1974, A&A, **32**, 197

[204] Peebles P. J. E., 1980, *The Large-Scale Structure of the Universe*, Princeton Univ. Press, Princeton (P80)

[205] Peebles P. J. E., Groth E. J., 1975, ApJ, **196**, 1

[206] Perna R., Di Matteo T., 2000, ApJ, **542**, 68

[207] Perrotta F., Magliocchetti M., Baccigalupi C., Bartelmann M., De Zotti G., Granato G.L., Silva L., Danese L., 2003, MNRAS, **338**, 623

[208] Phleps S., Peacock J. A., Meisenheimer K., Wolf C., 2006, A&A in press, astro-ph/0506320

[209] Pierpaoli E., Borgani S., Scott D., White M., 2003, MNRAS, **342**, 163

[210] Pierpaoli E., Perna R., 2004, MNRAS, **354**, 1005

[211] Porciani C., Magliocchetti M., Norberg P., 2004, MNRAS, **355**, 1010

[212] Postman M., 1999, in Evolution of large scale structure : from recombination to Garching, edited by A. J. Banday, R. K. Sheth, L. N. da Costa. ("Proceedings of the MPA- ESO cosmology conference, Garching, Germany, 2-7 August 1998".), p.270

[213] Pozzi F., Gruppioni C., Oliver S. et al., 2004, ApJ, **609**, 122

[214] Press W. H., Schechter P., 1974, ApJ, **187**, 425

[215] Prestage R. M., Peacock J. A., 1989, MNRAS, **230**, 131, erratum **236**, 959

[216] Puget J. L. Abergel A., Bernard J-P., Boulanger F., Burton W. B. et al., 1996, A&A, **308**, L5

[217] Reach W. T., Dwek E., Fixsen D. J. et al., 1995, ApJ, **451**, 188

[218] Readhead A. C. S., Taylor G. B., Pearson T. J., Wilkinson P. N., 1996, ApJ, **460**, 634

[219] Readhead A. C. S., Mason B. S., Contaldi C. R. et al., 2004, ApJ, **609**, 498

[220] Rebolo R., Battye R.A., Carreira P. et al., 2004, MNRAS, **353**, 747

[221] Rees M. J., Phinney E. S., Begelman M. C., Blandford R. D., 1982, Nature, **295**, 17

[222] Regan M. W., Thornley M. D., Helfer T. T., Sheth K., Wong T., Vogel S. N., Blitz L., Bock D. C. J., ApJ, 2001, **561**, 218

[223] Rengelink R. B., Röttgering H. J. A., 1999, in Röttgering H.J.A., Best P.N., Lehnert M.D., eds, Proc. Colloq. The Most Distant Radio Galaxies. Royal Netherlands Acad. Arts and Sciences, Amsterdam, p.399

[224] Rengelink R. B., Tang Y., de Bruyn A. G., Miley G. K., Bremer M. N., Röttgering H. J. A., Bremer M. A. R., 1997, A&AS, **124**, 259

[225] Ricci R., et al., 2004, MNRAS, **354**, 305

[226] Ricci R., Sadler E.M., Ekers R.D., Staveley-Smith L., Wilson W.E., Kesteven M.J., Subrahmanyan R., Walker M.A., Jackson C.A., De Zotti G., 2004, MNRAS, **354**, 305

[227] Richards E.A., 2000, ApJ, **533**, 611

[228] Rodighiero G., Fadda D., Gregnanin A., Lari C., Franceschini A., 2003, in Gry C. Peschke S., Matagne J., Garcia-Lario P., Lorente R., Salama A., eds, ESA SP-511, Exploiting the ISO Data Archive. Infrared Astronomy in the Internet Age. ESA Publications Division, Noordwijk, p.321

[229] Romano D., Silva L., Matteucci F., Danese L., 2002, MNRAS, **334**, 444

[230] Rowan-Robinson M., 2001, ApJ, **549**, 745

[231] Rowan-Robinson M., Benn C. R., Lawrence A., McMahon R. G., Broadhurst T. J., 1993, MNRAS, **263**, 123

[232] Russell D. M., Ellison S. L., Benn C. R., 2006, MNRAS, **367**, 412

[233] Sadler E. M. et al., 2002, MNRAS, **329**, 227

[234] Sadler E. M. et al., 2006, submitted to MNRAS (astro-ph/0603437)

[235] Sanders D. B., 1999, Ap&SS, **266**, 331

[236] Sanders D. B., Mirabel F., 1996, ARA&A, **34**, 749

[237] Saracco P. et al., 2004, A&A, **420**, 125

[238] Saunders W., Rowan-Robinson M., Lawrence A., 1992, MNRAS, **258**, 134

[239] Saunders W., Rowan-Robinson M., Lawrence A., Efstathiou G., Kaiser N., Ellis R. S., Frenk C. S., 1990, MNRAS, **242**, 318

[240] Sawicki M., 2002, AJ, **124**, 3050

[241] Sawicki M., Webb T. M. A., 2005, ApJ, **618**, 67

[242] Scheuer P. A. G., 1957, Proc. Cambridge Phil. Soc., **53**, 764

[243] Scheuer P. A. G., 1974, MNRAS, **166**, 329

[244] Schlegel D. J., Finkbeiner D. P., Davis M., 1998, ApJ, **500**, 525

[245] Scoccimarro R., Colombi S., Fry J.N., Frieman J.A., Hivon E., Melott A., 1998, ApJ, **496**, 586

[246] Scoccimarro R., Sefusatti E., 2004, PhRvD, **69**, 103513

[247] Scott S. E., Fox M. J., Dunlop J. S. et al., 2002, MNRAS, **331**, 817

[248] Scott D., White M., 1999, A&A, **346**, 1

[249] Seldner M., Peebles P. J. E., 1981, MNRAS, **194**, 251

[250] Seljiak U., Zaldarriaga M., 1996, ApJ, **469**, 437

[251] Serjeant S. et al., 2003, MNRAS, **344**, 887

[252] Shankar F. Lapi A., Salucci P., De Zotti G., Danese L., 2006, ApJ, **643**, 14

[253] Shaver P. A., Pierre M., 1989, A&A, **220**, 35

[254] Sheth R. K., Tormen G., 1999, MNRAS, **308**, 119

[255] Silva L., De Zotti G., Granato G.L., Maiolino R., Danese L., 2005, MNRAS, **357**, 1295

[256] Silva L., Granato G.L., Bressan A., Danese L., 1998, ApJ, **509**, 103

[257] Simpson C., Eisenhardt P., 1999, PASP, **111**, 691

[258] Smail I., Chapman S. C., Blain A. W., Ivison R. J., 2003, in Colless M., Staveley-Smith L. eds, ASP Conf. Ser. Vol. 216, Maps of the Cosmos. Astron, Soc. Pac., San Francisco (astro-ph/0311285)

[259] Smail I., Ivison R.J., Blain A.W., Kneib J.-P., 2002, MNRAS, **331**, 495

[260] Smith R. E. et al., 2003, MNRAS, **341**, 1311

[261] Snellen I. A. G., Schilizzi R. T., Miley G. K., et al. 2000, MNRAS, **319**, 445

[262] Soifer B. T., Neugebauer G., 1991, AJ, **101**, 354

[263] Soifer B. T., Boehmer L., Neugebauer G., Sanders D. B., 1989, AJ, **98**, 766

[264] Somerville R. S., Lemson G., Sigad Y., Dekel A., Kauffmann G., White S. D. M., 2001, **320**, 289

[265] Somerville R. S., Primack J. R., Faber S. M., 2001, MNRAS, **320**, 504

[266] Spergel D. N. et al., 2003, ApJ, **148**, 175

[267] Spergel D. N. et al., 2006, submitted to ApJ, astro-ph/0603449

[268] Stevens J. A. et al., 2003, Nature, **425**, 264

[269] Stevens J. A., Page M. J., Ivison R. J., Smail I., Carrera F. J., 2004, ApJ, **604**, 17

[270] Sugiyama N., 1995, ApJs, **100**, 281

[271] Szapudi I., 2004, ApJ, **605**, L89

[272] Szapudi I., Meiksin A., Nichol R.C., 1996, ApJ, **473**, 15

[273] Szapudi I., Postman M., Lauer T.R., Oegerle W., 2001, ApJ, **548**, 114

[274] Szapudi I., Szalay A. S., 1998, ApJ, **494**, L41

[275] Takeuchi T. T., Ishii T. T., 2004, ApJ, **604**, 40

[276] Takeuchi T. T., Ishii T. T., Hirashita H., Yoshikawa K., Matsuhara H., Kawara K., Okuda H., 2001, PASJ, **53**, 37

[277] Taylor A. N., Watts P.I.R., 2000, MNRAS, **314**, 92

[278] Terasranta H. et al., 1998, A&AS, **91**, 121

[279] Thomas D., Maraston C., Bender R., 2002, Ap&SS, **281**, 371

[280] Tinti S., Dalacasa D., De Zotti G., Celotti A., Stanghellini C., 2005, A&A, **432**, 31

[281] Toffolatti L., Argüeso Gómez F.A., De Zotti G., Mazzei P., Franceschini A., Danese L., Burigana C., 1998, MNRAS, **297**, 117

[282] Totsuji H., Kihara T., 1969, PASJ, **21**, 221

[283] Trager S. C., Faber S. M., Worthey G., Ganzález J. J., 2000a, AJ, **119**, 1645

[284] Trager S. C., Faber S. M., Worthey G., Ganzález J. J., 2000b, AJ, **120**, 165

[285] Umemura M., 2001, ApJ, **560**, L29

[286] Van Waerbeke L., Mellier Y., Hoekstra H., 2005, A&A, **429**, 75

[287] Venemans B. P. et al., 2002, ApJ, **569**, L11

[288] Verde L., Jimenez R., Kamionkowski M., Matarrese S., 2001, MNRAS, **325**, 412

[289] Waldram E. M., Pooley G. G., Grainge K. J. B., Jones M. E., Saunders R. D. E., Scott P. F., Taylor A. C., 2003, MNRAS, **342**, 915

[290] Wang W., Cowie L., Barger A., 2004, ApJ, **613**, 655

[291] Webb T. M., Eales S. A., Lilly S. J., Clements D. L., Dunne L., Gear W. K., Ivison R. J., Flores H., Yun M., 2003, ApJ, **587**, 41

[292] Webster A., 1976, MNRAS, **175**, 61

[293] Werner M. W., Gallagher D. B., Irace W. R., 2004, AdSpR, **34**, 600

[294] Willot C. J., Rawlings S., Blundell K. M., Lacy M., Eales S. A., 2001, MNRAS, **322**, 536

[295] Wilman R. J., Röttgering H. J. A., Overzier R. A., Jarvis M. J., 2003, MNRAS, **339**, 695

[296] Windhorst R. A., Fomalont E. B., Partridge R. B., Lowenthal J. D., 1993, ApJ, **405**, 498

[297] Xu C., Lonsdale C. J., Shupe D. L., O'Linger J., Masci F., 2001, ApJ, **562**, 179

[298] Xu C. K., Lonsdale C. J., Shupe D. L., Franceschini A., Martin C., Schiminovich D., 2003, ApJ, **587**, 90

[299] Zehavi I., Weinberg D. H., Zheng Z. et al., 2004, ApJ, **608**, 16

[300] Zehavi I., Zheng Z., Winberg D. H. et al., 2005, ApJ, **630**, 1

[301] Zhang P., Pen U., Wang B., 2002, ApJ, **577**, 555

[302] Zirbel E. L., 1996a, ApJ, **473**, 144

[303] Zirbel E. L., 1996b, ApJ, **473**, 713

[304] Zirbel E. L., 1997, ApJ, **476**, 489